Thermodynamic approach to Generating functions and Nonequilibrium Dynamics

by

James M. Hickey, MSci.

Thesis submitted to the University of Nottingham

for the degree of Doctor of Philosophy

October 2014

Abstract

This thesis investigates the dynamical properties of equilibrium and nonequilibrium systems, both quantum and classical, under the guise of a thermodynamic formalism. Large deviation functions associated with the generating functions of time-integrated observables play the role of dynamical free energies and thus determine the trajectory phase structure of a system. The 1d Glauber-Ising chain is studied using the time-integrated energy as the dynamical order parameter and a whole curve of second order trajectory transitions are uncovered in the complex counting field plane. The leading dynamical Lee-Yang zeros of the associated generating function are extracted directly from the time dependent high order cumulants. Resolving the cumulants into constituent contributions the motion of each contribution's leading Lee-Yang zeros pair allows one to infer the positions of the trajectory transition points. Contrastingly if one uses the full cumulants only the positions of those closest to the origin, in the limit of low temperatures, can be inferred. Motivated by homodyne detection schemes this thermodynamic approach to trajectories is extended to the quadrature trajectories of light emitted from open quantum systems. Using this dynamical observable the trajectory phases of a simple "blinking" 3-level system, two weakly coupled 2-level systems and the micromaser are studied. The trajectory phases of this observable are found to either carry as much information as the photon emission trajectories or in some cases capture extra dynamically features of the system (the second example). Finally, the statistics of the time-integrated longitudinal and transverse magnetization in the 1d transverse field quantum Ising model are explored. In both cases no large deviation function exists but the generating functions are still calculable. From the singularities of these generating functions new transition lines emerge. These were shown to be linked to: (a) the survival probability of an associated open system, (b) $\mathcal{PT}$-symmetry, (c) the temporal scaling of the cumulants and (d) the topology of an associated set of states.

List of Publications

The work described in this thesis has resulted in several publications and preprints in the past few years. The manuscripts directly related to the work in this thesis are as follows:

Chapter 3:

1. **James M. Hickey**, Christian Flindt, and Juan P. Garrahan, *Trajectory phase transitions and dynamical Lee-Yang zeros of the Glauber-Ising chain*, Phys. Rev. E **88**, 012119 (2013).

Chapter 4:

2. **James M. Hickey**, Sam Genway, Igor Lesanovsky, and Juan P. Garrahan, *Thermodynamics of Quadrature Trajectories in Open Quantum Systems*, Phys. Rev. A **86**, 063824 (2012).

Chapter 5:

3. **James M. Hickey**, Sam Genway, Igor Lesanovsky, and Juan P. Garrahan, *Time-integrated observables as order parameters for full counting statistics transitions in closed quantum systems*, Phys. Rev. B **87**, 184303 (2013).

4. **James M. Hickey**, Sam Genway, and Juan P. Garrahan, *Dynamical phase transitions, time-integrated observables and geometry of states*, Phys. Rev. B **89**, 054301 (2014).

5. **James M. Hickey**, Emanuele Levi, and Juan P. Garrahan, *Cumulants of time-integrated observables of closed quantum systems and $\mathcal{PT}$-symmetry, with an application to the quantum Ising chain*, Phys. Rev. B **90**, 094301 (2014).

Other Related Publications:

6. **James M. Hickey**, *Timescales, dynamical phase transitions and* 3*rd order phase transitions in the* 1*d anisotropic XY model*, arXiv:1403.5515 (2014).

7. **James M. Hickey**, and Sam Genway, *Fluctuation Theorems and the Generalised Gibbs Ensemble in Integrable Systems*, Phys. Rev. E **90**, 022107 (2014).

8. Sam Genway, **James M. Hickey**, Juan P. Garrahan, and Andrew Armour, *Dynamical Phases in the Full Counting Statistics of the Resonant-Level Model*, arXiv:1212.5200 (2012).

9. **James M. Hickey**, Christian Flindt, and Juan P. Garrahan, *Intermittency and dynamical Lee-Yang zeros of open quantum systems*, arXiv:1407.3963(2014).

10. **James M. Hickey**, Sam Genway, and Juan P. Garrahan, *Signatures of many-body localization without disorder and the relation to a glass transition*, arXiv:1405.5780 (2014).

Acknowledgements

This thesis would not have been possible to write without the support, friendship and guidance of many people. Firstly I thank my primary supervisor Juan P. Garrahan for years of stimulating discussions, guidance and good ideas! The constant supply of good and interesting ideas along with your enthusiasm for science have made my time at Nottingham very enjoyable as well as educational. To my secondary supervisor Igor Lesanovsky I am indebted to you for your wealth of ideas and support throughout my years at Nottingham.

I also thank the friends I made in the Department during my time at Nottingham. I have learnt so much from Sam, Mike, Rob, Suz and Ben; to name but a few, and have also had some great times outside of science too. To my friends from Cambridge for your enduring companionship, I thank you. In particular I extend a big thank you to Dave, Paul and Sophie for all the fun evenings and weekends they've given me away from physics.

To my family, I am deeply grateful for all the support and love they've provided me over the past 3 years. Finally, and most importantly, I thank Sarah for being the kindest person I've ever met and always making me smile throughout the PhD.

Contents

List of Figures

1. Introduction

Equilibrium statistical mechanics is a many-body theory which describes a system in thermal equilibrium with a surrounding environment [1, 2]. It captures the properties of the system of interest through a probabilistic approach, as the complexity of the problem does not allow for a full deterministic solution. This theory provides the microscopic foundations for thermodynamics, which only focuses on the macroscopic properties of a system and where the concept of microscopic details is foreign. Originally developed to describe the behaviour of ideal gases and magnets, taken together these theories have a broad range of applicability ranging from the classical to the quantum, from the practical (e. g. engines etc.) to the abstract (e. g. Bose-Einstein condensates etc.). It also describes one of the most remarkable and ubiquitous of collective phenomena, the phase transition [3]. A phase transition is marked by a singular change of a macroscopic observable upon tuning an appropriate system parameter, such as temperature. The occurrence of a phase transition manifests as nonanalyticities in the system's free energy, which may be derived from the central object of statistical mechanics, the partition sum. There is, however, one area of science which appears to be beyond statistical mechanics' reach of applicability, that is *nonequilibrium dynamics*. Contrary to initial intuition, surprisingly, it is possible to extend both thermodynamics and statistical mechanics to this area of physics.

The seeds of this extension were sown by Ruelle [4] who developed a thermodynamic formalism for dynamical systems; this was later developed into a full "thermodynamics of trajectories" [5–14]. A particularly useful ensemble within this formalism, and perhaps the most intuitive, is the fixed trajectory length ensemble known as the s-ensemble. The basic principle behind this approach is to understand the dynamical properties of complex many-body systems by considering ensembles of trajectories in a manner analogous to ensembles of configurations in equilibrium statistical physics. One area where this thermodynamic formalism has provided insight has been in the study of glassy systems, where upon cooling there is a change in the dynamical properties of the system without any apparent structural changes [5, 15–28]. One school of thought proposes that the emergence of glassy behaviour is not due to an equilibrium phase transition but due to highly correlated dynamical behaviour [15].

To gain more insight into the dynamical behaviour of these glassy systems the full distributions associated with dynamical observables needed to be studied. This approach revealed the existence of two distinct phases in the space of trajectories, an equilibrium liquid phase and an inactive glassy phase, which may be probed using the field s which is conjugate to the dynamical observable of interest [29–37]. In the equilibrium liquid phase the trajectories are active and have more than the typical amount of particle motion while in the inactive glassy case there is less particle activity. The physical dynamics of these models ($s = 0$) occurs precisely at coexistence between these phases leading to the emergence of glassy behaviour without any structural changes. Beyond the glass problem this approach allows one to study classical stochastic systems [38] within a generalized thermodynamic framework by focussing on the "free energies" and partition sums associated with these dynamical (time-integrated) observables [4, 6]. The analytic structure of these functions characterizes the *trajectory phase behaviour* of the system and analogous to equilibrium thermodynamics there can exist trajectory

phase transitions.

The purpose of this thesis is to develop this thermodynamic approach to dynamics in both the classical and quantum context. Chapter 2 provides a brief primer on this thermodynamic approach to dynamics, recapping all the necessary mathematical tools for both the quantum and classical cases. In both cases this approach was developed in parallel through advancements in quantum optics [39, 40], electronic transport [41, 42] and classical stochastics [38, 43] over the past few decades and relies heavily on large deviation theory [44–46].

Furthermore the last decade has also seen many advances in the experiments involving ultra cold atoms. Motivated by these advances in realising highly tunable open and closed quantum systems [47–50], we develop this approach for the case of dynamics in open dissipative and closed quantum systems. In Chapter 3 we examine how one may use the cumulants of the time-integrated energy to extract the Lee-Yang zeros [51, 52] of the associated dynamical partition sum and hence the location of these trajectory phase transitions [53]. Chapter 4 examines the trajectory phase diagram associated with quadrature measurements in several open quantum systems [54]. The formulation of the s-ensemble in terms of a quantum stochastic calculus is vital to studying this dynamical observable and the study of this new dynamical observable reveals new trajectory phase transitions in these systems.

Subsequently in Chapter 5 we study the dynamics of the 1d quantum Ising chain in a transverse field by analyzing the behaviour of the time-integrated magnetization. This model is the paradigm of a quantum phase transition where on tuning the transverse field the ground state will change in a singular fashion from being ferromagnetic in nature to paramagnetic at the static quantum critical points [55]. We uncover a whole curve of transition points associated with the time-integrated

magnetization of which the static critical points are just the end points [56]. We examine the behaviour of the states associated with these transition points and characterize their topology using the Berry phase and Chern number [57–64]. Moreover considering the time-integrated longitudinal magnetization we show how a spontaneously-broken parity time-reversal [65–71] (or $\mathcal{PT}$) symmetry impacts the temporal behaviour of the cumulants of this observable [72].

Finally in Chapter 6 we discuss the work presented in this thesis as a whole and conclude with an outlook of potential future work.

2. Thermodynamic Approach - Master Equations and Quantum Quenches

The success of the thermodynamic approach to science can be measured in how far reaching and long lasting its application and relevance has been. With applications in a broad variety of topics which include transport, phase transitions, black holes and even more mundane everyday examples such as engines, its reach is unquestionable. Developed in the 19th century this formalism describes macroscopic systems interacting with even larger environments but is underpinned by a well-defined microscopic theory known as statistical mechanics [1, 2]. Together they describe the equilibrium properties of systems coupled to an environment but the mathematical quantities which define the theory have a more general context and so this formalism may be extended to other situations beyond systems in equilibrium.

The central mathematical objects when studying the canonical statistical mechanics of any system are the canonical partition function and free energy. These objects describe the statistical physics of a system allowed to exchange energy with a large environment. This leads to a natural emergence of the inverse tempera-

ture $\beta = (k_B T)^{-1}$, here k_B is the Boltzmann constant and T is the temperature, as a Lagrange multiplier used to fix the average energy of the system of interest. However it also plays has a secondary role, as differentiating the free energy with respect to β generates the cumulants of the system's energy. Therefore one can consider the partition function and free energy density respectively as the (unnormalized) moment (MGF) and cumulant generating functions (CGF) of the system's energy. Viewed in this light one can consider classical thermodynamics to be defined in terms of generating functions of the system's energy and the analytic form of these encode all information of our system of interest, i. e. singularities in the free energy mark the onset of a phase transition [1]. Statistical mechanics is very well understood and can be used to explain all equilibrium phenomena provided one has access to these quantities. From this brief introduction a natural question then arises: if this approach is defined by generating functions can it be extended to nonequilibrium phenomena and dynamics? In particular can it be used to describe a new type of nonequilibrium phase transition or dynamical phase transition? The answer to both these questions is yes and will form the primary focus of this thesis.

This Chapter introduces the necessary theoretical background for the remainder of the thesis and the systems to be studied. Firstly, a brief overview of the canonical ensemble followed by a primer on large deviation theory [46], which underpins thermodynamics [4], and a classification scheme of phase transitions used in this thesis will be given. Following this there will be a description of the systems of interest, which include both classical and quantum stochastic systems as well as closed quantum systems. In the first two types of system, large deviations associated with dynamical observables describe the thermodynamics of trajectories, the so-called s-ensemble, of these systems. This approach will then be extended to closed quantum systems by considering the generating functions of time-integrated observables which may be estimated via full counting statistics. Moreover these

closed quantum systems may be put out of equilibrium via a protocol known as a quantum quench. The return amplitude, known as the Loschmidt echo [73], is the moment generating function of the work done during this protocol and in the large system size limit also has a large deviation form. Singularities in this large deviation function emerge as nonanalyticities in the real time dynamics of the quench [74–78] and are dubbed dynamical phase transitions (DPTs) [64, 79–81].

2.1 Basic Thermodynamics and Large Deviations

This Section focusses on the canonical ensemble in thermodynamics introducing it from first principles and highlighting the importance of large deviation functions, such as the free energy and entropy density.

2.1.1 Statistical Mechanics-The Canonical Ensemble

Consider an isolated system made up of N interacting particles, at any point in time the state of the system may be described by the positions of the particles $\underline{\mathbf{r}}$ and their momenta $\underline{\mathbf{p}}$. These $2DN$ scalar values, where D is the dimensionality the system, identify a point known as the system's representative point x which lives in a $2DN$ dimensional space known as **phase space**. The evolution of the representative point is determined by the system's Hamiltonian. In the thermodynamic (large system size) limit we now assume the state of the system is completely determined by a set of extensive macroscopic variables $(Y_1, \ldots, Y_r)$, each of which is a function of the representative point x. From this it is clear that the system's representative point must live in some *accessible* region of phase space where these variables possess their thermodynamic value [1]. This region of accessible phase

space is denoted Γ and it's volume is $|\Gamma|$. One must note that although knowledge of the accessible phase space and the representative points dynamics is enough to completely describe the system, in practice the number of degrees of freedom is often too large to admit a deterministic solution. Therefore we have only really outlined the mathematical preliminaries and not really gained much in the way of physical insight. If no deterministic solution is feasible a probabilistic approach is necessary. The next step is crucial in formulating equilibrium statistical physics and was proposed by Boltzmann, it is known as the fundamental postulate

$$S = k_B \ln|\Gamma|. \tag{2.1}$$

The relationship in Eq. (2.1), relating the thermodynamic entropy S to the phase space volume, cannot be proven but can be shown to hold the desired properties of a thermodynamic entropy, i. e. concavity, monotonicity etc. Using this idea of an accessible phase space we can define a probability distribution $P(x)$ which is non-zero only within Γ and is the probability of the system having a representative point $x' \in [x, x + dx]$. With this distribution we can see the true power of equilibrium statistical mechanics: it allows us to calculate the expectation value of extensive observables $A(x)$ which are not necessarily thermodynamic variables. Assuming almost all of the accessible phase space corresponds to A's equilibrium

value[1], a^*, this is simply calculated using

$$a^* = \langle A(x) \rangle = \int_\Gamma dx A(x) P(x). \tag{2.2}$$

The realisation of a specific distribution $P(x)$ over the accessible representative points defines an *ensemble*. Taking $P(x) = 1/|\Gamma|$ to be uniform over the accessible region of phase space corresponds to the *microcanonical ensemble*. We now consider the most important ensemble in equilibrium statistical mechanics, it is defined by the system of interest exchanging energy with a much larger reservoir R. In this instance the extensive variable of interest is the energy, E, and its corresponding thermodynamic intensive variable is temperature T. The system and reservoir can exchange energy freely and at equilibrium they possess the same temperature. Furthermore, due to the reservoir's much larger size, this temperature is independent of the energy of the system of interest. Noticing that the system plus reservoir is defined by the pair (x_R, x), where x_R is the reservoir's representative point and x is the system's, we may calculate the equilibrium values a^* of any system extensive observable $A(x)$ within the system plus reservoir's microcanonical ensemble via

$$a^* = \frac{1}{|\Gamma|} \int_\Gamma dx_R dx A(x). \tag{2.3}$$

The region of accessible phase space is determined by the total energy E, which is

[1]Here we note that to connect equilibrium thermodynamics with Hamiltonian dynamics one often appeals to chaos and the ergodic hypothesis. These ideas are invoked to explain how through deterministic evolution a system's extensive variables obtain their equilibrium values but are not necessarily a requirement for equilibrium statistical physics to hold [82]. We simply note that a much weaker but necessary condition required for equilibrium statistical physics to hold is that at long times (and in the large system size limit) a system's trajectory spends most of its time in the region of phase space where extensive observables obtain their equilibrium value.

fixed, along with other thermodynamic variables which we are not specifically interested in. The total Hamiltonian is assumed to be of the form $H_{total} \approx H_R(x_R) + H_{sys}(x)$ and so we may write

$$\begin{aligned} a^* &= \frac{1}{|\Gamma|}\int dx_R dx A(x)\delta(H_{sys}(x) + H_R(x_R) - E) \\ &= \frac{1}{|\Gamma|}\int dx A(x)\int dx_R\ \delta(H_R(x_R) - (E - H_{sys}(x))). \end{aligned} \tag{2.4}$$

The integral over the reservoir is simply the accessible region of phase space when the reservoir's energy is $E - H_{sys}$. Using the fundamental postulate we express this in terms of the reservoir entropy and find the integral over x_R is simply $\exp(S_R(E - H_{sys})/k_B)$; recalling the reservoir is much larger than the system the entropy may be Taylor expanded

$$\exp(\frac{S_R(E - H_{sys})}{k_B}) \approx \exp(\frac{S_R(E)}{k_B})\exp(-\frac{1}{k_B}\frac{\partial S_R}{\partial E}H_{sys}). \tag{2.5}$$

Identifying $\partial S_R/\partial E$ as the inverse temperature $1/T$ the expectation value of Eq. (2.4) is

$$\langle A\rangle = \frac{1}{\mathcal{N}}\int dx A(x)e^{-\beta H_{sys}}, \tag{2.6}$$

where the normalization $\mathcal{N}$ is a fundamental quantity known as the **partition function**:

$$Z = \mathcal{N} = \int dx e^{-\beta H_{sys}}. \tag{2.7}$$

In essence we have defined a new probability distribution $P(x) = e^{-\beta H_{sys}}/Z$ or in the language of statistical mechanics a new ensemble, the *canonical ensemble* [1]. It is also possible to show that **in the thermodynamic limit** the average of observables is dominated by the region of phase space where the system's internal energy is equal to its equilibrium value E^*. This ensures that in the thermodynamic limit the expectation values calculated in the both the microcanonical and canonical ensemble are identical. It is also implies that the partition function is

related to the system's entropy and equilibrium energy via

$$\begin{aligned} Z &= \int dx e^{-\beta H_{sys}} = \int dE' dx \delta(E' - H_{sys}) e^{-\beta E'} \\ &= \int dE' e^{-\beta(E' - TS(E'))} \\ &\approx \exp(-\beta(E^* - TS(E^*))) = \exp(-\beta F(E^*)), \end{aligned} \tag{2.8}$$

where $F(E^*)$ is the system's free energy. This completes the brief introduction to equilibrium statistical physics. Although the derivation of these objects has been heavily reliant on the notion of equilibrium; we will see in the next section that the main quantity of interest, the free energy, is only a specific case of a general class of large deviation functions.

2.1.2 Large Deviation Principle

In this part the large deviation (LD) principle [46] is introduced in a heuristic manner using a simple problem before connecting this approach with equilibrium statistical mechanics and the canonical ensemble. The definitions provided here are not rigorous and only serve as a simple primer for the remainder of the thesis. For the interested reader there are many reviews which deal with the more formal aspects and subtleties behind large deviation theory.

Consider the simple problem of n independent identically distributed random variables, X_i where $i \in 1, 2, \ldots n$, which are drawn from a Gaussian distribution with variance σ^2 and mean μ

$$P(X_i = x) = \frac{1}{\sqrt{2\pi\sigma^2}} e^{-\frac{(x-\mu)^2}{2\sigma^2}}. \tag{2.9}$$

As these are independent random variables the probability of drawing a sequence $x = (x_1, x_2, \ldots, x_n)$ from the Gaussian distribution is simply the product of their

individual probability densities

$$P(x) = P(x_1, x_2, \ldots, x_n) = P(x_1)P(x_2)\ldots P(x_n). \tag{2.10}$$

From this it is easy to see that the sample mean, $S_n = n^{-1}\sum_i X_i$, has a probability density

$$\begin{aligned} P(S_n = s) &= \int \delta(S_n(x) - s)P(x)dx \\ &= \langle \delta(S_n - s)\rangle \\ &= \sqrt{\frac{n}{2\pi\sigma^2}} e^{-\frac{n(s-\mu)^2}{2\sigma^2}}. \end{aligned} \tag{2.11}$$

This result is expected as the sum of Gaussian random variables should also be Gaussian distributed. In the large n limit this density takes a large deviation form, as the $\sqrt{n}$ term is subdominant to the decaying exponential term in Eq. (2.11), and thus

$$P(S_n = s) \asymp e^{-nJ(s)}, \tag{2.12}$$

where the LD function is $J(s) = (s-\mu)^2/2\sigma^2$. We further note the symbol "$\asymp$" denotes that the probability distribution is dominated by an exponentially decaying term in the limit $n \to \infty$. The only value of S_n which does not decay exponentially is $S_n = \mu$ and so the distribution of this variable will become dense around the mean

$$\lim_{n\to\infty} P(S_n \in [\mu - \epsilon, \mu + \epsilon]) = 1. \tag{2.13}$$

Here ϵ is any positive number and whenever this limit holds S_n will converge to the mean. This property is known as the Law of Large Numbers.

This example illustrates the basic approximation associated with the LD principle. In this principle the probability obeys a scaling law of the form $P_n \approx e^{-nI}$, where n is a large parameter and I is some positive constant. Although intuitive, the idea behind this scaling form should be clear, that is, in the limit of large n the dominant

behaviour of P_n is an exponential decay in n. Also in the context of continuous random variables the LD function I need not be constant, as demonstrated above. A useful result associated with the LD principle is the Gärtner-Ellis theorem [46] which connects the LD functions of the moment generating function (MGF) and probability distribution. Considering a random variable A, which depends on parameter n, the scaled cumulant generating function is defined as

$$\theta(s) = \lim_{n\to\infty} \frac{1}{n} \log\langle e^{-nsA}\rangle, \tag{2.14}$$

where $s \in \mathbb{R}$ and

$$\langle e^{-nsA}\rangle = \int_{\mathbb{R}} e^{-snA} P(A) dA. \tag{2.15}$$

This scaled cumulant generating function (CGF) is an LD function, provided it exists and is differentiable at all $s \in \mathbb{R}$ the Gärtner-Ellis theorem states that the variable A satisfies a large deviation principle

$$P(A) \asymp e^{-nI(A)}. \tag{2.16}$$

These LD functions are related by a Legendre-Fenchel transform $\theta(s) = -\min_a[I(a) + sa]$ which may be heuristically considered as the saddle-point approximation applied to Eq. (2.15). Building on this brief introduction in LD theory we now illustrate the connection between LD theory and equilibrium statistical mechanics [4, 46].

As in the previous section, consider a system of N interacting particles: according to equilibrium statistical physics the system may then be described as being distributed across an ensemble of microstates ψ. The set of these microstates is denoted Ω_N and is simply the N-fold product of each individual particle's state space. The energetics of this system is determined by the Hamiltonian $E_N(\psi)$, from this we straightforwardly define a mean energy per particle $\epsilon_N(\psi) = E_N(\psi)/N$. The system is now to be modelled abstractly; treating the microstate ψ as a random

variable determined by a prior probability measure $P(d\psi)$ which in many cases is $\propto d\psi$ due to Liouville's theorem.

Now that the problem has been formally set out, how does LD theory come into play? LD theory becomes relevant when one considers the thermodynamic limit $N \to \infty$. In this limit the interactions between the particles means the system behaves in a coarse-grained manner and is determined by a few macroscopic variables known as a *macrostate*, $M_N(\psi)$. The system is now characterized by a subset of microstates called the equilibrium microstates, which are the most probable set of macrostates in the ensemble. In essence the thermodynamic description of the system stems from the *Law of Large Numbers* and the convergence in probability of the macrostates around the equilibrium microstates often obeys a LD principle.

The discussion above focussed on the unconstrained problem, if this problem obeys a large deviation principle one may show that the constrained problem, i. e. fixed energy (microcanonical ensemble), obeys a LD principle. The formal details proving this may be found in Ref. [46]; here we simply list the relevant LD functions related to the canonical ensemble. From the last section we write a discretized version of the partition sum is

$$\begin{aligned} Z(\beta) &= \sum_i e^{-\beta\epsilon_i} \\ &\asymp e^{-N\beta f(\beta)}, \end{aligned} \tag{2.17}$$

where $f(\beta)$ is the free energy density of the problem, this is the LD function associated with the unnormalized MGF of the system's energy (the partition sum). Similarly, the probability of being in a macrostate with energy density u also follows a large deviation principle, $P(u) = e^{-N\beta s(u)}$, where the LD function $s(u)$ is the entropy density. These LD functions essentially define the properties of the system in the canonical ensemble and their analytic form has many physical

consequences. Their most relevant property, in relation to this thesis, is how singular features in the free energy density mark phase transitions. In the next Section a basic background to equilibrium phase transitions will be provided but it is important to remember that the formalism discussed is applicable to LD functions beyond those associated with the energy of the system of interest.

2.2 Order Parameters and Phase Transitions

Phase transitions are marked by singular changes in the macroscopic properties of the system under tuning a system parameter. They are ubiquitous in nature and nearly everyone has observed simple examples such as water changing to a gas upon heating to $\sim 373K$ in normal conditions (i. e. one atmosphere of pressure) or freezing to form a solid upon cooling. These transitions emerge as a collective phenomenon in many-body systems with non-trivial interactions and so are often difficult to describe in full without resorting to powerful tools such as renormalization group theory. However the basics of phase transition theory are quite simple and intuitive and so will be the focus of this Section.

Phase transitions manifest themselves as singular features in the analytic structure of the free energy. As such there are many types of phase transitions and a classification system was introduced by Ehrenfest. This system is based on the derivatives of the free energy: a nth order phase transition is marked by a discontinuity in the nth derivative of the free energy and all lower order derivatives are smooth. In the conventional approach to phase transitions only first and second order phase transitions are usually considered and so we will introduce their basic phenomenology. However in this thesis we will also encounter third order transitions as defined by Ehrenfest's classification.

To observe a phase transition it is necessary to study an observable which can distinguish between the different phases. This observable is the **order parameter** of the system and it changes in a singular fashion when the system undergoes a transition from one phase to another. Two pedagogical examples of a phase transition are the liquid-gas transition and the ferromagnet-paramagnet transition; these are systems which exhibit first and second order transitions respectively. In the first case a suitable order parameter is the particle density ρ, at ambient pressure this observable changes discontinuously when the system's temperature crosses its boiling point T_c. In the second example the interaction between the magnetic dipoles seeks to align the dipoles ferromagnetically and enhance the magnetization while thermal fluctuations seek to disorder the system. A good order parameter for this system is the total magnetization M. This macroscopic order parameter varies smoothly as a function a T. However if one instead considers the corresponding susceptibility, $\partial_T M$, this diverges at the critical point T_c, both of these cases are shown in Fig. 2.1[2].

Although we have only considered two simple examples of a static phase transition in the canonical ensemble, this thesis will focus on *dynamical "free energies"* which capture temporal correlations of complex many-body systems and analogous to the cases discussed above may undergo *dynamical/trajectory phase transitions* [6, 7, 9, 29, 53, 54, 56]. Therefore in studying these new generalized free energies it will be necessary to consider *dynamical* order parameters to characterize this new phase

[2]If one now considers ρ as a function of pressure (P) and T we find a line of 1st order transitions which ends at a critical point in the (P,T) plane. Similarly in the second example we now consider M as a function of a magnetic field H and T. Below T_c the ground state is ferromagnetic and aligns with the field H in a symmetry breaking process. The $H = 0$ line then forms a 1st order transition line between two symmetry broken states where the spins are aligned in opposite directions. This 1st order line ends at the critical point T_c above which the system is paramagnetic. It should be clear that when extended to the (P,T) and (H,T) planes the behaviour of the order parameters of these two systems is very similar.

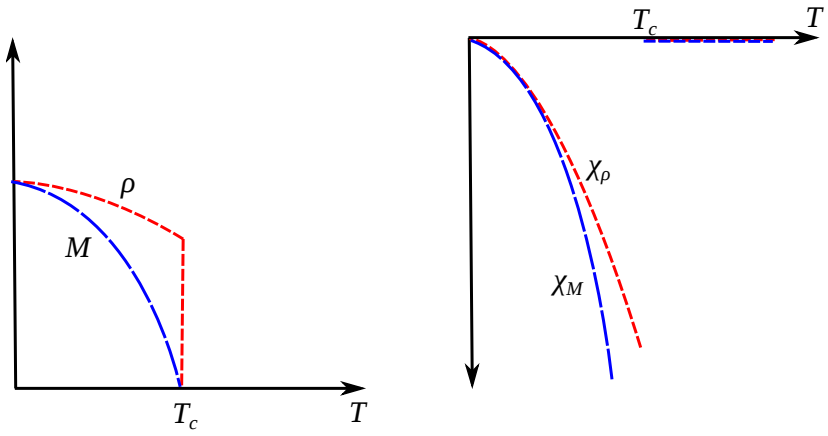

Figure 2.1: The panel on the left shows both 1st and 2nd order transitions where the order parameter changes discontinuously and continuously at T_c respectively. Both transitions result in a diverging susceptibility at T_c, as shown in the panel on the right.

behaviour. The remaining Sections of this Chapter will focus on describing the types of systems studied in the remainder of the thesis and how they relate to LD theory, thermodynamics and phase transitions.

2.3 Classical Systems

Equilibrium statistical physics emerged prior to quantum mechanics and so it is appropriate this thesis includes a study of a classical nonequilibrium many-body system. The type of nonequilibrium dynamical systems we are interested in are stochastic in nature and obey Markovian Master equations. Such stochastic processes play an important role in many areas from economics to life sciences and are often the subject of interdisciplinary research. This Section will briefly derive the classical Master equation associated with a continuous time Markov process before describing how these stochastic systems may be understood using

the s-ensemble formalism [7, 8, 29].

2.3.1 Stochastic Processes and Master Equations

In essence a process is a sequence of configurations $\{\mathcal{C}_i(t_i)\}$ where t_i, $i = 1, \ldots, n$, are discrete times at which the state of the system is recorded. As such the temporal evolution of a state may be described by a process and if this evolution involves some element of randomness, i. e. in the step $\mathcal{C}_i(t_i) \to \mathcal{C}_{i+1}(t_{i+1})$, this process is called a **stochastic process**. This randomness is not compatible with the deterministic Hamiltonian dynamics and instead result from the effects of environmental degrees of freedom which are traced out. One of the most famous examples of a stochastic process is **Brownian motion** where the effects of collisions with external particles generates an effective random fluctuating force. Due to the random nature of these processes it is necessary to consider all possible sequences $\{\mathcal{C}_i(t_i)\}$ and to each realization assign a probability $P(\mathcal{C}_n, t_n; \ldots; \mathcal{C}_1, t_1)$. This probability carries all of the information about the process and the dynamics of the system [38].

There are many different types of stochastic process and therefore the form of the probability distribution may change dramatically from process to process. We therefore will discuss a few general types of stochastic process before proceeding. Firstly, a *stationary* process is one where the distribution P is invariant under time translation of all its arguments; from this it follows $\dot{P} = 0$. A completely random process is one where the distribution is completely independent of its history

$$P(\mathcal{C}_n, t_n; \ldots; \mathcal{C}_1, t_1) = P(\mathcal{C}_1, t_1) \prod_{i=2}^{n} P(\mathcal{C}_i, t_i | \mathcal{C}_{i-1}, t_{i-1}; \ldots; \mathcal{C}_1)$$
$$= \prod_i P(\mathcal{C}_i, t_i), \tag{2.18}$$

here $P(a|b)$ is the joint probability of recording event a given event b has been recorded. In this instance the full distribution is just the product of the distributions of n independent random variables and so lacks any intrinsic correlation. Therefore the dynamics described by such a process would not be expected to exhibit any interesting phenomena. The simplest non-trivial process which may capture rich dynamical phenomena is a **Markovian process**. These processes are defined by joint probability distributions where the current state of the system is only dependent on the previous configuration and so can be considered *memoryless*,

$$P(\mathcal{C}_n, t_n | \mathcal{C}_{n-1}, t_{n-1}; \ldots; \mathcal{C}_1, t_1) = P(\mathcal{C}_n, t_n | \mathcal{C}_{n-1}, t_{n-1}). \tag{2.19}$$

This property defines a very specific dynamics captured by the *Chapman-Kolmogorov* relationship [38]. Consider initializing the system in configuration $\mathcal{C}_i$ at a time t_i, the probability of observing the system in configuration $\mathcal{C}$ at a time t is given by $P(\mathcal{C}, t; \mathcal{C}_i, t_i)$. This is the *transition probability* of the system and may be formally expressed as an integral over the probability to be in an intermediate configuration $\mathcal{C}'$ at time t' prior to the transition,

$$P(\mathcal{C}, t; \mathcal{C}_i, t_i) = \int d\mathcal{C}' P(\mathcal{C}, t; \mathcal{C}', t'; \mathcal{C}_i, t_i)$$
$$= \int d\mathcal{C}' P(\mathcal{C}, t | \mathcal{C}', t'; \mathcal{C}_i, t_i) P(\mathcal{C}', t'; \mathcal{C}_i, t_i) \tag{2.20}$$
$$= \int d\mathcal{C}' P(\mathcal{C}, t | \mathcal{C}', t') P(\mathcal{C}', t'; \mathcal{C}_i, t_i),$$

where the final line is obtained using the Markovian property defined by Eq. (2.19). Although formally exact the Chapman-Kolmogorov relationship does not become

useful until one considers the limit $|t - t'| \ll |t - t_i|$. In this limit the integral decomposes into three pieces: the transition probability of interest, the probability to reach an intermediate state $\mathcal{C}'$ just prior to t and the probability of transitioning from $\mathcal{C}' \to \mathcal{C}$ in a time $|t-t'|$. To see this consider $|t-t'| \equiv \delta t$ to be infinitesimally small and expanding $P(\mathcal{C}, t|\mathcal{C}', t - \delta t)$ to lowest order in δt one finds

$$P(\mathcal{C}, t|\mathcal{C}', t') = \delta(\mathcal{C} - \mathcal{C}')(1 - \delta t \int d\mathcal{C}'' W(\mathcal{C}''|\mathcal{C}')) + \delta t \; W(\mathcal{C}|\mathcal{C}') + \mathcal{O}(\delta t^2). \quad (2.21)$$

This is a very good approximation in the limit $|t - t'| \to 0$ as the probability of transitions to a state $\mathcal{C}$ at a time t is dominated by stationary terms of order $\mathcal{O}(1)$ and transition terms of $\mathcal{O}(\delta t)$. The $\mathcal{O}(\delta t)$ terms are comprised of losses out of state $\mathcal{C}'$ to another state $\mathcal{C}''$ and inputs from transitions from $\mathcal{C}'$ to $\mathcal{C}$; the transition rates associated with these processes are defined as $W(A|B) \equiv \partial_t P(A|B)$.

Substituting this into Eq. (2.20) we arrive at the so-called **Master equation**

$$\partial_t P(\mathcal{C}, t) = -r(\mathcal{C})P(\mathcal{C}, t) + \sum_{\mathcal{C}'} W(\mathcal{C}|\mathcal{C}')P(\mathcal{C}', t), \quad (2.22)$$

where for ease of reading we now denote $P(\mathcal{C}, t; \mathcal{C}_i, t_i) \equiv P(\mathcal{C}, t)$, $r(\mathcal{C}) = \sum_{\mathcal{C}'} W(\mathcal{C}'|\mathcal{C})$ is the escape rate and we have converted the integral to a discrete summation. It is often convenient to write this equation in matrix notation [8, 13, 53, 83]

$$\partial_t |P(t)\rangle = \mathbb{W}|P(t)\rangle, \quad (2.23)$$

where the vector $|P(t)\rangle$ contains the probabilities $P(\mathcal{C}, t)$ and the stochastic matrix $\mathbb{W}$ has matrix elements

$$\langle \mathcal{C}|\mathbb{W}|\mathcal{C}'\rangle = W(\mathcal{C}|\mathcal{C}') - r(\mathcal{C})\delta_{\mathcal{C},\mathcal{C}'}. \quad (2.24)$$

In this pedagogical derivation we have assumed that the stochastic process is not only Markovian but also continuous in time, that is the variable used to characterize the process (in this case the configuration $\mathcal{C}(t)$) changes continuously in

time. This Master equation can be used to describe the dynamics of complex many-body systems. Thus not much can be said about the Master equation in general, but if this equation describes a physical system at long times it should relax to an equilibrium distribution as described by equilibrium statistical physics. Furthermore as a physical system should be described by a microscopic Hamiltonian whose dynamics is preserved under time reversal, the condition $\dot{P}_{eq}(\mathcal{C}) = 0$ translates into **detailed balance**:

$$W(\mathcal{C}|\mathcal{C}')P_{eq}(\mathcal{C}') = W(\mathcal{C}'|\mathcal{C})P_{eq}(\mathcal{C}). \tag{2.25}$$

2.3.2 The s-ensemble

As previously stated a general analysis of the Master equation is very difficult and beyond detailed balance not much information can be gleaned. However changing tack and approaching this dynamical equation from a thermodynamic perspective may provide some new insight or at a least a new physical perspective on the problem. Under the Master equation the system can be considered to evolve along a particular trajectory defined by the set of configurations it visits. Now rather than considering ensembles of microstates we may consider equivalent ensembles of trajectories and use the language of equilibrium statistical physics to understand this problem.

Rather than considering microstates with fixed energy E and system size N, as we do in the *microcanonical* ensemble, we now consider histories of the system between an initial time $\tau = 0$ and final time $\tau = t$. To define our new trajectory microcanonical ensemble [8, 13] we examine statistics of a time extensive observable A_t, and from this we denote $\Gamma_{dyn.}$ as the fraction of histories with a given

value of A_t. We may now apply a thermodynamic formalism [6] provided

$$\lim_{t\to\infty} \frac{\log \Gamma_{dyn.}(ta_t, t)}{t} \to -\phi(a_t). \tag{2.26}$$

Here $a_t = A_t/t$ is the temporal density of A_t and provided $\phi(a_t)$ is finite the system obeys a LD principle and a thermodynamic formalism can be applied where now time plays the extensive role of volume. In this approach the observable a_t plays the role of a *dynamical order parameter* and although in principle it is arbitrary, it is pragmatic to choose an observable that may provide some insight into the dynamics of the problem. For example, if a conductor is connected to two large leads and a voltage is dropped across it, the relevant dynamical order parameter for this nonequilibrium process would be the total charged current transferred. Having essentially defined the dynamical equivalent of the microcanonical ensemble we can equally define a dynamical partition sum by introducing a time-intensive field conjugate to the time-extensive observable A_t,

$$Z_A(s,t) = \sum_{A_t} \Gamma_{dyn.}(A_t, t) e^{-sA_t}. \tag{2.27}$$

The above sum is over all realizations of the observables A_t, and the "counting field" s is taken to be real. The above partition sum is the MGF of A_t and so the moments of A_t are obtained via differentiation, $\langle A_t^n \rangle = (-1)^n \partial_s^n Z_A(s,t)|_{s\to 0}$. Similarly the cumulant generating function (CGF) is given through the logarithm, $\Theta_A(s,t) = \log Z_A(s,t)$. Tuning s away from 0 can be considered to bias the system away from its set of typical trajectories, thus providing information about the rare events of the system. In the large time limit this partition sum takes an LD form:

$$Z_A(s,t) \approx e^{t\theta(s)}, \tag{2.28}$$

and this scaled CGF is related to $\phi(a_t)$ via the Legendre transformation $\theta(s) = -\min_{a_t}(\phi(a_t) + sa_t)$. Pursuing the thermodynamic analogy, the quantity $\phi(a_t)$ is equivalent to a dynamical entropy density and $\theta(s)$ is a dynamical free energy

density [29, 30, 83, 84]. Analogous to equilibrium thermodynamics this free energy may possess singular features which mark **trajectory phase transitions**. The order parameter for this transition is the observable A_t in the 's-biased' ensemble: $\langle A_t \rangle_s = \langle A_t e^{-sA_t} \rangle / Z_A(s,t)$. This dynamical order parameter is simply $-\partial_s \theta(s)$ and we will also examine the corresponding susceptibility $\chi_s = \partial_s^2 \theta(s)$. It is important to note that although the s-field is not necessarily physically tunable nonetheless singular features in the generating functions have implications on the form of the full distribution $P(A_t, t)$ [5] and hence the moments at $s = 0$, this is shown in Fig. 2.2. Below we summarize the important quantities introduced so far in this Section and their equilibrium statistical physics analogs.

s-ensemble	Equil. Stat. Phys.
t (time)	N (volume)
s	β
$\Gamma_{dyn.}(A_t, t)$	$\Gamma(E, N)$
$\phi(A_t/t)$ (Rate function)	$s(E/N)$ (Entropy density)
$Z_A(s,t)$ (MGF)	$Z(\beta, N)$ (Partition function)
$\Theta_A(s,t)$ (CGF)	$F(\beta, N)$ (Free Energy)
$\theta(s)$ (dyn. free energy density)	$f(\beta)$ (free energy density)
χ_s (dyn. susceptibility)	χ (static susceptibility, i. e. χ_M in Sec. 2.2)

To extract the LD function $\theta(s)$ we must first consider the probability, $P(\mathcal{C}, A_t, t)$, of being in a certain configuration $\mathcal{C}$ having measured a value A_t. Summing this probability over all configurations yields the microcanonical counting function $\Gamma_{dyn.}(A_t, t)$. Laplace transforming $P(\mathcal{C}, A_t, t)$ and writing in vector notation we have:

$$|P(s,t)\rangle = \sum_{A_t} |P(A_t, t)\rangle e^{-sA_t}, \tag{2.29}$$

the overlap of this probability vector with the flat state $\langle -| \equiv (1, 1, \ldots, 1)$ yields

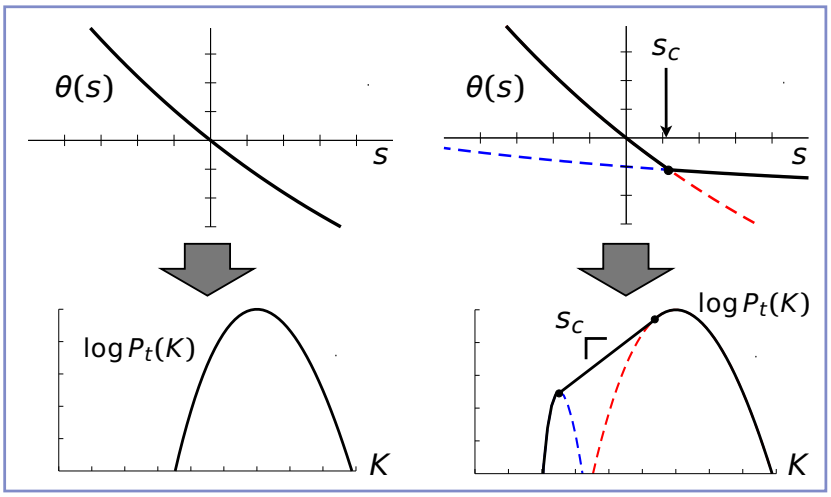

Figure 2.2: A smooth $\theta(s)$ implies that the distribution associated with the observable K is unimodal. In the right panels we see a trajectory transition point implies that the full distribution $P_t(K)$ has "fat-tails" where the contributions from each trajectory phase are visible.

the MGF. This s-biased probability vector's temporal evolution is not generated by the stochastic operator $\mathbb{W}$ but instead it evolves under a deformed Master equation with Master operator $\mathbb{W}_s$. Within this formalism the operator $e^{-\mathbb{W}_s}$ plays the role of a transfer operator, $Z_A(s,t)$ is similar to a boundary partition function and t is essentially the length of the "boundary". At $s = 0$ this transfer operator is a real square matrix with positive entries and in accordance with the *Perron-Frobenius* theorem (combined with the Krein-Rutman theorem) it possesses a unique largest real eigenvalue. Turning on s the uniqueness of this eigenvalue is no longer guaranteed and the spectral gap of $\mathbb{W}_s$ may close resulting in a trajectory phase transition.

Thus we have demonstrated that the trajectory phase properties may be examined by exact diagonalization of the deformed Master operator $\mathbb{W}_s$. How the s-bias deforms the Master operator depends on the type of observable A_t one is interested in. There are two general classifications of observable in this formalism,

observables that increment when the system changes configuration and observables which continuously vary in time, which we call type $\mathcal{A}$ and $\mathcal{B}$ observables respectively [8]. Beginning with type $\mathcal{A}$ observables, given K changes in configuration and increment $\alpha(\mathcal{C}, \mathcal{C}')$ between configuration changes, they are formally defined as

$$\mathcal{A} = \sum_{i=1}^{K} \alpha(\mathcal{C}_i, \mathcal{C}_{i+1}). \tag{2.30}$$

Now the probability of being in a state $\mathcal{C}$ at a time t where the dynamical observable takes a value $\mathcal{A}$ evolves under

$$\partial_t P(\mathcal{C}, \mathcal{A}, t) = \sum_{\mathcal{C}'} W(\mathcal{C}'|\mathcal{C}) P(\mathcal{C}', \mathcal{A} - \alpha(\mathcal{C}', \mathcal{C}), t) - r(\mathcal{C}) P(\mathcal{C}, A, t). \tag{2.31}$$

Laplace transforming Eq. (2.31) and collecting the probabilities $P(\mathcal{C}, s, t)$ into a vector it is easy to show

$$\begin{aligned} \partial_t |P(s,t)\rangle &= \mathbb{W}_s |P(s,t)\rangle, \\ \langle \mathcal{C}|\mathbb{W}_s|\mathcal{C}'\rangle &= W(\mathcal{C}'|\mathcal{C}) e^{-s\alpha(\mathcal{C}', \mathcal{C})} - r(\mathcal{C})\delta_{\mathcal{C},\mathcal{C}'}. \end{aligned} \tag{2.32}$$

Considering now type $\mathcal{B}$ observables they are related to configuration dependent observables $b(\mathcal{C})$ formally by

$$\mathcal{B} = \sum_{i=1}^{K} (t_{i+1} - t_i) b(\mathcal{C}) = \int_0^t dt' b(\mathcal{C}(t')), \tag{2.33}$$

where we take the time spent in $\mathcal{C}_i$ as $t_{i+1} - t_i$ and in the sum we define $t_1 = 0$ and $t_K = t$. The function $\mathcal{C}(t')$ which appears in the integral representation thus takes the value $\mathcal{C}_i$ for $t_i < t' < t_{i+1}$. Examining the probability $P(\mathcal{C}, \mathcal{B}, t)$ this obeys a modified Master equation

$$\partial_t P(\mathcal{C}, \mathcal{B}, t) = \sum_{\mathcal{C}'} W(\mathcal{C}'|\mathcal{C}) P(\mathcal{C}', \mathcal{B}, t) - r(\mathcal{C}) P(\mathcal{C}, \mathcal{B}, t) - b(\mathcal{C}) \partial_{\mathcal{B}} P(\mathcal{C}, \mathcal{B}, t). \tag{2.34}$$

Repeating the above analysis and Laplace transforming this distribution and writ-

ing the result in matrix notation we find

$$\begin{aligned}\partial_t|P(s,t)\rangle &= \mathbb{W}_s|P(s,t)\rangle,\\ \langle\mathcal{C}|\mathbb{W}_s|\mathcal{C}'\rangle &= W(\mathcal{C}'|\mathcal{C}) - (r(\mathcal{C}) + sb(\mathcal{C}))\delta_{\mathcal{C},\mathcal{C}'}.\end{aligned} \tag{2.35}$$

Both deformed Master equations, for type $\mathcal{A}$ and $\mathcal{B}$ observables, have the formal solution

$$|P(s,t)\rangle = e^{\mathbb{W}_s t}|P(0)\rangle, \tag{2.36}$$

where $|P(0)\rangle$ is the initial state of the system. Taking the overlap with flat state $\langle -|$ we find the time dependent MGF is given by

$$Z(s,t) = \langle -|e^{\mathbb{W}_s t}|P(0)\rangle. \tag{2.37}$$

Finally it is worth noting this deformed Master operator can be decomposed into its left $|L_n\rangle$ and right eigenvectors $|R_n\rangle$: $\mathbb{W}_s = \lambda_0|R_0\rangle\langle L_0| + \lambda_1|R_1\rangle\langle L_1| + \ldots$, where $\lambda_0 \geq \lambda_1 \geq \lambda_2 \ldots$ are the eigenvalues of the deformed Master operator and $\lambda_0 = \theta(s)$.

2.4 Open Quantum Systems

Another type of nonequilibrium dissipative system of interest are open quantum systems. Specifically we are interested in open systems which are described by a density matrix whose evolution is Markovian in nature and obeys a Lindblad Master equation [40, 85–87]. Analogous to classical Master equations the effects of the environment, whose degrees of freedom are traced out, is to input stochastic noise into the system's evolution. In this approach the system-environment interaction may be treated within an input-output formalism and this interaction leads to dissipation where the system may emit quanta into the bath over the course of

its evolution [39, 40, 87]. The observer may then perform measurements on the environment and describe the evolution of the system in terms of the time-records of these measurements. These time-records play the same role as the configurational changes in the last Section and define the trajectories of the open system. To define a thermodynamics of trajectories associated with these types of systems it is instructive to derive the Lindblad Master equation using quantum stochastic calculus [40] and that is where this Section begins.

2.4.1 Lindblad Master Equation

Modelling the environment as a continuum of Harmonic oscillators the Hamiltonian for the joint system plus environment is given by

$$H_{tot} = H_{sys} + H_{bath} + H_{int}, \tag{2.38}$$

where the bath Hamiltonian and interaction are

$$\begin{aligned} H_{bath} &= \int_0^\infty d\omega\ \omega b^\dagger(\omega) b(\omega), \\ H_{int} &= i\int_0^\infty d\omega\ \kappa(\omega)(L - L^\dagger)(b(\omega) + b^\dagger(\omega)). \end{aligned} \tag{2.39}$$

Firstly we recall that we have set $\hbar = 1$, and we treat the heat bath as being bosonic in nature and has raising (lowering) operators $b^\dagger(\omega)$ ($b(\omega)$) which obey the usual canonical commutation relations: $[b(\omega'), b^\dagger(\omega)] = \delta(\omega - \omega')$. For simplicity when describing the interaction we consider the case of the system connected to a single heat bath via a single set of operators (L and $L^\dagger$), however this derivation can be easily extended to multiple L operators and baths if desired. Moreover the coupling $\kappa(\omega)$ is also assumed to be smooth.

We begin by assuming that the bare system dipole L evolves as $L(t) = Le^{-i\omega_0 t}$, where ω_0 is the *resonance frequency* of the system. Therefore the system will be

coupled predominantly to frequencies centred about ω_0, hence we impose a cutoff in interaction Hamiltonian ϑ,

$$H_{int}^{\vartheta} = i\int_{\omega_0-\vartheta}^{\omega_0+\vartheta} d\omega\ \kappa(\omega)(L - L^{\dagger})(b(\omega) + b^{\dagger}(\omega)). \tag{2.40}$$

The cutoff is then assumed to be $\vartheta \ll \omega_0$, which implicitly assumes a separation of timescales where the bare system's frequency is much larger than the cutoff which is also much larger than the decay rates and the typical frequencies associated with the system's dynamics [40, 87]. Moreover the coupling within this regime is assumed to be constant in this frequency range $\kappa(\omega) = \sqrt{\gamma/2\pi}$.

Switching to the interaction picture the interaction Hamiltonian becomes

$$H_{int}^{\vartheta}(t) = i\int_{\omega_0-\vartheta}^{\omega_0+\vartheta} d\omega\sqrt{\frac{\gamma}{2\pi}}(Le^{-i\omega_0 t} - L^{\dagger}e^{i\omega_0 t})(b(\omega)e^{-i\omega t} + b^{\dagger}(\omega)e^{i\omega t}). \tag{2.41}$$

The separation of timescales implies that the terms $e^{\pm i(\omega+\omega_0)t}$ oscillate very rapidly over the relaxation time and will average to zero compared to $e^{\pm i(\omega-\omega_0)t}$. Thus we neglect these terms, making the so-called *rotating wave approximation* [40, 88], and obtain

$$H_{int}^{\vartheta}(t) = i\sqrt{\gamma}(b^{\vartheta}(t)^{\dagger}L - h.\ c.), \tag{2.42}$$

where

$$b^{\vartheta}(t) = \frac{1}{\sqrt{2\pi}}\int_{\omega_0-\vartheta}^{\omega_0+\vartheta} d\omega b(\omega)e^{-i(\omega-\omega_0)t}. \tag{2.43}$$

Under these approximations the time evolution operator $U^{\vartheta}(t)$ in the interaction picture and obeys

$$\frac{d}{dt}U^{\vartheta}(t) = -iH_{int}^{\vartheta}U^{\vartheta}(t), \tag{2.44}$$

where the separation in timescales implies that in the weak coupling limit $\gamma \ll 1$ the relaxation timescale is $\gg 1/\vartheta$. Therefore we may consider all frequencies about ω_0 to be relevant in describing the evolution and take $\vartheta \to \infty$ and rewrite $b^{\vartheta}(t) \to b(t)$. The effects of the bath fields can be described via an input-output

formalism where in effect one can consider the bath as driving the system with noise fields ($b^{(\dagger)}(t)$) which interact with the system at a time t. These input fields then "exit" the system and the output is given by the Heisenberg evolution of these fields under an appropriate stochastic evolution operator such as the one described below. In this weak coupling limit these noise terms obey the commutation relation $[b(t), b^\dagger(t')] = \delta(t - t')$ and so the bath effectively plays the role of **white noise**.

In typical quantum optical set ups there are many external laser fields in the vicinity of ω_0 which leads to a time dependent $H_{sys}(t)$, so it is often convenient to consider a reference frame where this explicit time dependence has been removed. This leads to a residual time independent H_{sys} appearing in the appearing in the Schrödinger equation, which we simply label as H for the remainder of this thesis. This all leads to a general evolution equation

$$\frac{d}{dt}U(t) = (-iH + \sqrt{\gamma}b^\dagger(t)L - \sqrt{\gamma}L^\dagger b(t))U(t). \tag{2.45}$$

This may be recast as a *stochastic Schrödinger equation*

$$dU(t) = (-iHdt + \sqrt{\gamma}dB^\dagger(t)L - \sqrt{\gamma}dB(t)L^\dagger)U(t), \tag{2.46}$$

where the increments are defined as

$$\begin{aligned} B^{(\dagger)}(t) &= \int_0^t b^{(\dagger)}(s)ds, \\ dB^{(\dagger)}(t) &= B^{(\dagger)}(t + dt) - B^{(\dagger)}(t), \\ dB(t) &= [dB^\dagger(t)]^\dagger. \end{aligned} \tag{2.47}$$

The stochastic equation in Eq. (2.46) is of Stratonovich form and hence captures the noncommutability of the system-bath operators in the Heisenberg representation as defined by H_{tot}. For ease of use this may be converted to a stochastic equation of Itō form, where the increments do commute with system observables, simply by manipulating Eq. (2.46) using the formal definitions of both types of

stochastic integrals [40]

$$\int_{t_0}^{t} g(t')dB(t') = \lim_{n\to\infty} \sum_{i=1}^{n} g(t_i)[B(t_{i+1}) - B(t_i)] \ (\mathbf{I}),$$
$$\int_{t_0}^{t} g(t')dB(t') = \lim_{n\to\infty} \sum_{i=1}^{n} \frac{g(t_i) + g(t_{i+1})}{2}[B(t_{i+1}) - B(t_i)] \ (\mathbf{S}). \tag{2.48}$$

Above (**I**/**S**) denotes Itō/Stratonovich integrals respectively and we can see the stochastic integrals in the Itō formalism are evaluated strictly in the past, hence the system operator $g(t')$ commutes with the increment. This leads to the Itō stochastic Schrödinger equation

$$dU(t) = ((-iH - \frac{1}{2}\gamma L^\dagger L)\ dt + \sqrt{\gamma}dB^\dagger(t)L - \sqrt{\gamma}dB(t)L^\dagger)U(t), \tag{2.49}$$

where we will consider the quantity $H - i\frac{\gamma}{2}L^\dagger L$ as an effective non-Hermitian Hamiltonian H_{eff}. Now as with regular Itō stochastic calculus the quantum stochastic calculus does not obey the regular rules of calculus and one must define an associated Itō table to describe how the increments behave. For simplicity in this instance we assume the bath begins in a vacuum state $b(t)|\text{vac}\rangle = 0$, using the definition of the increments in Eq. (2.47) it can be shown the only non-zero combination of $dB(t)$ and $dB^\dagger(t)$ is

$$\begin{aligned} dB(t)dB^\dagger(t) &= dt, \\ dB^\dagger(t)dB(t) &= 0, \\ [dB(t)]^2 &= [dB^\dagger(t)]^2 = 0. \end{aligned} \tag{2.50}$$

From this brief journey into quantum stochastics we are ready to derive the Lindblad Master equation. Initializing the system in a pure state described by the total density operator $\rho(t) = |\Psi(t)\rangle\langle\Psi(t)|$, using the *stochastic Schrödinger equation* it is simple to derive the equation of motion for the stochastic density operator which

describes the evolution of the system plus heat bath

$$\begin{aligned} d\rho(t) &\equiv \rho(t+dt) - \rho(t) \\ &= U(t+dt,t)\rho(t)U^\dagger(t+dt,t) - \rho(t) \\ &= -i(H_{eff}\rho(t) - \rho(t)H_{eff})\ dt + \gamma dB^\dagger(t)L\rho(t)L^\dagger dB(t) \qquad (2.51) \\ &+ \sqrt{\gamma}dB^\dagger L\rho(t) + \rho(t)\sqrt{\gamma}dB(t)L^\dagger. \qquad (2.52) \end{aligned}$$

Here the evolution operator $U(t',t)$ evolves the state from time $t \to t'$. Taking the trace over the bath degrees of freedom and using the Itō rules from Eq. (2.50) we readily arrive at the Lindblad Master equation [85, 86]

$$\dot{\rho}_{sys} = -i[H,\rho_{sys}] + \sum_i \gamma_i L_i \rho_{sys} L_i^\dagger - \frac{\gamma_i}{2}\{L_i^\dagger L_i, \rho_{sys}\}, \qquad (2.53)$$

where ρ_{sys} now denotes the system density matrix, we have also generalized to many dissipation channels and $\{\bullet,\bullet\}$ denotes the anti-commutator. This equation consists of two parts, the non-unitary evolution defined by H_{eff} which describes the "no-jump" evolution of the system and the recycling terms $L_i\rho_{sys}L_i^\dagger$ which capture the emission of quanta from the system to the bath.

The similarity between the Lindblad Master equation and classical Master equation described in the previous Section does not end with their underlying physics being stochastic in nature. The Lindblad Master equation may also be considered *Markovian* in the sense that the correlation time of the bath is much shorter than that of the system and the evolution operator $V(t',t)$ has the semi-group property

$$V(t,t_1)V(t_1,t_0) = V(t,t_0). \qquad (2.54)$$

Furthermore the dynamics generated by this Master equation can be decomposed into constituent trajectories. However rather than being a history of configurational changes it is continuous measurements which describe the trajectories. This *unravelling* [40, 87] depends on the choice of observable measured but in all cases

their contributions can be combined to determine $\rho_{sys}(t)$ for the system. These measurements define the **trajectories** of these open quantum systems [29, 39, 40].

2.4.2 Thermodynamics of Quantum Jump Trajectories

Perhaps the most natural observable to analyze in a dissipative system is the time-record of emissions into the bath [29, 30, 84]. To examine the full distribution of this observable we resort to a **quantum version** of the *s-ensemble* and begin by defining the total number of photons counted up to a time t,

$$K(t) \equiv \int_0^t dt' \; b^\dagger(t')b(t'). \tag{2.55}$$

Here $K(t)$ is the counting process whose generating function will define the s-ensemble in this system. To examine the dynamical behaviour of this counting process it is necessary to consider the stochastic increment $dK(t)$ and its associated Itō rules. This operator has eigenvalues which are the number of photons counted in the interval $(t, t+dt]$ and has the associated Itō table

$$\begin{aligned} dK(t)dK(t) &= dK(t), \\ dB(t)dK(t) &= dB(t), \qquad (2.56) \\ dK(t)dB^\dagger(t) &= dB^\dagger(t). \qquad (2.57) \end{aligned}$$

and all other products involving $dK(t)$ vanish. These rules allow us to redefine the increment as $dK(t) \equiv dB^\dagger(t)dB(t)/dt$ and only use the vacuum Itō rules defined in Eq. (2.50). With these rules we consider the dynamical evolution of the associated generating function of this process. Before this there is a small subtlety to clarify, in the input-output picture the increments considered so far describe how the bath changes upon interacting with the system at a time t. This input field would then

exit the system and be detected by an external detector, therefore one should really examine the statistics of the *output* field. A detailed discussion of this may be found in Ref. [40]. Here we give the main result

$$\begin{aligned}\tilde{V}_t[s] &= \exp(-s\int_0^t dK(t')),\\ Z(s,t) &= \mathrm{Tr}_{sys}\mathrm{Tr}_B(\tilde{V}_t[s]\rho(t)) = \mathrm{Tr}_{sys}(\rho_s(t)),\end{aligned} \tag{2.58}$$

where ρ_s is the s-biased system density matrix, Tr_B and $Z(s,t)$ denote the trace over the bath degrees of freedom and the *dynamical partition sum* of the quantum jump trajectories respectively. In the long time limit this generating function will obey a LD principle [46] and so this process will have an associated dynamical free energy $\theta(s)$. From Eq. (2.58) the stochastic increment of the characteristic operator $\tilde{V}_t[s]$ can be deduced by expanding the exponential and using the Itō rules to obtain

$$d\tilde{V}_t[s] = \tilde{V}_t[s](e^{-s}-1)dK(t). \tag{2.59}$$

Combining this with the stochastic density operator increment (see Eq. (2.51)) and the vacuum Itō rules one can readily trace out the bath degrees of freedom to find

$$\begin{aligned}\dot{\rho}_s &= \mathbb{W}_s(\rho_s)\\ &= -i[H,\rho_s] + \sum_i e^{-s}\gamma_i L_i\rho_s L_i^\dagger - \frac{\gamma_i}{2}\{L_i^\dagger L_i,\rho_s\}.\end{aligned} \tag{2.60}$$

Here the deformed Master operator $\mathbb{W}_s$ has a largest real eigenvalue which once again corresponds to $\theta(s)$ [29]. Above we are examining the total emission statistics but depending on which jump process statistics one wishes to examine, one may add/remove factors of e^{-s} in front of the appropriate recycling terms. The trajectory phases of this process are characterized by the 1st and 2nd derivatives of $\theta(s)$ which are referred to as the **activity** and **dynamical susceptibility**

respectively. Positive s biases the system towards inactive trajectories while negative s probes ensembles of active trajectories. Here, again, singular features in $\theta(s)$ mark trajectory phase transitions and using the Legendre transform one may obtain the probability of having measured K photons in a time t,

$$P_t(K) = \mathrm{Tr}_{sys}(\rho^K_{sys}(t)) \approx e^{-t\phi(K/t)}, \tag{2.61}$$

where ρ^K_{sys} is the system density matrix projected onto the subspace where K events have occurred [29, 30, 54, 84].

2.4.3 Mapping to an Equilibrium Phase Transition

The dynamics described by the Lindblad Master equation, see Eq. (2.53), generates a matrix product state (MPS) [89, 90] on the environmental degrees of freedom [91–93]. Using this fact, it was later shown that the quantum jump trajectory phases can be mapped to the ground state phases of a 1d spin chain [94]. To see this we consider the evolution of the density matrix ρ over a short time interval δt using a Kraus map description:

$$\rho(t+\delta t) = K_0\rho(t)K_0 + \sum_{i\neq 0} K_i\rho(t)K_i^\dagger. \tag{2.62}$$

The Kraus operators in Eq. (2.62) are $K_0 = e^{-i\delta t H}\sqrt{1-\delta t\sum_i \gamma_i L_i^\dagger L_i}$ and $K_i = e^{-i\delta t H}\sqrt{\gamma_i \delta t}L_i$. The first Kraus operator K_0 describes the nonunitary no jump evolution while $K_{i\neq 0}$ represents the quantum jump associated with the Lindblad operator L_i. Applying the Kraus map repeatedly generates the dynamics of the Lindblad Master equation and produces a quantum jump trajectory. Initializing the system in a state $|i\rangle$ the probability of a trajectory $\{n_1, n_2, \ldots, n_M\}$ (here n_i

represents the jump channel at step i, i. e. L_{n_i}) after M steps is

$$p_{n_1,n_2,\ldots,n_M} = \sum_f |\langle f|K_{n_M}\ldots K_{n_2}K_{n_1}|i\rangle|^2. \tag{2.63}$$

The sum in Eq. (2.63) is over a basis of final system states $\{|f\rangle\}$. For specificity we consider a dissipative open system with N jump operators. The jump trajectory probabilities can be encoded in a MPS which is generated by letting the system interact sequentially with a spin chain of $(N+1)$-dimensional spins [91–94]. The quantum state, of the system+spin chain, after M steps is then given by

$$|\Psi\rangle = \sum_f |f\rangle \otimes |\psi(f)\rangle, \tag{2.64}$$

where $|\psi(f)\rangle$ is the unnormalized MPS:

$$|\psi(f)\rangle = \sum_{n_m,\ldots n_2,n_1=0}^{N} \langle f|K_{n_M}\ldots K_{n_1}|i\rangle|n_1,\ldots n_M\rangle. \tag{2.65}$$

From this we see $|\Psi\rangle$ encodes the entire ensemble of quantum jump trajectories where each basis state $|n_1\ldots n_M\rangle$ represents a quantum jump trajectory and the associated amplitude is directly related to $p_{n_1,\ldots,n_M}$. This formal connection illustrates that s-ensemble trajectory phase transitions, which are encoded in the temporal correlations of quantum jumps, will become visible in the spatial correlations of the MPS spin chain [94].

2.5 Closed Quantum Systems

The preceding Sections focussed on stochastic systems, both quantum and classical, and a thermodynamic approach to the relevant stochastic variables in these nonequilibrium settings. This thermodynamic approach to the generating functions emerged in the classical community from the works of Ruelle [4] and others [6–8, 13] before being extended to the open quantum system case [29, 30].

Casting this approach in the context of a *closed quantum system* is difficult as observables are not stochastic variables and a Law of Large Numbers may not exist. The key observation is that the observables of interest in the previous cases are **time-integrated** along the trajectory. We therefore may ask about the generating functions of such time-integrated observables and although a LD principle may not apply we may still search for singular features in an appropriately scaled CGF [56, 72]. The generating functions of such observables may be calculated using methods of **full counting statistics (FCS)** [41, 42, 95–100].

This Section covers two separate topics: the first part provides an overview of how to construct these generating functions for a general quantum mechanical observable [41, 97]. The remainder describes a nonequilibrium protocol known as a quantum quench, and how LD theory emerges in the statistics of the work done during this protocol. At finite times singular features may emerge in the generating function of the work done marking a new type of **dynamical phase transition (DPT)**.

2.5.1 Time-Integrated observables

In classical stochastic systems and open quantum systems there is a well-defined probability distribution associated with each variable that can be measured. Such a probabilistic description is not possible in quantum mechanics, hence one can not construct a classical phase space which is directly linked to the wavefunction of the system [40, 97]. Despite this one can consider a *quasi-probability* distribution known as the **Wigner function** [40] which depends on a *position* coordinate x and *conjugate momentum* p. Although this looks similar to the phase space picture of equilibrium statistical mechanics it may take negative values and thus may not be considered a true probability distribution. Another concern when trying to

define the MGF of time-integrated observables is causality. These observables do not depend locally on time and time-ordering is crucial to avoid problems with causality, these problems were tackled by Nazarov et al. [97]; here we outline the main result and relate it to the Wigner function of an ancillary measurement device.

A closed quantum system's evolution is determined by its Hamiltonian H. We are interested in the moments of a time-integrated observable

$$Q_t \equiv \int^t q(t')dt', \tag{2.66}$$

where $q(t')$ is the observable of interest written in the Heisenberg representation. The MGF of this observable is constructed from a related non-Hermitian operator and its associated non-unitary evolution operator $T_t(s)$ which are defined by the equations [56, 64, 72]

$$T_t(s) \equiv e^{-itH_s},\ H_s \equiv H - \frac{is}{2}q. \tag{2.67}$$

From these definitions the MGF of Q_t is given by

$$Z(s,t) = \langle T_t^\dagger(s)T_t(s)\rangle = \mathrm{Tr}(T_t(s)\rho_{sys}T_t^\dagger(s)), \tag{2.68}$$

where ρ_{sys} is the system of interest's density matrix. To see this is the correct MGF we switch to the interaction picture by setting $T_t(s) \to U_t^\dagger T_t(s) U_t$ where U_t is the unitary evolution operator generated by H. In this reference frame one readily sees

$$Z(s,t) = \langle \overrightarrow{\mathcal{T}} e^{-\frac{s}{2}\int^t q(t')dt'} \overleftarrow{\mathcal{T}} e^{-\frac{s}{2}\int^t q(t')dt'}\rangle, \tag{2.69}$$

where $\overleftarrow{\mathcal{T}}$ ($\overrightarrow{\mathcal{T}}$) denotes time ordering (anti-time ordering). These operators take care of causality and the moments of Q_t are generated through the derivatives of $Z(s,t)$, $\langle Q_t^n\rangle = (-1)^n\partial_s^n Z(s,t)|_{s\to 0}$. The logarithm of the MGF defines the cumulant generating function, $\Theta(s,t) \equiv \log Z(s,t)$. The moments and cumulants

generated by these functions are constructed from all possible time orderings of the operator $q(t')$.

These functions form a definition of the full counting statistics (FCS) of this observable. However in contrast to usual definitions of FCS we take the "counting field" s to be real [56]. Adapting our approach from earlier we examine the analytic properties of the CGF away from $s = 0$ using an appropriately scaled CGF

$$\theta(s) = \lim_{N\to\infty, t\to\infty} \frac{\Theta(s,t)}{Nt}, \tag{2.70}$$

where N represents the system size. Although it seems the MGF obeys an LD principle this is not the case, *a priori* there is no well defined probability distribution associated with Q_t. To see if $\theta(s)$ is indeed an LD function we must examine how $Z(s,t)$ is related to a measurement scheme, if any.

We now consider a detector with conjugate position and momenta coordinates denoted by the operators x and p respectively [97]. Connecting this to the system such that the detector's position couples directly to q we obtain a new *system plus detector* Hamiltonian

$$H_{total} = H - xq. \tag{2.71}$$

From this the Heisenberg equations of motion for the detector's conjugate momenta are directly related to Q_t via

$$\dot{p}(t) = q. \tag{2.72}$$

Considering the full system plus ancilla density matrix, where the detector is initialized in the state $\rho^i_{anc.}$, to find the ancilla density matrix at a time t we evolve it under H_{total} and trace over the system degrees of freedom

$$\rho^f_{anc.}(x^+, x^-) = \mathrm{Tr}_{sys}\langle x^+|e^{-iH_{total}t}\rho_{sys}\rho^i_{anc.}e^{iH_{total}t}|x^-\rangle, \tag{2.73}$$

where $|x^{\pm}\rangle$ are position basis states for the detector[3] Setting $x^{\pm} = x \pm \frac{z}{2}$ then this equation may be rewritten as

$$\rho^f_{anc.}(x+\frac{z}{2}, x-\frac{z}{2}) = Z(x+\frac{z}{2}, x-\frac{z}{2}, t)\rho^i_{anc.}(x+\frac{z}{2}, x-\frac{z}{2}) \ , \tag{2.74}$$
$$Z(x+\frac{z}{2}, x-\frac{z}{2}, t) = \mathrm{Tr}_{sys.}\Big(e^{-i(H-x-\frac{z}{2})t}\rho_{sys}e^{i(H-x+\frac{z}{2})t}\Big).$$

The Wigner representation of the detector density matrix is simply its Fourier transform [40]

$$\rho(x,p) = \int \frac{dz}{2\pi} e^{-ipz}\rho(x+\frac{z}{2}, x-\frac{z}{2}), \tag{2.75}$$

this *quasi-phase space* representation of the density matrix allows one to consider the Wigner function $\rho(x,p)$ as being a quasi-probability distribution. It may not be considered a real probability distribution as it can be negative due to interference effects arising from the quantum mechanical nature of the system. Fourier transforming Eq. (2.74) and applying the convolution theorem the MGF is related to the propagator connecting the initial and final states of the detector:

$$\rho^f_{anc.} = \int \ dp_1 \ P_t(x, p-p_1)\rho^i_{anc.}(x, p_1), \tag{2.76}$$

$$Z(x+\frac{z}{2}, x-\frac{z}{2}, t) = \int \ dp \ e^{ipz} \ P_t(x,p). \tag{2.77}$$

[3]It is worth noting that this formalism may be recast in the language of Keldysh field theory. In this language the MGF $Z(x+\frac{z}{2}, x-\frac{z}{2}, t)$ is the Keldysh partition function where the field z couples to a purely quantum vector field. Setting $z = is$ one can see that the effect of s is to exponentially suppress or enhance the contribution of this vector field to the MGF. This is intimately linked with the existence (or lack thereof) of a LD principle. If the MGF in this field theoretic setting is well described by a saddle point approximation then a LD principle will exist. The action of this field theory is usually extensive in system size N, i. e. the quantum fluctuations are exponentially suppressed with system size and one can approximate the MGF as $\exp(N\Theta(s,t))$, it may not be extensive in t. For finite s the quantum fluctuations are suppressed with increasing time and so at long times a further saddle point approximation may be made, i. e. $\Theta(s,t) \approx t\theta(s)$, and we obtain a LD function for $s \neq 0$.

Setting $x = 0$ and analytically continuing z to the imaginary axis such that $z = is$ we see that the MGF as defined in FCS is essentially the bilateral Laplace transform of the propagator $P_t(0, p)$. It is clear from Eq. (2.76) that as the Wigner function of the detector is not necessarily positive then neither is the positivity of $P_t(x, p)$ guaranteed. Therefore although the MGF is well-defined in general for the closed system case an associated probability distribution is not. An important case is when $P_t(x, p)$ is independent of x, in this instance one can integrate Eq. (2.76) over x and can consider the integrated Wigner function as the probability distribution for the detector to have a momentum p and the propagator is the probability of the momentum shift between the initial and final state of the detector [97].

2.5.2 Quantum Quench-Work done and Dynamical Phase Transitions

In the study of nonequilibrium dynamics of closed quantum systems one of the most common nonequilibrium protocols implemented is known as a *quantum quench* [74, 76–78]. The protocol is as follows: the system is first initialized in the ground state $|0_{\lambda_0}\rangle$ of a Hamiltonian $H(\lambda_0)$ which depends on the tunable global parameter λ_0. This global parameter is then instantaneously changed from $\lambda_0 \to \lambda_\tau$ and the ground state is allowed to evolve under the new Hamiltonian $H(\lambda_\tau)$.

The properties of this protocol have been studied in detail, such studies focussed on: thermalization, the emergence of a generalized Gibbs ensemble in the long time limit, statistics of the work done and universality, singularities in the return probability etc. The remainder of this Section will recap some important results and background relating to the work done and return amplitude resulting from this protocol [75].

Consider a closed quantum system with N degrees of freedom, such that the internal energy of the system is extensive with N. On performing a quench the work done (W_N) is determined by the initial state ($|0_{\lambda_0}\rangle$) and the eigenvalues ($E^n_{\lambda_\tau}$) and eigenvectors ($|\psi^n_{\lambda_\tau}\rangle$) of the final Hamiltonian $H(\lambda_\tau)$. The work done can be calculated from a two point measurement scheme, whereby we first measure the energy of the initial state, then evolve the system under the quench dynamics and measure the energy of the final state. Within this scheme the work done is a stochastic variable with probability density

$$P(W_N) = \sum_{n\geq 0} |\langle\psi^n_{\lambda_\tau}|0_{\lambda_0}\rangle|^2 \delta(W_N - (E^n_{\lambda_\tau} - E^0_{\lambda_0})). \tag{2.78}$$

The Laplace transform of this variable defines the generating function of the work done, $G(s) = \langle 0_{\lambda_0}|e^{-s(H(\lambda_\tau)-H(\lambda_0))}|0_{\lambda_0}\rangle$, and in the large N limit this function takes a large deviation form

$$G(s) \asymp e^{-Nf(s)}, \tag{2.79}$$

where the LD function is directly related to the return probability of the system and singularities in this function may mark dynamical phase transitions (DPTs) [64, 79, 81].

To establish this connection we consider the time evolved quenched state $|\psi(t)\rangle = e^{-iH(\lambda_\tau)t}|0_{\lambda_0}\rangle$; the return probability which defines the probability of the state returning to the initial state after a time t is simply [73]

$$\begin{aligned} L(t) &= |\langle\psi(t)|0_{\lambda_0}\rangle|^2 \\ &= |\langle 0_{\lambda_0}|e^{-iH(\lambda_\tau)t}|0_{\lambda_0}\rangle|^2 = |G(it)|^2. \end{aligned} \tag{2.80}$$

In the large N limit $L(t)$ also obeys a large deviation principle with a large deviation function $l(t) = 2\mathrm{Re}(f(it))$. This establishes the connection between the CGF of the work done and the return probability. Analogous to thermodynamics $l(t)$ would play the role of a free energy and so singular features in this LD function

mark a new type of nonequilibrium phase transitions known as *dynamical phase transitions* (**DPTs**) [64, 79–81]. However, in contrast to both equilibrium statistical physics and trajectory phase transitions where the transitions are driven by either a thermodynamic or "counting field", here it is the nonequilibrium temporal evolution which drives the system across these new phase transitions. To see how singular features can emerge in this LD function we consider the return amplitude under the framework of the Lee-Yang (Fisher zeros) theory of equilibrium phase transitions.

Formally the return amplitude is directly related to the boundary partition function

$$Z(L) = \langle \psi_a | e^{-LH} | \psi_b \rangle. \tag{2.81}$$

This quantity is simply the MGF of the work done but with different boundary conditions. Taking identical boundaries $|\psi_{a,b}\rangle = |0_{\lambda_0}\rangle$ and analytically continuing the boundary length L to the complex plane, $L \to \beta \in \mathbb{C}$, we readily see if $\beta = it$ the analytically continued boundary partition function is the return amplitude. This partition function has Fisher zeros [101] which lie in the complex β plane, these zeros may lie on the real time axis (equivalent to the imaginary L axis) when the quenched state $|\psi(t)\rangle$ is orthogonal to the initial state. In the thermodynamic limit these zeros coalesce and form a transition line which may intersect the real time axis. This results in the emergence of nonanalyticities in the rate function $l(t)$ which are the so-called DPTs. Figure 2.3 shows the emergence of DPTs in the 1d transverse field Ising model (TFIM) [55] when quenched across its quantum critical point [79].

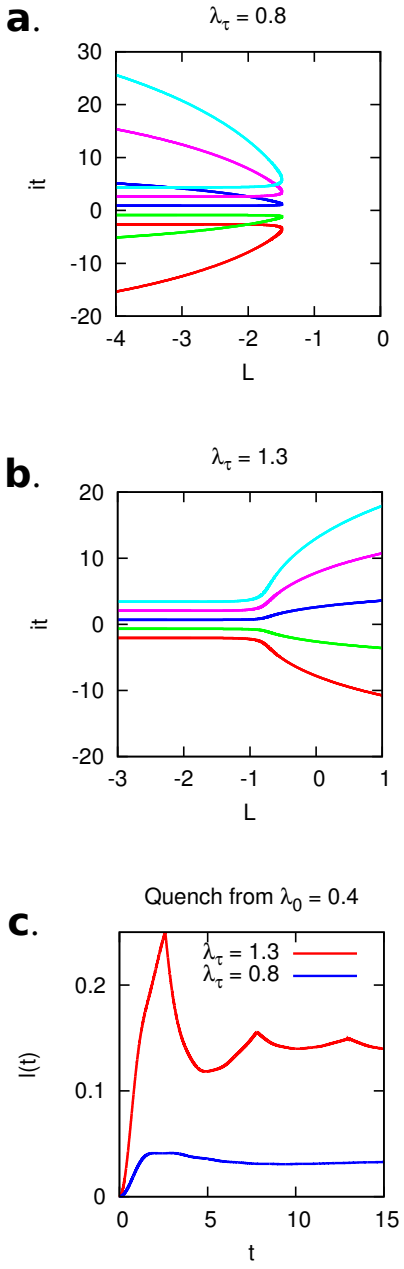

Figure 2.3: Studying the ground state of the TFIM under a quench in the transverse field from $\lambda_0 = 0.4 \rightarrow \lambda_\tau$. (a) We see the Fisher zeros for $\lambda_\tau = 0.8$ do not cross the real time axis. (b) Quenching across the critical point ($\lambda_c = 1$) the zeros cross the real time axis leading to the singular points manifesting in $l(t)$ as shown in (c).

3. Dynamical Lee-Yang zeros of the 1d Glauber-Ising Chain

The formalism of the previous Chapter highlights the generality of the thermodynamic formalism and similarities between nonequilibrium stochastic problems and equilibrium statistical mechanics. There is, however, a crucial difference between the latter two problems: to probe a phase transition in equilibrium statistical physics one simply has to tune an appropriate driving field. Within the s-ensemble formalism the trajectory phase transition is driven by the "counting field", s, which is often not simply related to physically accessible parameters [6, 7, 9, 10, 34, 35, 102, 103]. Furthermore these trajectory phase transitions may only be observed in the long time limit, i. e. at times much larger than the typical relaxation timescales of the problem, which are often beyond the reach of experiment or simulation in practice.

Recently a potential solution [53] to the above problems was proposed based on a generalization of the Lee-Yang theory of phase transitions to these dynamical systems [51, 52, 104–106]. Specifically a formal connection between the zeros of the MGF of the dynamical observable of interest with the short time behaviour of its high order cumulants was established. In particular it was shown that one can infer the value of the s-field where a trajectory phase transition occurs from

the motion of these dynamical Lee-Yang zeros. This formalism was applied to two kinetically constrained models of glass formers, the Frederickson-Andersen model [107] and the hard East model [27], which both possess a first order phase transition at $s = 0$ in the trajectories of the activity (e. g. the number of spin-flips per unit time).

In this Chapter we begin by recapping the connection between these dynamical Lee-Yang zeros and the high order cumulants [53, 100, 108, 109] of the desired observable. We will then apply this method to another many-body stochastic system which, unlike the previous models, possesses a continuum of 2nd order trajectory phase transitions in the complex s plane. We focus on the example of the 1d Glauber-Ising chain [110] and examine the high order cumulants of the time-integrated energy [13, 83]. This model, along with the appropriate dynamical observable, admits an analytic treatment and so we do not need to rely on numerical simulation to extract the high order cumulants, as was the case for the KCM study. This Chapter is organized as follows, in Sec. 3.1 we describe the Lee-Yang zero method reported in Ref. [53]. We then in Sec. 3.2 discuss the Glauber-Ising chain and calculate the full time dependent MGF of the time-integrated energy before examining the trajectory phase diagram of this system in Sec. 3.3. In Sec. 3.4 we show how one may infer the full trajectory phase diagram using the mode-resolved high order cumulants of the time-integrated energy. Finally in Sec. 3.5 we present a full analysis without using the mode-resolved cumulants and, at low temperatures, demonstrate that the dominant singularities associated with the long wavelength modes may be extracted. However, at higher temperatures other modes play a role in the fluctuation properties of the system and it becomes difficult to extract the associated trajectory transition points [83].

3.1 Lee-Yang Zeros Method

Close to a trajectory transition point (s_c) the MGF is dominated by two large nearly degenerate eigenvalues of the deformed Master operator, $\lambda_0(s)$ and $\lambda_1(s)$. When $s \simeq s_c$ the MGF in Eq. (2.37), of a dynamical observable $\mathcal{B}_t$, may be approximated by these two largest eigenvalues

$$Z(s,t) \simeq c_0(s)e^{-\lambda_0(s)t} + c_1(s)e^{-\lambda_1(s)t}, \tag{3.1}$$

where the initial conditions of the system are stored in the coefficients $c_0(s)$ and $c_1(s)$. This approximation is valid close to equilibrium where the contributions from all the other eigenvalues are small and can be neglected. Within this approximation we find that the zeros of the MGF are given by

$$\lambda_0(s) = \lambda_1(s) + \frac{\log[c_0(s)/c_1(s)] + i(2j+1)\pi}{t}, \tag{3.2}$$

where j is an integer. In the long time limit, $t \to \infty$, this equation reduces to $\lambda_0(s) = \lambda_1(s)$ thus showing that the zeros of the MGF will converge to the trajectory transition point $s = s_c$. The task now is to extract the motion of these zeros directly from the high order cumulants of the dynamical observable of interest. To reveal the connection between these two we express the MGF in terms of Lee-Yang zeros using the Hadamard factorization theorem,

$$Z(s,t) = e^{a(t)s} \prod_j \frac{s_j(t) - s}{s_j(t)}. \tag{3.3}$$

Here $s_j(t)$ is the jth zero of the MGF at a time t and $a(t)$ is a real function which is independent of the trajectory bias s. Furthermore as the MGF is a real function of real s these Lee-Yang zeros must appear as complex conjugate pairs at all times. Using this factorization we readily find the time dependent CGF

$$\Theta(s,t) = a(t)s + \sum_j \{\log[s_j(t) - s] - \log[s_j(t)]\}, \tag{3.4}$$

differentiating this function with respect to $-s$ we see the cumulants of our observable $\mathcal{B}_t$ (as defined in Eq. (2.33)) are given by

$$\langle\langle \mathcal{B}_t^n \rangle\rangle = a(t)\delta_{n,1} + (-1)^{(n-1)}(n-1)! \sum_j \frac{e^{-in\text{arg}[s_j(t)]}}{|s_j(t)|^n}. \tag{3.5}$$

Here we use the polar coordinate notation $s_j(t) = |s_j(t)|e^{i\text{arg}[s_j(t)]}$. In accordance with Darboux's theorem [111, 112] the zeros of the MGF correspond to logarithmic singularities in the CGF which, in turn, determine the high order derivatives (i. e. the cumulants) of the CGF. For large n the summation in Eq. (3.5) is dominated by the leading Lee-Yang zero pair closest to the origin. Denoting this pair $s_0(t)$ and $s_0^*(t)$, we may approximate the sum in Eq. (3.5) as [53, 100, 108, 109, 112, 113]

$$\langle\langle \mathcal{B}_t^n \rangle\rangle \approx (-1)^{(n-1)}(n-1)! \frac{2\cos[n\text{arg}s_0(t)]}{|s_0(t)|^n}. \tag{3.6}$$

From this we see that the cumulants grow factorially with the cumulant order n and oscillate as function of any parameter which changes the polar angle of the leading Lee-Yang zeros. This behaviour has been observed experimentally in the high order cumulants of the charge transferred through a quantum dot [100, 114, 115]. Furthermore we may invert the relationship and determine the position of the leading Lee-Yang zeros directly from the cumulants via the matrix equation [53, 108, 109, 116]

$$\begin{bmatrix} 1 & -\frac{\kappa_n^{(+)}}{n} \\ 1 & -\frac{\kappa_{n+1}^{(+)}}{n+1} \end{bmatrix} \cdot \begin{bmatrix} -(s_0 + s_0^*) \\ |s_0|^2 \end{bmatrix} = \begin{bmatrix} (n-1)\kappa_n^{(-)} \\ n\kappa_{n+1}^{(-)} \end{bmatrix}, \tag{3.7}$$

where given the ratio of consecutive cumulants, $\kappa_n^{(\pm)}(t) \equiv \langle\langle \mathcal{B}_t^{n\pm1} \rangle\rangle / \langle\langle \mathcal{B}_t^n \rangle\rangle$, one may readily solve for the zeros. Thus by measuring the finite time cumulants of the unbiased $s = 0$ dynamics, either through experiment or simulation, one may infer the location of the leading Lee-Yang zero pair as they move towards the location of a trajectory phase transition with increasing time [53, 83]. We will apply this

approach to a model which has a whole curve of trajectory phase transitions, the 1d Glauber-Ising chain.

3.2 Glauber-Ising Chain

The 1d Glauber-Ising chain consists of N classical spins, where the spin at site i is $S_i = \pm 1$, subject to periodic boundary conditions and whose total energy is given by

$$E = -\frac{J}{2}\sum_i S_i S_{i+1}. \tag{3.8}$$

This interaction is ferromagnetic when $J > 0$ and the sum is taken over all sites in the periodic chain. The system evolves under Glauber stochastic dynamics where the rate for flipping the spin at site i is given by

$$\Gamma_i = \frac{\Gamma}{1 + e^{\beta \Delta E_i}}, \tag{3.9}$$

where β is simply the inverse temperature and $\Delta E_i = J S_i (S_{i-1} + S_{i+1})$ is the energy cost to flip the spin. The overall spin flip rate, that is the spin flip rate at $\beta = -\infty$, is set by Γ. This stochastic dynamics obeys detailed balance and in the long time limit converges to a stationary state described by the Boltzmann distribution. While this equilibrium distribution is quite simple, the dynamical relaxation to this stationary regime is complex and may show very rich behaviour. In our investigation we focus on a type $\mathcal{B}$ dynamical observable the time-integrated energy, which is simply related to the time dependent energy function $E(t)$ by

$$\mathcal{E}_t = \int^t dt' E(t'). \tag{3.10}$$

To examine the dynamical fluctuations of $\mathcal{E}_t$ we evaluate its time dependent MGF. To do this we proceed along the analytic route described in Ref. [13] and introduce

the domain wall variables

$$n_i = \frac{1}{2}(1 - S_i S_{i+1}), \tag{3.11}$$

these variables correspond to the number of domain walls ($n_i = 0, 1$) between the sites i and $i + 1$. Using these variables the energy function simplifies to

$$E = J \sum_i (n_i - 1/2). \tag{3.12}$$

Furthermore we may express the Master operator $\mathbb{W}$ describing the stochastic Glauber dynamics of this system in terms of Pauli spin matrices by defining

$$\sigma_i^z = 2(n_i - 1/2), \tag{3.13}$$

together with the usual spin raising (σ_i^+) and lowering operators (σ_i^-). Within this spin representation the presence of a domain wall corresponds to a spin-up state and the absence of a wall corresponds to a spin-down state. Moreover this representation is useful as the energy function is now $E = \frac{J}{2} \sum_i \sigma_i^z$ and the energy cost to flip a spin also has a simple functional form $\Delta E_i = -J(\sigma_i^z + \sigma_{i-1}^z)$. The generator for the stochastic time evolution may then be expressed in terms of spin operators [13, 117]:

$$\mathbb{W} = \frac{\Gamma}{2} \sum_i \left(2\sigma_i^+ \sigma_{i+1}^- + \gamma \sigma_i^- \sigma_{i+1}^- + \lambda \sigma_i^+ \sigma_{i+1}^+ + (\lambda - 1)\sigma_i^z - 1 \right), \tag{3.14}$$

where we've introduced the parameters $\gamma = 2/(1 + e^{-2J\beta})$ and $\lambda = 2 - \gamma$. From Eq. (2.35) the biased dynamics of the time-integrated energy are then generated by $\mathbb{W}_s = \mathbb{W} - s\frac{J}{2} \sum_i \sigma_i^z$.

We also note that the LD statistics for the anti-ferromagnetic Glauber-Ising chain ($J \leftrightarrow -J$) may be obtained by simultaneously changing the sign of s and β. The cumulants of the time integrated energy are measured in units of energy and time, that is J and Γ^{-1}, and for the remainder of this Chapter we set $J = 1$ and

$\Gamma^{-1} = 1$. Furthermore, as the dynamical observable of interest is time-reversal symmetric (see Appendix A) the deformed Master operator may be symmetrized using a similarity transform to obtain the non-Hermitian matrix

$$\mathbb{H}_s = e^{\beta E/2}\mathbb{W}_s e^{-\beta E/2}, \tag{3.15}$$

where E is the diagonal energy operator. This matrix $\mathbb{H}_s$ is non-Hermitian as we explicitly consider complex s biases, and it takes the form of a non-Hermitian Hamiltonian for a quantum spin chain

$$\begin{aligned}\mathbb{H}_s = \frac{1}{2}\sum_i \Big(&\frac{1+\sqrt{\gamma\lambda}}{2}\sigma_i^x\sigma_{i+1}^x + \frac{1-\sqrt{\gamma\lambda}}{2}\sigma_i^y\sigma_{i+1}^y \\ &+ (\lambda - 1 - s)\sigma_i^z - 1\Big),\end{aligned} \tag{3.16}$$

where s plays the role of a complex transverse magnetic field. One limit of particular interest is when $\beta = 0$, that is $\gamma = \lambda = 1$, and we take s to be real. In this limit the generator of the biased dynamics maps directly onto the Hamiltonian of the 1d transverse field quantum Ising model. To evaluate the MGF and CGF for all values of β, we focus on the case where s is real and then in the long time and large system size limit we analytically continue our answer into the complex s plane. The Hamiltonian $\mathbb{H}_s$ may be diagonalized via a Jordan-Wigner transformation followed by a Bogoliubov rotation (see Appendix B) yielding

$$\mathbb{H}_s = -\sum_k [\epsilon_k(s)(c_k^\dagger c_k - 1/2) + 1/2], \tag{3.17}$$

where $c_k^\dagger$ and c_k are fermionic creation and annihilation operators. The dispersion is given by $\epsilon_k(s) = \sqrt{(s - \lambda + 1 - \cos k)^2 + \gamma\lambda \sin^2 k}$ and, restricting N to be even, the wavevectors take values

$$k = \frac{\pi n}{N},\ n = -N+1, -N+3, \ldots, N-1. \tag{3.18}$$

Taking the initial state of the system to be the equilibrium distribution under the similarity transformation this becomes the ground state $|0\rangle$ of the $s = 0$ quantum

spin Hamiltonian and the MGF becomes

$$Z(s,t) = \langle 0|e^{t\mathbb{H}_s}|0\rangle. \tag{3.19}$$

This quantity is directly related to the boundary partition function of the system with identical boundaries, a Hamiltonian $-\mathbb{H}_s$ and a boundary of length t. Analytically continuing $t \to it$ we see it is also directly related to the return amplitude of the system under a quantum quench. The dynamical Lee-Yang zeros of this associated boundary system coalesce in the long time and large system size limits to form trajectory phase transitions while the Fisher zeros result in DPTs as described in Sec. 2.5.2. Using the diagonalized form of $\mathbb{H}_s$ we readily obtain

$$Z(s,t) = \prod_{k>0} \underbrace{e^{t(\epsilon_k(s)-1)} \cos^2 \alpha_k^s (1 + \tan^2 \alpha_k^s e^{-2t\epsilon_k(s)})}_{Z_k(s,t)}, \tag{3.20}$$

where the angles α_k^s are related to the difference in Bogoliubov angles required to diagonalize $\mathbb{H}_s$ and $\mathbb{H}_{s=0}$ (see Appendix B). Note that in deriving the above expression we have also used the fact that $\epsilon_k(s) = \epsilon_{-k}(s)$ and $Z_k = Z_{-k}$.

From this we see that the CGF takes the form

$$\Theta(s,t) = \sum_{k>0} \log Z_k(s,t) = \sum_{k>0} \Theta_k(s,t), \tag{3.21}$$

where it is clear from the above expression that each k mode contributes independently to the cumulants of the time-integrated energy with a corresponding term $\Theta_k(s,t)$ contributing to the total CGF. Equations (3.20) and (3.21) are the main results of this Section as they will allow us to probe the time dependence of the fluctuations of the time-integrated energy. A final note is that in the limit of long times and large system sizes the MGF takes an LD form $Z(s,t) \approx e^{tN\theta(s)}$, where the dynamical free energy is given by

$$\theta(s) = \int_0^\pi \frac{dk}{2\pi} [\epsilon_k(s) - 1]. \tag{3.22}$$

The analytic structure of $\theta(s)$ allows us to determine the full trajectory phase diagram [13, 83]. For all finite N and t the Hadamard factorization of the MGF will hold as the possible values that $\mathcal{E}(t)$ may take are bounded from above and below. However even in the thermodynamic limit, where this factorization does not hold, using appropriately scaled cumulants the method to extract the leading zeros is still expected to work. Although trying to access the k-resolved cumulants, as described by $\Theta_k(s,t)$, may be difficult in practice as the mode occupation numbers become dense on the interval $[0,\pi]$ in this limit.

3.3 Trajectory Phase Diagram

Having obtained the LD function $\theta(s)$ we are now ready to examine the full trajectory phase diagram of the 1d Glauber-Ising chain. To simplify the analysis it is better to consider the finite N LD function and split it up into its constituent k mode contributions, $\theta(s) = \sum_{k>0} \epsilon_k(s) - 1 = \frac{1}{2}\sum_k \theta_k(s)$. Taking s to be real to begin with, the dynamical free energies of each k mode $\theta_k(s)$ are singular with a square-root branch cut when $\epsilon_k(s) = 0$. The solutions to the equations $\epsilon_k(s) = 0$ give a series of 2nd order continuous trajectory phase transition points s_c. Requiring a real bias s the only k modes with a solution are $k = 0, \pi$ and

$$s_c^{\pm}(\beta) = \lambda - 1 \pm 1. \tag{3.23}$$

When $|s| < |s_c|$ the trajectories are paramagnetically ordered, and so these singularities from the $k = 0$ and $k = \pi$ modes separate the paramagnetically ordered regime from the antiferromagnetic and ferromagnetic trajectories respectively. These phase transitions form a continuous curve in the β-s plane as shown in Fig. 3.1. Promoting s to a full complex field we find that every k mode contribution $\theta_k(s)$ is singular with a square-root branch cut for some complex s_c. Solving

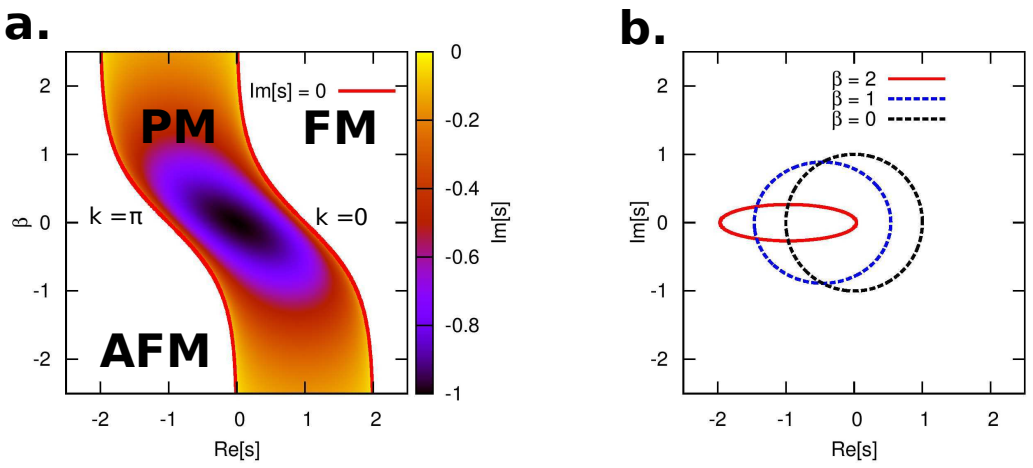

Figure 3.1: (a) The trajectory phase diagram projected onto the plane of β and the real part of the counting field $\mathrm{Re}[s]$. Trajectory phases are separated by a surface of transition points in the β-s plane. In the $\mathrm{Im}[s] = 0$ plane the paramagnetically ordered trajectories are separated from the (anti-)ferromagnetically ordered trajectories by two transition lines (solid red lines above) emerging from the $k = 0, \pi$ modes. When $\beta > 0$ and $s = \mathrm{Re}[s] + i\mathrm{Im}[s] > 0$ the trajectories are either paramagnetic (labelled PM above) or ferromagnetic (labelled FM above) in nature; the complex transition points separate these two. In contrast when $\beta < 0$ and $s < 0$ the trajectories are either paramagnetic in nature or anti-ferromagnetically ordered (labelled AFM above). (b) At fixed β the trajectory transition lines form closed curves in the complex s plane, these curves approach the unit circle as $\beta \to 0$.

$\epsilon_k(s) = 0$ we find the transition point s_c as a function of k and β:

$$s_c(k, \beta) = \lambda - 1 + \cos k + i\sqrt{\gamma\lambda}\sin k. \tag{3.24}$$

In the thermodynamic limit the wavevector k becomes continuous over the interval $[-\pi, \pi]$ and so for fixed β the transition points form a closed curve in the complex s plane. When $\beta > 0$ this curve is elliptical, as $\gamma\lambda \neq 1$, however upon increasing the temperature the curves approach the unit circle, see Fig. 3.1. At infinite temperature the curve is in fact the unit circle as $\gamma = \lambda = 1$, this is in accordance with the Lee-Yang theory of the associated 1d transverse field quantum Ising model [55].

3.4 Mode-Resolved Cumulants

With the description of the trajectory phase diagram completed, we now apply the method described in Sec. 3.1 to detect signatures of the trajectory phase transitions found in the previous Section. We begin by considering the contributions to cumulants from each individual k at finite times, see Eqs. (3.20) and (3.21). We refer to these contributions as the k-resolved cumulants which are defined as

$$\langle\langle \mathcal{E}_t^n \rangle\rangle_k = (-1)^n \partial_s^n \Theta_k(s, t)|_{s\to 0}. \tag{3.25}$$

From this we extract the k-resolved cumulants, Fig. 3.2 shows the resolved cumulants of order $n = 6, 7, 8, 9$ as a function of time with a fixed $k = \pi/4$. The scale in Fig. 3.2 is logarithmic, this implies the cumulants crossing zero corresponds to a downward spike. We then use Eq. (3.7) to extract the leading Lee-Yang zeros from the finite time cumulants and track their motion in the complex counting

field plane as a function of time. The motion of these zeros (the open circles) along with the full curve of transition points and the relevant transition points associated with the particular $k = \pi/4$ mode (red spots) are shown in Fig. 3.3. It is clear that as time increases the leading Lee-Yang zeros approach the related trajectory transition point. This allows one to deduce the location of the trajectory transition points in the complex s plane from these finite time k-resolved cumulants, which are obtained from the physical $s = 0$ system dynamics.

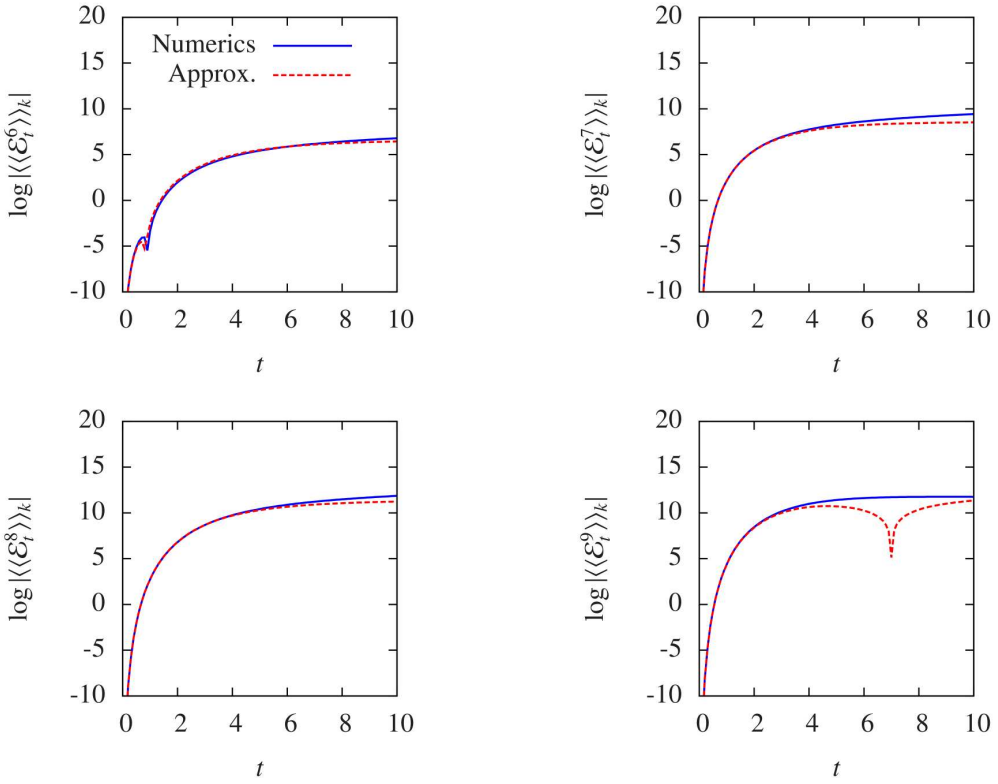

Figure 3.2: The mode-resolved cumulants (full lines) for orders $n = 6, 7, 8, 9$ are plotted together with the approximation (dashed lines) based on the extracted leading pair of Lee-Yang zeros for $\beta = 0.5$. The agreement at short times is apparent and going to longer times it becomes clear that the approximation fails.

Checking for self-consistency we use the extracted zeros to reconstruct the k-resolved cumulants using the approximation in Eq. (3.6). The results from this approximation (dashed lines) together with the exact curves are shown in Fig. 3.2. At short times the approximation holds very well but at longer times the agreement decreases. This reduction in agreement is due to higher order Lee-Yang zeros beginning to move towards the transitions points and so may not be neglected. This is also reflected in the deviation in the convergence of the leading zeros from the transition points, however the approximation may be improved by considering higher order cumulants. The eventual breakdown of this approximation at longer times is not shown here but it should be clear from Fig. 3.2 that the position of the trajectory transition points can be extracted before this occurs.

3.5 Full Analysis

In this Section we consider the full cumulants extracted from $\Theta(s,t)$ which are simply the sum of the k-resolved contributions,

$$\langle\langle \mathcal{E}_t^n \rangle\rangle = \sum_k \langle\langle \mathcal{E}_t^n \rangle\rangle_k. \tag{3.26}$$

The approximation in Eq. (3.6) only includes the leading Lee-Yang pair of zeros. This pair converges to at most two distinct points in the complex s plane, thus we cannot extract the full form of the transition line which is in contrast to using the k-resolved cumulants. All is not lost however, as in certain instances there are a few transition points close to $s = 0$ which dominate the dynamical fluctuations of the time-integrated energy. At infinite temperature, $\beta = 0$, all of the transition points lie on the unit circle and are equidistant from the origin. Lowering the temperature the trajectory transition line forms a shifted ellipse, where a few points on the ellipse are now close to $s = 0$ and so will dominate the dynamics

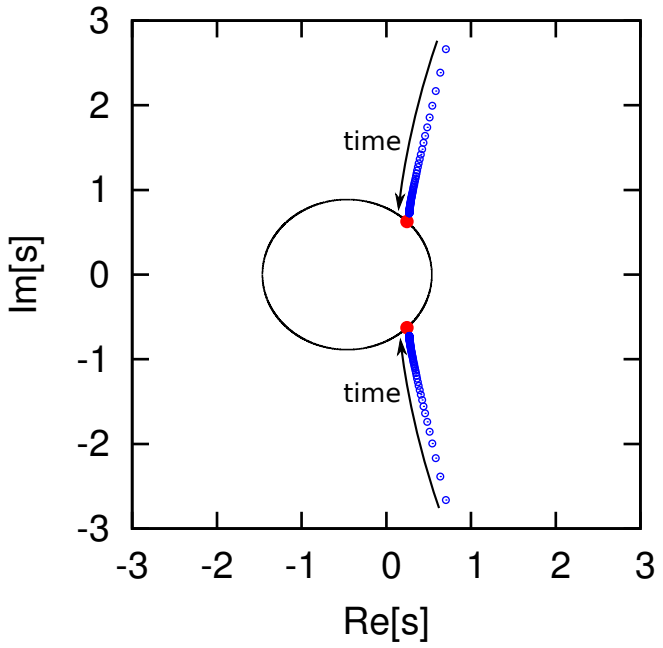

Figure 3.3: The Lee-Yang zeros (open circles) extracted from the high order cumulants moves towards the trajectory transition points (filled circles) on the closed curves, here $\beta = 0.5$ and the transition points are associated with the $k = \pi/4$ mode.

of the system and hence the cumulants of the time-integrated energy. From this we expect our method to remain applicable in the low temperature regime where only a few transition points are relevant to the dynamics. Furthermore this low temperature regime is interesting as thermal fluctuations are suppressed and the temporal evolution of the high order cumulants is determined solely by the intrinsic properties of the model. Conversely at higher temperatures the method is expected to not be successful in locating the transition points.

The dynamical Lee-Yang zeros extracted from Eq. (3.7) in both the low and high temperature regimes are shown in Fig. 3.4. In the low temperature regime the leading Lee-Yang pair move towards the transition points closest to the origin with increasing time. These singularities closest to $s = 0$ are associated to the low k mode contributions to the high order cumulants, which are the dominant contributors at these low temperatures. In the high temperature ($\beta = 0$) regime the picture changes drastically, now all k modes contribute significantly to the high order cumulants and so all the singularities are important. One may still attempt to extract numerical values for the leading Lee-Yang pair using Eq. (3.7) but the approximation in Eq. (3.6) is no longer valid. We thus expect many zeros to contribute meaningfully to the cumulants and hence the extracted zeros should be meaningless, this is confirmed by their lack of convergence to any transition point as shown in Fig. 3.4.

Having examined the trajectory phases of a classical stochastic system using a dynamical Lee-Yang framework, we will now examine a series of open quantum systems. More specifically, in the subsequent Chapter we will extend the thermodynamic approach to quantum jump trajectories to diffusive quadrature trajectories and examine what new dynamical information these ensembles of quadrature trajectories encode.

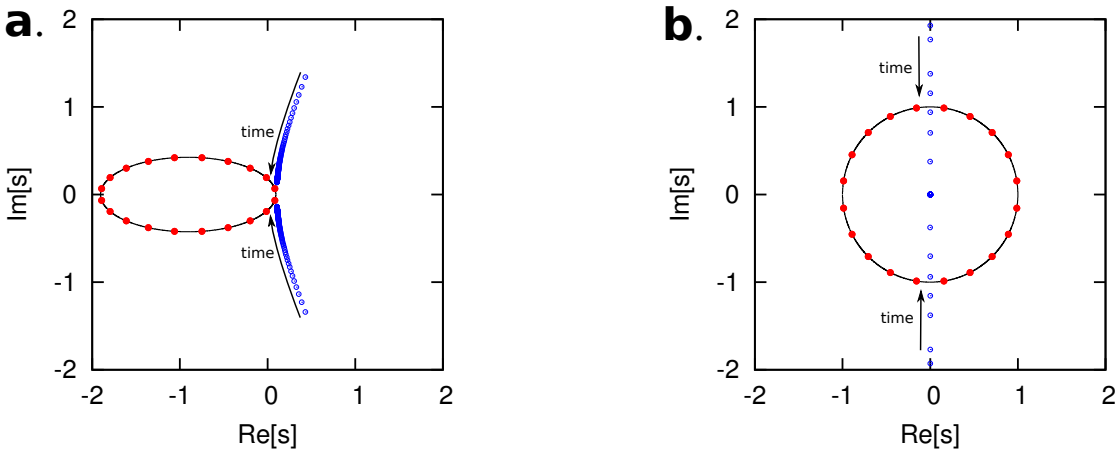

Figure 3.4: The extracted dynamical Lee-Yang zeros (open circles), from the cumulants of order $n = 6, 7, 8, 9$, for a spin chain with N = 20 spins. (a) The high order cumulants of the time-integrated energy are dominated at low temperatures ($\beta = 1.5$) by transition points close to $s = 0$ associated with the long-wavelength modes. The extracted Lee-Yang zeros move towards these dominant transition points as time increases. (b) In the high temperature limit ($\beta = 0$) all modes contribute equally towards the dynamical fluctuations and so all the transition points are equidistant from the origin. Therefore the extracted zeros do not move towards any singularity in this regime.

4. Open Quantum Systems and Quadrature Trajectories

The extension of trajectory thermodynamics (or s-ensemble) of classical stochastic systems to open quantum systems described by a Lindblad Master equation is relatively straightforward, see Sec. 2.4.2. However in the case of an open quantum system the trajectories are defined not as system configurational changes but continuous time-records of some property of the quanta emitted by the system [29, 40]. The most natural dynamical observable to characterize such trajectories is simply the total number of emissions, K, up to a time t. The statistics of this observable obeys a LD principle and in short one may invoke a thermodynamic formalism as described in Sec. 2.4.2. This Chapter focusses on extending this thermodynamic approach to other dynamical order parameters in open quantum systems. Taking motivation from experiments using homodyne detection schemes we will focus on the trajectories of the quadratures of light emitted from dissipative systems [54]. We study this new order parameter in a simple driven 3-level system and two coupled 2-level systems before examining a many-body system, the micromaser [30, 88, 118, 119]. These examples highlight how one can uncover different trajectory phases not only from the statistics of photon emissions but also the quadratures of the light, and in some instances uncover trajectory phases not captured by the photon activity. To further compare and contrast this new type of

order parameter with the activity ($\langle K\rangle_{s'}/t$) we also ask what is the typical behaviour of one order parameter in biased ensembles of trajectories of the other. This problem could be of interest with regards to simulations of the trajectory biased dynamics of such dissipative open quantum systems.

4.1 Extended trajectory ensembles

4.1.1 The s-ensemble for quadrature trajectories

Trajectory phases of open quantum systems were previously [29] characterized by their photon activity, $k_{s'} = -\theta'_K(s')$, and dynamic susceptibility, $\chi_{s'} = \theta''_K(s')$. To evaluate these quantities the deformed Master operator $\mathbb{W}_{s'}$, see Eq. (2.60), must be diagonalized and the largest real eigenvalue is the associated dynamical free energy $\theta_K(s')$. We now consider characterizing the trajectory phases of the system in terms of the X and Y quadratures of the light emitted into the bath. These are defined as $(b+b^\dagger)/2$ and $-i(b-b^\dagger)/2$ respectively, where we recall b ($b^\dagger$) are the lowering (raising) operators of the bath. Correspondingly the dynamical order parameters used to distinguish the different quadrature trajectory phases are $x_s = \langle X\rangle_s/t$ and $y_s = \langle Y\rangle_s/t$, which we both generically refer to as *quadrature activities*. These quadrature operators define axes of an optical phase space and so further insight may be obtained by considering a generalized quadrature

$$X^\alpha = \cos\alpha\ X + \sin\alpha\ Y, \tag{4.1}$$

where the angle α is with respect to the X quadrature axis in phase space, see Fig. 4.1. For these quadratures we consider scaled marginal distributions $P(X^\alpha) \simeq e^{-\phi(x^\alpha)}$, where $\phi(x^\alpha)$ is the "entropy density" of these quadrature trajectories which can be extracted via the Legendre transform of the associated dynamical "free

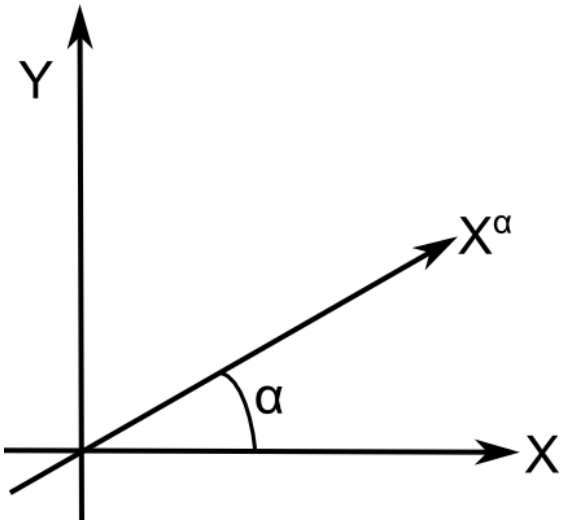

Figure 4.1: The axes of an optical phase space are defined by the X and Y quadratures. The generic quadrature X^α is then simply a rotation of the X quadrature axis.

energy" $\theta_{X^\alpha}(s)$.

The deformed Master operator $\mathbb{W}_s$ associated with the quadratures X^α may be determined by recognizing that its stochastic Itō increment is given by

$$dX^\alpha(t) = \frac{1}{2}(e^{-i\alpha}dB(t) + e^{i\alpha}dB^\dagger(t)), \tag{4.2}$$

where $dB(t)$and $dB^\dagger(t)$ are the usual bath increments. The s-biased operator $\mathbb{W}_s$ determines the evolution of the s-biased reduced density operator $\rho_s(t)$ which is given by

$$\rho_s(t) = \mathrm{Tr}_B(\exp(-s\int^t dX^\alpha(t'))\rho(t)) = \mathrm{Tr}_B(V_t[s]\rho(t)), \tag{4.3}$$

where the trace is over the bath degrees of freedom. To perform this trace we consider the increment of this s-biased density matrix

$$d[\rho_s] = \mathrm{Tr}_B\{d[V_t[s]]\rho + V_t[s]d[\rho] + d[V_t[s]]d[\rho]\}, \tag{4.4}$$

the first two terms appear in standard calculus while the final term appears due to the stochastic nature of the increments.

Using the Itō calculus set out in Eq. (2.50) we expand the characteristic operator $V_t[s]$ to first order in dt and find

$$d[V_t[s]] = V_t[s](\frac{s^2}{8}dt - sdX^\alpha). \tag{4.5}$$

Recalling the increment of the stochastic density operator [40], see Eq. (2.51), we may now evaluate the increment $d[\rho_s]$ to lowest order in dt: term by term the RHS of Eq. (4.4) is

$$\begin{aligned}
\mathrm{Tr}_B(d[V_t[s]]\rho) &= \frac{s^2}{8}\rho_s dt, \\
\mathrm{Tr}_B(V_t[s]d[\rho]) &= \mathbb{W}(\rho_s)dt, \\
\mathrm{Tr}_B(d[V_t[s]]d[\rho]) &= -\sum_i \frac{\sqrt{\gamma_i}s}{2}(e^{-i\alpha}L_i\rho_s + e^{i\alpha}\rho_s L_i^\dagger)dt.
\end{aligned} \tag{4.6}$$

Here $\{L_i\}$ are the Lindblad operators of the dissipative system, γ_i is the associated decay rate of channel i and the operator $\mathbb{W}$ generates the regular Lindbladian evolution with these jump operators. Combining all of these we find the generalized master equation

$$\begin{aligned}
\dot{\rho}_s(t) &= \mathbb{W}_s(\rho_s) \\
&= -i[H,\rho_s] + \sum_i \gamma_i L_i\rho_s L_i^\dagger - \frac{\gamma_i}{2}\{L_i^\dagger L_i, \rho_s\} \\
&\quad - \sum_i \frac{\sqrt{\gamma_i}s}{2}(e^{-i\alpha}L_i\rho_s + e^{i\alpha}\rho_s L_i^\dagger) + \frac{s^2}{8}\rho_s,
\end{aligned} \tag{4.7}$$

where H is the system self Hamiltonian. The MGF of the quadratures is simply $Z(s,t) = \mathrm{Tr}_{sys}(\rho_s(t))$ and in the long time limit this assumes an LD form with a dynamical free energy $\theta_{X^\alpha}(s)$, which corresponds to the largest real eigenvalue of $\mathbb{W}_s$.

To distinguish between the thermodynamics of quadrature and jump trajectories we will always consider the jump trajectories to be biased by a field s' and the

quadratures by a field s. Finally we note that throughout this Chapter we will denote the quadrature activity x_s^α (**the absence of the subscript s** implies the activity of interest is **evaluated at $s = 0$**, i. e. $x \equiv x_{s=0}$) and the corresponding quadrature susceptibility $\chi_s^{X^\alpha}$. This concludes the introduction of the s-ensemble of quadrature trajectories; before presenting our results for various models we discuss the concept of doubly biased trajectory ensembles.

4.1.2 Doubly Biased Ensembles

Thus far we have provided the theoretical formalism for a thermodynamic approach to diffusive quadrature trajectories. In this Section we introduce the abstract concept of doubly biased ensembles where we ask about the properties of the trajectories of an already biased system. For example consider the following question, what are the properties of the quadrature trajectories for a system biased such that it emits more/less than the typical number of quanta? To answer this we first bias the system with the field s', conjugate to the total number of emitted photons K, and ask what form the generating function for the quadratures takes in this biased system [54]. To this end we introduce a doubly biased density operator $\rho_{ss'}$ which incorporates information[1] on the statistics of both trajectory ensembles,

$$\rho_{ss'} = \mathrm{Tr}_B(\tilde{V}_t[\frac{s'}{2}]V_t[s]\tilde{V}_t[\frac{s'}{2}]\rho(t)). \tag{4.8}$$

The ordering of the characteristic operators for the quantum jumps ($\tilde{V}_t[s']$) and quadratures ($V_t[s]$) is important due to the noncommutability of the two observables. Considering the stochastic increment of $\rho_{ss'}$ one may formally trace out the bath using the appropriate Itō calculus to readily find this doubly biased master

[1]Specifically derivatives of the trace of $\rho_{ss'}$ with respect to $-s$ evaluated at $s = 0$ give the quadrature statistics of a system biased by s'.

density matrix obeys a new generalized Master equation

$$\dot{\rho}_{ss'}(t) = \mathbb{W}(\rho_{ss'}) + (e^{-s'} - 1)\sum_i \gamma_i L_i \rho_{ss'} L_i^\dagger + \frac{s^2}{8}\rho_{ss'} - \frac{s e^{-s'/2}}{2}\sum_i \sqrt{\gamma_i}(e^{-i\alpha} L_i \rho_{ss'} + e^{i\alpha}\rho_{ss'} L_i^\dagger). \tag{4.9}$$

Taking the limits $s, s' \to 0$ we obtain the regular trace-preserving Lindbladian evolution. This equation may once again be written in matrix form with a superoperator $\mathbb{W}_{ss'}$ which possesses a largest real eigenvalue $\theta_{K,X^\alpha}(s, s')$, this LD function encapsulates the long time quadrature trajectory statistics of this biased system. Moreover we note that in the limit of $s \to 0$ we obtain the dynamical free energy associated with the quantum jump trajectories $\theta_K(s')$ [29, 84]. With this new CGF the natural quantity to examine is the typical quadrature activity/susceptibility in this jump biased ensemble and so we examine derivatives of $\theta_{K,X^\alpha}(s, s')$ w. r. t. s evaluated in the limit $s \to 0$.

Similarly we can probe the statistics of the quantum jump trajectories in a quadrature biased system by changing the ordering of the characteristic operators and defining a new doubly biased density matrix

$$\rho_{s's}(t) = \mathrm{Tr}_B(V_t[\frac{s}{2}]\tilde{V}_t[s']V_t[\frac{s}{2}]\rho(t)). \tag{4.10}$$

This new biased density operator obeys the generalized Master equation

$$\dot{\rho}_{s's}(t) = \mathbb{W}(\rho_{s's}) + (e^{-s'} - 1)\sum_i \gamma_i L_i \rho_{s's} L_i^\dagger + \frac{s^2}{8}\rho_{s's} - \frac{s(e^{-s'} + 1)}{4}\sum_i \sqrt{\gamma_i}(e^{-i\alpha} L_i \rho_{s's} + e^{i\alpha}\rho_{s's} L_i^\dagger). \tag{4.11}$$

Solving for the LD function $\theta_{X^\alpha,K}(s', s)$ the typical value for the photon activity $k_{s'=0}$ for different quadrature biases s may be extracted via differentiation. In the coming Sections we exemplify the formalism introduced in this Section using a few simple quantum optical systems and the micromaser.

4.2 Simple Open Optical Systems

4.2.1 Driven Three-Level System

The first example we consider is a dissipative 3-level system which is driven by two resonant lasers between $|0\rangle$ and the excited states $|1\rangle$ and $|2\rangle$ with Rabi frequencies Ω_1 and Ω_2 respectively. Along with this there is a *single* decay channel $|1\rangle \to |0\rangle$ with an associated decay rate κ as depicted in Fig. 4.2(a). This decay transition results in the emission of photons and is considered the active or light line transition while the state $|2\rangle$ is an inactive level. When $\Omega_1 \gg \Omega_2$ the photon emission trajectories are intermittent [29, 39, 120] displaying both "bright" and "dark" periods, this is due to the system spending significant periods of time in the state $|2\rangle$ before the active state becoming populated again resulting in emission. This intermittency was previously shown [29] to manifest itself as a dynamical crossover in *jump activity* $k_{s'}$ at $s' = 0$. In the $s' < 0$ regime the system is highly active and the dynamics are dominated by the levels $|1\rangle$ and $|0\rangle$, tuning s' through 0 the system crossovers over to an inactive regime $s' > 0$ where the dynamics are dominated by very long periods where the dark $|2\rangle$ state is occupied. Having understood the dynamics of this system in terms of quantum jumps we now characterize it in terms of its quadrature statistics before examining the doubly biased statistics and its phase space portraits of the marginal distributions of the quadratures.

Considering the quadrature trajectories, the generalized Master operator $\mathbb{W}_s$ is of the form given in Eq. (4.7) with a single set of Lindblad operators L and $L^\dagger$ and one decay rate κ, due to the null decay rate between $|2\rangle$ and $|0\rangle$. In this system these Lindblads have a simple form $L = |0\rangle\langle 1|$ and the Hamiltonian for this system is simply

$$H = \sum_{i=1}^{2} \Omega_i (c_i + c_i^\dagger), \tag{4.12}$$

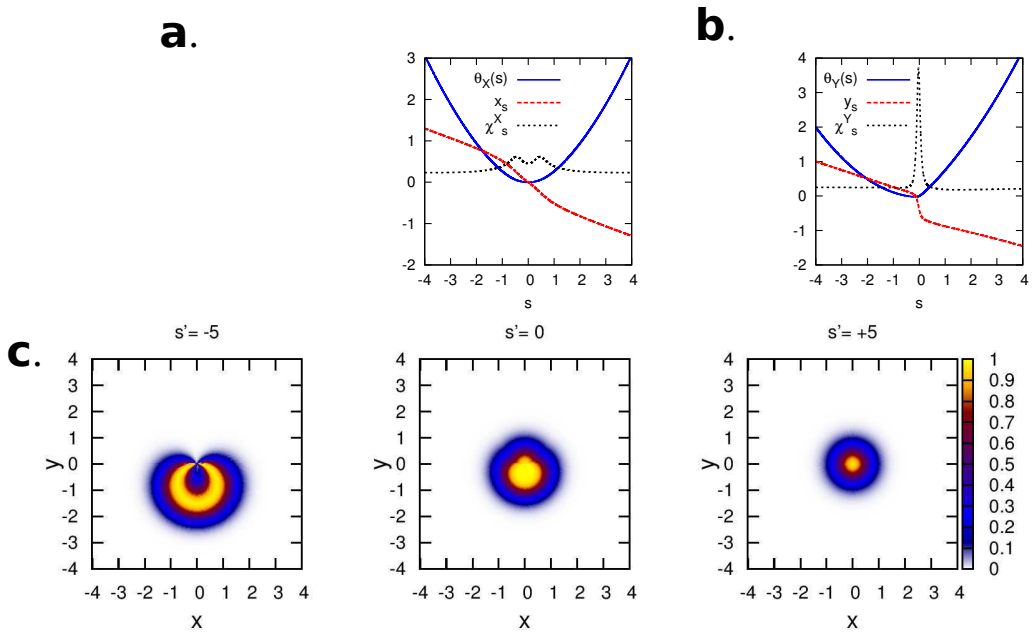

Figure 4.2: (a) Schematic of 3-level system coupled to a vacuum driven by two resonant lasers with Rabi frequencies Ω_1 and Ω_2. (b) The X quadrature statistics are symmetric about $s = 0$ and in the limit $|s| \gg 1$ the LD function is simply that of a driven 2-level system. In contrast the Y quadrature activity has a rounded step at $s = 0$ marked by a peak in the dynamical susceptibility. (c) Phase space portraits of the 3-level system at different photon biases s'; the axes are labelled x and y which denote the X and Y quadrature activities at $s = 0$. Making the system more photon active the plot moves away from the origin in the negative y direction while making it more inactive the plot becomes centred about the origin.

where c_i ($c_i^\dagger$) is the lowering (raising) operator $|0\rangle\langle i|$ ($|i\rangle\langle 0|$). The dynamical free energy $\theta_{X^\alpha}(s)$ for each α is obtained via exact diagonalization of $\mathbb{W}_s$, and in this Section we focus on the special case of $\kappa = 4\Omega_1$, $\Omega_2 = \Omega_1/10$ and we fix $\Omega_1 = 1$. We begin by examining the biased ensembles of trajectories associated with the X quadrature statistics. We find that $\theta_X(s)$ is symmetric in s and exhibits no "sharp" crossovers which would be indicative that the system is intermittent, this is shown in Fig. 4.2(b). On the other hand, the Y quadrature activity y_s does exhibit a crossover along with a corresponding peak in its susceptibility χ_s^Y at $s = 0$, as shown in Fig. 4.2(b).

Previously the crossover in $k_{s'}$, studied in Ref. [29], attributed the crossover to a change in the effective behaviour of the system. For $s' < 0$ the system, it was argued, behaved as if it were a 2-level system comprised only of the levels $|0\rangle$ and $|1\rangle$. While the inactive phase ($s' > 0$) was due to the dark state $|2\rangle$ being occupied for long periods of time such that photon emission could not occur. In this instance we propose that the crossover in y_s is due to the same change in dynamics associated with the crossover in photon emission k'_s. To support this claim we examine consider the typical quadrature statistics within ensembles of jump biased trajectories and construct phase space portraits of the system for various s' biases. These portraits are plots of $e^{-\phi(x^\alpha)}$ $\forall\alpha$ in the optical phase space obtained by solving the doubly biased Master equation (4.9) and applying the appropriate Legendre transformation.

We first examine the phase space portraits in the photon-inactive regime, $s' = 5$, here the portrait is centred close on the origin and appears almost like a vacuum suggesting $|2\rangle$ is occupied for large periods of time, see Fig. 4.2(c). Although it must be noted it is not a true vacuum as both the photon activity and y_s are small but nonzero. Tuning s' to the photon-active phase $s' = -5$, the phase space portrait changes dramatically and in fact it is very similar to the portraits of a 2-

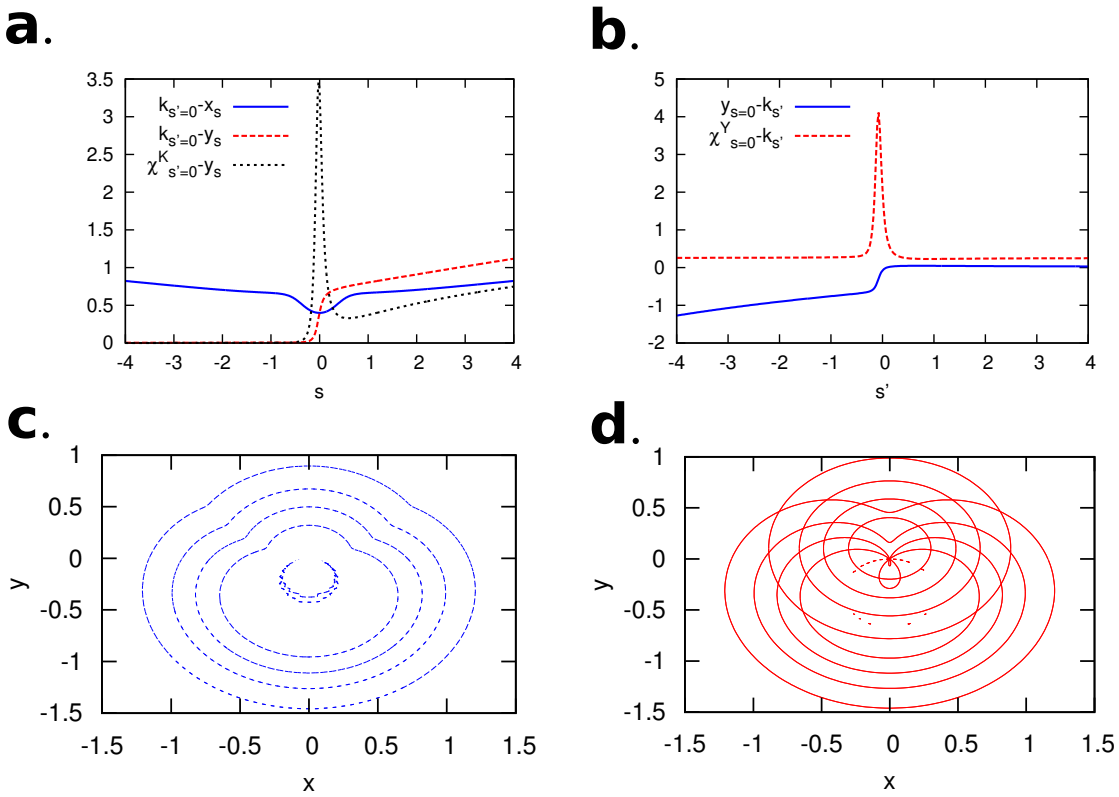

Figure 4.3: (a) Plots of the typical photon activity in biased quadrature trajectory ensembles. Biasing the X quadrature the photon activity grows irrespective of the sign s. However the photon activity exhibits a crossover from an active to an inactive phase at $s = 0$ when we consider biasing the Y quadrature. Furthermore the system is more photon active when we bias the system towards negative Y quadrature activity. (b) Similarly the typical Y quadrature activity exhibits a crossover at $s' = 0$ as we bias the photon activity of our system. Again the sign of y is indicative of the magnitude of k. (c) Contour plots of marginal distributions of the typical trajectories of a driven 2-level system plus a shifted photon inactive ($s' = +5$ and shifted by 0.1 along the y direction). This plot is very similar to the portrait of the unbiased 3-level dynamics shown in (d), highlighting that the physical dynamics can be considered as being composed of an active 2-level plus an inactive 2-level system.

level systems also biased to the photon active regime $s' = -5$, see Refs. [29] and [54] for details. Finally considering the unbiased $s' = 0$ phase space portrait we find it appears to be some combination of the 2-level phase space portrait and the $s' = 5$ portrait of the 3-level system. This is illustrated more clearly in Fig. 4.3(c,d) where we present contour plots of a 2-level system's phase space portrait at $s' = 0$ with a shifted 3-level $s' = 5$ portrait and find it closely resembles the 3-level system's portrait at $s' = 0$. Thus demonstrating that the physical dynamics of the 3-level system effectively consists of an active 2-level system plus an inactive 2-level system (where the dynamics are dominated by long period where $|2\rangle$ is occupied) plus some "mixing" between the two.

With this qualitative examination complete, we now need to determine whether or not the crossover in $k_{s'}$ is the reason for the crossover in y_s and so we examine the typical jump statistics in the biased quadrature ensembles and vice-versa. To extract the LD functions $\theta_{X^\alpha,K}(s', s)$ and $\theta_{K,X^\alpha}(s, s')$ we diagonalize the Master operators given by Eqs. (4.9) and (4.11) respectively. Extracting $k_{s'=0}$ for both X and Y quadrature biases s we find the typical activity k shows no sharp features as bias the X quadrature, irrespective of the sign of s. However if we bias the Y quadrature, the activity k exhibits a crossover at $s = 0$ with a corresponding peak in its susceptibility χ_s. Furthermore when $s < 0$ the system becomes photon inactive while for $s > 0$ is a photon active state, that is to say more positive y_s leads to smaller than average k while the more negative y_s is the more photon active the system. This is shown in Fig. 4.3(a) and supports the assertion that the activities y_s and $k_{s'}$ may be used as equivalent order parameters in this system.

For completeness we examine $y_{s=0}$ for various s' biases, this is plotted in Fig. 4.3(b). Surprisingly the typical $s = 0$ quadrature activity in these biased ensembles exhibits the same correlation as that of k under a Y quadrature bias. This is surprising as the Y quadrature trajectories do not have an inactive regime but biasing

the photon trajectories to be inactive we find the typical y activity becomes very small in magnitude. Correspondingly when $s' < 0$ and the system is highly jump active $y_{s=0}$ is very negative, confirming that both $k_{s'}$ and y_s may be used as equivalent dynamical order parameters in this system. This connection has been found to hold in other systems such as the 2-level system and may be a trait present in many other dissipative optical systems. In conclusion, we note that the encoding of equivalent dynamical information in both the quadrature and jump activities is surprising, both due to their differing behaviour under biasing their trajectories and the noncommuting nature of the operators involved.

4.2.2 Two Coupled Two-Level Systems

In this Section we extend our study to a pair of coupled two-level systems driven by lasers of different polarization, this set up is depicted in Fig. 4.4(a). In the previous Section we have shown that crossovers in the jump activity are mirrored as crossovers in the quadrature activity, specifically y_s, highlighting that in certain systems these dynamical order parameters are equivalent. With these coupled two-level systems we show that this equivalence is not always the case, and that crossovers can occur in the quadrature activity without a corresponding crossover in the photon activity. This shows that the quadrature activity can be considered a dynamical order parameter in its own right and can capture dynamical information not present the photon activity.

The two weakly coupled two-level systems evolve under Markovian dissipative evolution with two jump operators: $L_I = c_I$ and $L_{II} = c_{II}$, where these operators are the lowering ladder operators of each two-level system, I and II, respectively, see Fig. 4.4(a). Both two-level systems have identical Rabi frequencies (Ω) and decay rates (κ), and throughout this Section we choose $\kappa = 4\Omega$ and fix $\Omega = 1$.

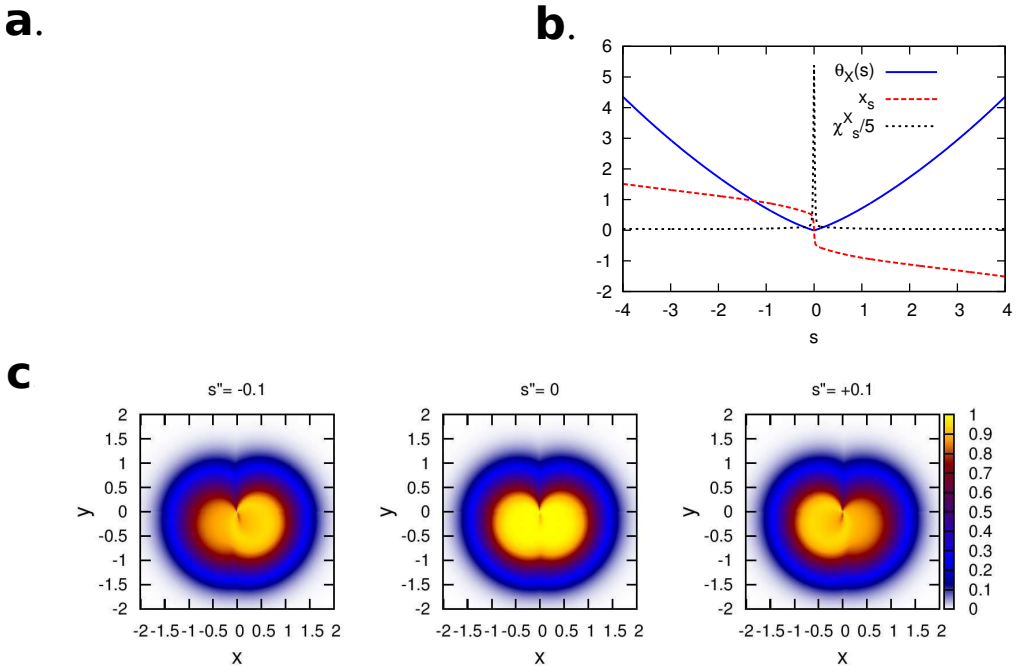

Figure 4.4: (a) Schematic diagram of two weakly coupled 2-level systems driven by resonant lasers of identical Rabi frequency Ω but of different polarization. (b) The X quadrature activity exhibits a crossover at $s = 0$, this is due to the different laser polarizations and is marked by a large peak in the susceptibility at $s = 0$. (c) Phase space portraits of the two weakly coupled 2-level systems at various X quadrature biases s''. For $s = -0.1, +0.1$ the probability distributions are concentrated about $x > 0$ and $x < 0$ respectively, whereas at $s'' = 0$ they are even functions of x. This change in distribution is indicative of the crossover in x_s at $s = 0$.

However the individual two-level systems are distinguished by the polarization of the driving laser, subsystem I is driven by a $\sigma_x - \sigma_y$ polarized laser and II is driven by a $\sigma_x + \sigma_y$ polarized laser. Combined with a weak coherent coupling between each subsystems ground state the self-Hamiltonian of this combined system is given by

$$\begin{aligned} H =& \Omega(c_I + c_I^\dagger - ic_I + ic_I^\dagger + c_{II}^\dagger + c_I I + ic_{II} - ic_{II}^\dagger) \\ &+ \lambda(|0\rangle\langle 2| + |2\rangle\langle 0|). \end{aligned} \tag{4.13}$$

The coherent coupling is chosen to be weak, $\lambda \ll \Omega$, and is fixed as $\lambda = \Omega/10$ in the presented results. Moreover the form of this coupling allows for the coherence between the two-level subsystems to be preserved. The similarity between the two subsystems in conjunction with the weak coupling results in preventing crossovers in the jump activity occurring. However the different driving laser polarizations can result in a transition in the space of quadrature trajectories.

Examining the Y quadrature, its statistics are featureless and do not capture the difference in each subsystems self-Hamiltonian but the X quadrature trajectories do display a crossover around $s = 0$ as shown in Fig. 4.4(b). This crossover sharpens as $\lambda \to 0$ and conversely becomes more diffuse as we increase the coupling. Either side of the crossover there exists two distinct phases, for $s < 0$ the X activity is positive due to emission of light of subsystem I. The second phase exists when $s > 0$, in this phase the light is predominantly emitted from subsystem II resulting in a negative X activity. The crossover at $s = 0$ is indicative that the physical dynamics of the total system is a combination of these two phases. To demonstrate that this is indeed the case we construct phase space portraits for each dynamical regime.

To construct these portraits we wish to examine the marginal distributions $e^{-\phi(x^\alpha)}$ for rare X quadrature trajectories. To this end, we consider the doubly biased

ensemble where we first bias the X quadrature statistics with a field s'' and then measure the typical x^α $\forall\alpha$ employing another generating function parameter s. This double bias scheme is of the same form as Eq. (4.8) but rather than biasing jumps and measuring quadratures, or vice-versa, we consider first biasing the X quadrature and measuring quadratures. This scheme leads to a new generalized Master equation

$$\begin{aligned}\dot{\rho_{ss''}}(t) =&\mathbb{W}(\rho_{ss''}) + \rho_{ss''}\frac{ss''}{4}\cos\alpha \\ &- \frac{s\sqrt{\kappa}}{2}\sum_i (e^{-i\alpha}c_i\rho_{ss''} + e^{i\alpha}\rho_{ss''}c_i^\dagger) \qquad (4.14)\\ &- \frac{s''\sqrt{\kappa}}{2}\sum_i (c_i\rho_{ss''} + \rho_{ss''}c_i^\dagger) + \frac{s''^2}{8}\rho_{ss''} + \frac{s^2}{8}\rho_{ss''}, \qquad (4.15)\end{aligned}$$

where the summation is over the two subsystems I and II. Biasing the system to rare X quadrature trajectories with s'' we then take derivatives of the associated LD function w. r. t. s and evaluate these derivatives in the limit $s \to 0$ to extract the typical quadrature activity in these biases ensembles $\forall\alpha$. With the typical activity and scaled CGF in hand we use the Legendre transformation to extract the probability distributions $e^{-\phi(x^\alpha)}$. Considering quadrature biases of $s'' = -0.1, 0,$ and 0.1 we find the typical behaviour, as described by the marginal distributions at $s = 0$, is composed of two distinct dynamical phases, see Fig. 4.4(c).

In this system the crossover of emission from one subsystem to another is not captured by the statistics of the quantum jump trajectories, highlighting that the quadrature activities as dynamical order parameters are not just equivalent to the jump activity and may in fact reveal extra trajectory phases which are not distinguishable through photon counting.

4.3 Micromaser

In this Section we consider a many-body system as a final example. The many-body problem we study consists of a set of two-level atoms interacting with a single resonant cavity mode which may leak photons into a surrounding thermal environment, this set-up is the so-called micromaser [30, 88, 118, 119]. The single-mode resonant cavity is pumped by the excited two-level atoms and we denote the total number of these atoms divided by the cavity lifetime (τ_c) to be N_{ex}. For simplicity we set the cavity lifetime to be unity and fix $N_{ex} = 100$ for the remainder of this Section. Depending on the atom-cavity coupling and the pump rate N_{ex} the distribution of the steady-state cavity occupation can change from being unimodal to bimodal [119]. With fixed N_{ex} increasing the coupling strength between the cavity mode and atoms we can reach many points in parameter space where the steady-state cavity occupation exhibits a bistability. At these bistable points a small increase in the coupling between the cavity and the atoms results in a crossover in the occupation number of the cavity, i. e. the occupation number changes dramatically in a discontinuous fashion. Previously it was shown that this bistability manifests itself as a bistability in the space of quantum jump trajectories [30] and using the number of atoms which exit the cavity in the ground state as a dynamical order parameter a rich trajectory phase diagram was constructed. In this Section we will study the statistics of the quadratures of light leaked into the thermal environment with two approaches. Firstly we will "extract" the associated LD function using a mean-field treatment before using exact diagonalization to determine the full LD function and produce phase diagrams for the system along with examining the doubly biased trajectory properties of the model.

After tracing out the bath and atom degrees of freedom the dynamics of the cavity

is purely Lindbladian in nature and so the cavity dynamics contain *no coherent* evolution terms, i. e. $H = 0$ in Eq. (2.53). There are four pairs of Lindblad operators, two associated with the atom-cavity interaction

$$\begin{aligned}\sqrt{\gamma_1}L_1 &= \sqrt{N_{ex}}a^\dagger \frac{\sin(\phi\sqrt{aa^\dagger})}{\sqrt{aa^\dagger}},\\ \sqrt{\gamma_2}L_2 &= \sqrt{N_{ex}}\cos(\phi\sqrt{aa^\dagger}),\end{aligned} \tag{4.16}$$

and another pair result from the cavity-bath environment,

$$\begin{aligned}\sqrt{\gamma_3}L_3 &= \sqrt{\nu+1}a,\\ \sqrt{\gamma_4}L_4 &= \sqrt{\nu}a^\dagger.\end{aligned} \tag{4.17}$$

In the above equations the atom-cavity interaction is encoded in the accumulated Rabi frequency ϕ, a ($a^\dagger$) is the cavity lowering (raising operator) and ν is the thermal occupation number of the bath. For simplicity we work with a zero temperature bath $\nu = 0$ and find the generalized Master equation describing the quadrature cumulants is given by

$$\begin{aligned}\dot{\rho_s} &= \mathbb{W}_s(\rho_s)\\ &= \mathbb{W}(\rho_s) - \frac{s}{2}(e^{-i\alpha}L_3\rho_s + e^{i\alpha}\rho_s L_3^\dagger) + \frac{s^2}{8}\rho_s.\end{aligned} \tag{4.18}$$

In this system the LD function of the quadratures statistics is independent of the angle α, this is due to the purely Lindbladian evolution, and so we restrict our study to the X quadrature statistics ($\alpha = 0$) of the leaked light from the cavity.

4.3.1 Mean-field Approximation

A well-known analytic solution [30, 119] exists for the $s = 0$ steady state of this model but this solution is not simply generalized to biased ensembles away from

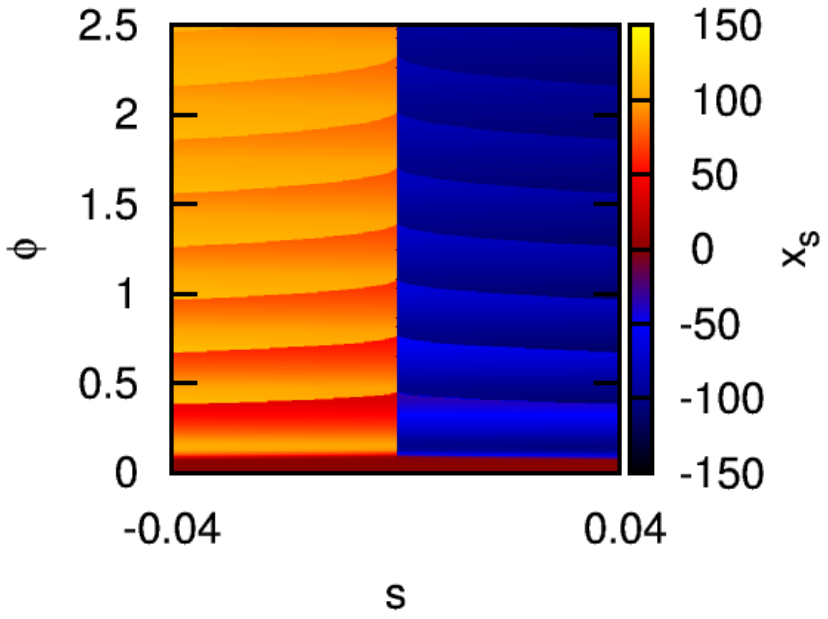

Figure 4.5: Mean-field theory result for the quadrature activity in the micromaser. This approach uncovers multiple first order transition lines in the activity either side of $s = 0$, which begin to bend as they approach $s = 0$. This diagram is very similar to that of the "atom" counting case of Ref.[31], highlighting similarities between the jump activity and quadrature activity.

$s = 0$. In the study of the quantum jump trajectories of this model much progress was made by assuming the right eigenmatrix associated with the LD function of the Master operator $\mathbb{W}_{s'}$ was diagonal in $a^\dagger a$. Using this mean-field approximation it was demonstrated that the cavity pump rate controlled the properties of the coexistence line at $s' = 0$. These results were then confirmed using exact diagonalization, moreover multiple first order transition lines were uncovered in the jump active regime ($s' < 0$) along with a single transition line in the photon inactive regime and a sole critical point located at $s' \approx 0$ and $\phi \approx 0.1$. In this study the generalized Master operator $\mathbb{W}_s$ in Eq. (4.18) generates off-diagonal terms in the density matrix and so the right eigenmatrices are generally not diagonal in $a^\dagger a$ for finite s. Close to $s = 0$ we will approximate the off-diagonal generating term in Eq. (4.18) with a diagonal one [54] given by

$$\begin{aligned} -\frac{s}{2}(a\rho_s + \rho_s a^\dagger) &= -a\rho_s a^\dagger + (a - \frac{s}{2})\rho_s(a^\dagger - \frac{s}{2}) - \frac{s^2}{4}\rho_s \\ &\approx -a\rho_s a^\dagger + e^{|s|}a\rho_s a^\dagger - \frac{s^2}{4}\rho_s. \end{aligned} \tag{4.19}$$

In this replacement we have assumed that $s \ll 1$ along with a and $a^\dagger$ being $\approx \sqrt{n}$, where n is the cavity occupation which is also assumed to be $\gg 1$. Furthermore we have used our prior experience that we expect the LD function of the X quadrature statistics to be an even function of s to introduce $|s|$ in the exponential. Thus for $s \ll 1$ we have introduced an approximate diagonal term to replace the off-diagonal piece of $\mathbb{W}_s$. With this crude approximation we can restrict our analysis to density operators which are diagonal in the number basis and so the generalized Master operator reduces to a smaller dimension operator in this space,

$$\begin{aligned} \mathbb{W}_s \to W_s =& N_{ex} a^\dagger \frac{\sin^2(\phi\sqrt{a^\dagger a + 1})}{\sqrt{a^\dagger a + 1}} - N_{ex}\sin^2(\sqrt{a^\dagger a + 1}) \\ &- a^\dagger a + e^{|s|}\sqrt{a^\dagger a + 1}a - \frac{s^2}{8}. \end{aligned} \tag{4.20}$$

To calculate the largest of W_s we employ a variational approach using a coherent

state ansatz, thus we set $a = e^{i\gamma}\sqrt{n}$ and $a^\dagger = e^{-i\gamma}\sqrt{n}$. Then to extract the LD function we solve the Euler-Lagrange equations, $\partial W_s/\partial\gamma = 0$ and $\partial W_s/\partial n = 0$, the first of which yields

$$\begin{aligned} a &= \sqrt{n}\Big(e^{-|s|}N_{ex}\frac{\sin^2(\phi\sqrt{n+1})}{n+1}\Big)^{1/2}, \\ a^\dagger &= \sqrt{n}\Big(e^{-|s|}N_{ex}\frac{\sin^2(\phi\sqrt{n+1})}{n+1}\Big)^{-1/2}. \end{aligned} \tag{4.21}$$

Substituting these into W_s, see Eq. (4.20), we obtain a variational "free energy" function, $\mathcal{F}_s(n)$, which we minimize with respect to n to obtain an estimate for the desired LD function,

$$\theta_X(s) \approx -\min_s \mathcal{F}_s(n). \tag{4.22}$$

This minimization was performed numerically and a trajectory phase diagram was constructed from the estimated $\theta_X(s)$, see Fig. 4.5. This trajectory phase diagram shows that multiple first order transitions occur in both the quadrature activity and cavity occupation as we tune s and ϕ. These transition lines bend upon approaching $s = 0$, and the first transition line ends at the point $s \approx 0,\ \phi \approx 0.1$. This point was originally identified as the critical point which controlled the photon number dynamics [30], and highlights once again that quadrature trajectories may also capture features associated with the quantum jump trajectories. However in this case the critical point is much more masked compared to the quantum jump trajectory phase diagram, even within our crude approximation scheme. Furthermore there are several implicit assumptions and limitations associated with this diagonal approximation. Firstly it becomes less accurate at larger values of ϕ where nonlinearities in the operator W_s become more important. It also implicitly assumes a normal ordering and that the average of products of the raising and lowering operators may be replaced by the products of their individual averages.

However crude this approach may be it still predicts multiple first order transitions in both the quadrature trajectories and the cavity occupation number n.

4.3.2 Full Numerical Diagonalization

We will now examine the exact form of the LD function extracted via exact diagonalization [84] of $\mathbb{W}_s$. To do this it is necessary to truncate the basis of the system, in this problem the number basis $|n\rangle$ is the natural basis to use to construct the matrix form of $\mathbb{W}_s$. Since we have set $N_{ex} = 100$ we should be able to restrict the maximum photon number to $n = 150$ without losing too much information. The form of $\mathbb{W}_s$ introduces coherences between different number states and our choice of truncated basis must allow these to be conserved. However as $\mathbb{W}_s$ is an $n^2 \times n^2$ matrix it is necessary to implement further truncations and we truncate the basis such that only coherences between number states with occupation number differing by less than m ($m < n$) are kept. In practice the values of m and n were tested numerically so that the results were not sensitive to the truncation and in this work we found the values $m = 15$ and $n = 150$ to be sufficient. Having constructed the matrix W_s it was diagonalized using an Arnoldi iterative scheme [84, 121, 122] and the LD function was extracted.

From the extracted $\theta_X(s)$, numerical derivatives were used to determine the quadrature activity and the eigenmatrix ρ_s was used to determine the cavity occupation number. The full trajectory phase diagram is shown in Fig. 4.6(a) where we see multiple first order transition lines which accumulate at the critical point $s = 0, \phi \approx 0.1$. Beyond $\phi \approx 0.1$ the transition lines do not accumulate at $s = 0$ but instead bend upon approaching the zero trajectory bias line. Comparing Figs. 4.5 and 4.6(a) it is apparent that up to $\phi \approx 0.7$ the mean-field predicts the values at which the transitions occur quite accurately. Furthermore just as in the

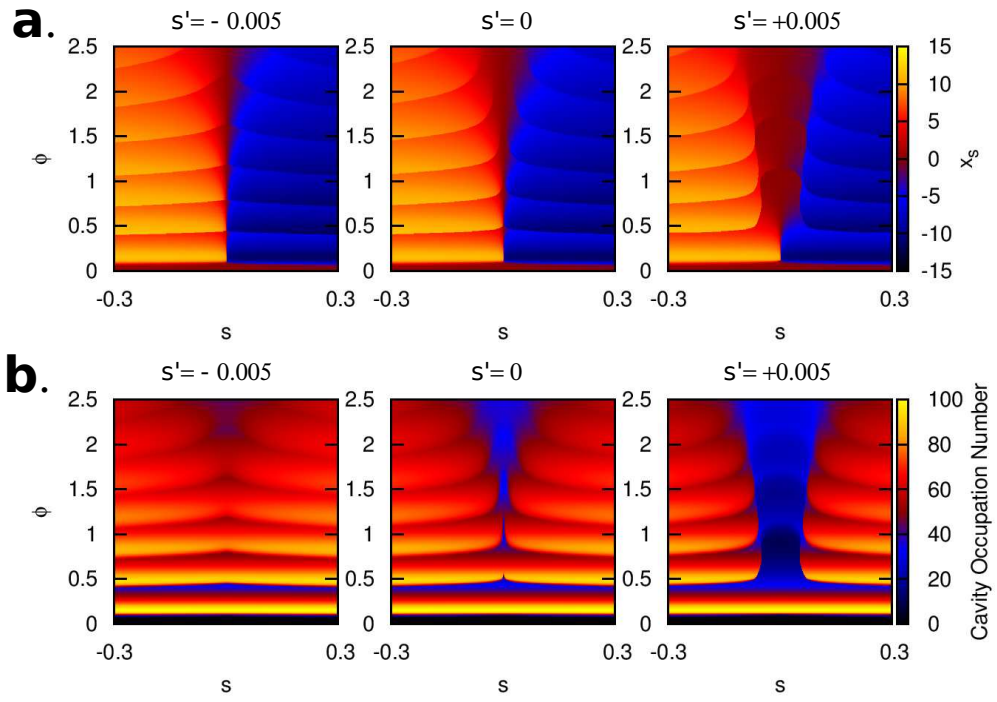

Figure 4.6: (a) Quadrature activity phase diagrams for various jump biased systems. In all cases there are multiple first order transition lines as we vary ϕ and s, which bend as they approach the origin which becomes more pronounced as the system is made more jump inactive. Comparing with the mean-field results there is good agreement up until $\phi \approx 0.7$, beyond which the agreement breaks down. (b) Cavity occupation number for doubly biased ensembles of trajectories. The transitions in the quadrature activity are marked by equivalent transitions in the cavity occupation. Furthermore bending of the transition lines approaching $s = 0$ correlates with the $s = 0$ dynamics possessing a lower occupation compared to the ensembles of rare trajectories.

quantum jump case these transitions correlate with the first order transitions in the cavity occupation number as shown in Fig. 4.6(b), clearly demonstrating that the cavity occupation number bistability manifests in the ensembles of quadrature trajectories [54].

We now examine the statistics of the quadrature trajectories having first placed the system in a higher or lower photon occupation state using the field s'. Depending on whether the system is in a higher ($s' < 0$) or lower ($s' > 0$) occupation state the first order transition lines either accumulate more at the $s = 0$ line or bend further away, respectively. This can be explained as follows, placing the system in a photon active phase ($s' < 0$) removes the low cavity number regions near $s = 0$, see Fig. 4.6(b), thus allowing the transition lines to accumulate closer to the $s = 0$ line. Conversely, making the system less active results in large low cavity number regions around $s = 0$ which "blow out" the transition lines as they approach $s = 0$, and ensures the cavity occupation number remains small unless s is large as seen in Fig. 4.6.

In this case although sharp crossovers occur in the quadrature activity, corresponding to crossovers in the cavity occupation, it is not clear that the physical $s = 0$ dynamics is composed of two distinct phases, one photon active the other photon inactive. This only becomes clear by examining the quantum jump trajectories [30], moreover the critical point also becomes more apparent when examining these trajectories. In conclusion both the quadrature and jump trajectories capture similar information, in contrast to the example of the two coupled two-level systems, but the information is much more readily gleaned from the latter trajectory ensemble.

We've now developed and studied the thermodynamics of trajectories formalism in both a classical stochastic setting and a series of open quantum systems. In

the next Chapter we will complete our study by examining the statistics of time-integrated observables in closed quantum systems taking inspiration from the thermodynamic approach of the previous Chapters. In particular we will focus on the example of the 1d transverse field quantum Ising model as it is analytically soluble and contains a wealth of physics.

5. Time-integrated Observables and the transverse field quantum Ising model

This Chapter focusses on providing a detailed exposition of analytical studies on singularities in the generating functions of time-integrated observables in closed quantum systems. In particular these analytics will focus on the long time functional form of these generating functions and the connection of singular features within said generating functions to a diverse set of concepts such as geometry [64], digital simulation using cold ion systems [56, 123, 124], $\mathcal{PT}$-symmetry breaking [68, 72] and dynamical phase transitions (DPTs) [64, 79]. To this end we focus on the TFIM throughout as it is both analytically soluble and is a paradigmatic model of a quantum phase transition [55]. This model consists of N spins and is described by the Hamiltonian

$$H = -\sum_i \sigma_i^z \sigma_{i+1}^z - \lambda \sum_i \sigma_i^x, \tag{5.1}$$

where, as usual, the operators $\sigma^{z,x}$ are Pauli spin operators and λ is the transverse field strength. In the thermodynamic limit there are two quantum critical points

at $\lambda = \pm 1$, where for $|\lambda| < 1$ the ground state is an ordered ferromagnetic state and for $|\lambda| > 1$ the ground state is a disordered paramagnet.

In the coming Sections we will examine the generating functions associated with the time-integrated transverse and longitudinal magnetization in the ground state of this model. We will begin with the former as it presents an analytically accessible form of the CGF thus allowing its singular points in the limit of long time and large system to be identified. We proceed to describe how one could use digital simulation in cold ion systems to experimentally probe such singular features. We then focus on the time-integrals of the longitudinal magnetization and find that the phase diagram, along the $s = 0$ axis, consists of two regimes where an appropriate $\mathcal{PT}$-symmetry of the deformed Hamiltonian, which forms the MGF, is either unbroken or broken. We demonstrate that the spontaneous breaking of this symmetry in the thermodynamic limit has a profound effect on the temporal behaviour of the cumulants of the time-integrated longitudinal magnetization, which may not be expected from the static properties of the ground state. The final Sections of this Chapter examine the properties of a set of appropriately normalized states which capture the singular features of the CGF of the time-integrated transverse magnetization. We discuss the geometric features of these states as characterized by the Berry phase [57] and Chern number [60]. We then perform a "quantum quench" on these states and find DPTs may emerge even far away from the quantum critical points.

5.1 Time-Integrated Transverse Magnetization

To examine the time integrals of the transverse magnetization we follow the formalism of Sec. 2.5.1 where the non-Hermitian H_s of Eq. (2.67) is defined using

the TFIM H and $q = \sum_i \sigma_i^x$. We are interested specifically in the statistics of $\int^t dt' \sum_i \sigma_i^x(t')$ in the ground state $|0\rangle$ of H at a fixed value of λ; we also recall $\sigma_i^x(t') \equiv e^{iHt}\sigma_i^x e^{-iHt}$. To examine the statistics of this time-integrated observable we need to evaluate the MGF, $Z(s,t)$, of the time-integrated magnetization. To do this we evaluate the expectation value shown in Eq. (2.68) using the ground state $|0\rangle$ of H at fixed value of λ and where $H_s \equiv H - \frac{is}{2}q$ is also at this same value of λ. We note that although this procedure formally constitutes a nonequilibrium evolution of $|0\rangle$ under $e^{-iH_s t}$ the quantities of interest are expectation values in the equilibrium ground state at λ. One may diagonalize the non-Hermitian H_s via a Jordan-Wigner transformation followed by a Bogoliubov rotation [55], which maps the spin Hamiltonian H_s to a free fermion model with a complex dispersion $\epsilon_k(s) = 2\sqrt{(\lambda + \frac{is}{2} - \cos k)^2 + \sin^2 k}$. In this Section we focus on the case where N is even and the boundary conditions are periodic. The quasi-particle wavevectors k are discrete and are given by $k = \pi n/N$, where $n = -N+1, -N+3, \ldots, N-1$. In its diagonal form $H_s = \sum_k \epsilon_k(s)(\bar{A}_k A_k - 1/2)$, which is slightly different from the diagonal form of the standard Ising model H as H_s is not Hermitian. This difference is reflected in the pair $(\bar{A}_k, A_k)$ which obey canonical fermionic commutation relations, $\{\bar{A}_{k'}, A_k\} = \delta_{k',k}$, but are not Hermitian conjugate $\bar{A}_k \neq A_k^\dagger$.

The initial ground state $|0\rangle$ of the unperturbed TFIM, i. e. $H_{s=0}$, may be expressed as a BCS state of H_s

$$|0\rangle \propto \bigotimes_{k>0} \left[\cos\alpha_k^s |0_k, 0_{-k}\rangle_s - i \sin\alpha_k^s |1_k, 1_{-k}\rangle_s\right]. \tag{5.2}$$

The symbol $\bigotimes$ stands for the direct product and the k-mode vacuum of H_s is $|0_k, 0_{-k}\rangle_s$ which is annihilated by the operators $A_{\pm k}$, $A_{\pm k}|0_k, 0_{-k}\rangle_s = 0$. The state $|1_k, 1_{-k}\rangle_s$ is a state occupied by a pair of fermions at wavevectors $\pm k$ and is generated from the vacuum state via $\bar{A}_k \bar{A}_{-k}|0_k, 0_{-k}\rangle_s = |1_k, 1_{-k}\rangle_s$. The complex angles α_k^s are equal to half the difference of the Bogoliubov angles, ϕ_k^s and $\phi_k^{s=0}$, used to diagonalize the unperturbed Hamiltonian and H_s. These Bogoliubov angles

are fixed such that H and H_s contain no "off-diagonal" terms in this free fermion picture and hence are given by $\tan\phi_k^s = \sin k/[\lambda + \frac{is}{2} - \cos k]$. Combined with the BCS form of Eq. (5.2) the full MGF (see Eq. (2.68)) may be evaluated directly,

$$\begin{aligned} Z(s,t) = \prod_{k>0} \quad & \left(|\cos\alpha_k^s|^2 \cosh\left[2\mathrm{Im}(\alpha_k^s)\right] e^{-2\mathrm{Im}(\epsilon_k^s)t} \right. \\ & + |\sin\alpha_k^s|^2 \cosh\left[2\mathrm{Im}(\alpha_k^s)\right] e^{2\mathrm{Im}(\epsilon_k^s)t} \\ & + \mathrm{i}\sin\alpha_k^s \cos\alpha_k^{-s} \sinh\left[2\mathrm{Im}(\alpha_k^s)\right] e^{-2\mathrm{iRe}(\epsilon_k^s)t} \\ & \left. - \mathrm{i}\sin\alpha_k^{-s} \cos\alpha_k^s \sinh\left[2\mathrm{Im}(\alpha_k^s)\right] e^{2\mathrm{iRe}(\epsilon_k^s)t} \right). \end{aligned} \tag{5.3}$$

Taking the logarithm the product over k becomes a sum and in the long time limit we find that the scaled CGF as defined in Eq. (2.70) is determined by the imaginary components of the complex energy spectrum,

$$\begin{aligned} \theta(s) &= \lim_{N,t\to\infty} \frac{\Theta(s,t)}{Nt} \\ &= \lim_{N\to\infty} \frac{2\sum_{k>0} |\mathrm{Im}\epsilon_k(s)|}{N} = \frac{1}{\pi}\int_0^\pi |\mathrm{Im}\epsilon_k(s)| dk. \end{aligned} \tag{5.4}$$

Above we used the identity $\frac{1}{N}\sum_{k>0} = \frac{1}{2\pi}\int dk$ which is valid in the limit $N \to \infty$. We note that the sign of imaginary part of the complex energy changes at a critical wavevector k_λ which is set by the transverse field strength, $k_\lambda = \cos^{-1}\lambda$. Using this fact we can evaluate the integral directly and after some algebra we find

$$\theta(s) = \begin{cases} \frac{4}{\pi}\mathrm{Im}\left[(1+\lambda_s)\ E\left(\frac{2\sqrt{\lambda_s}}{1+\lambda_s}\right)\right], & (\lambda, s) \notin \mathcal{D} \\ \frac{4}{\pi}\mathrm{Im}\left\{(1+\lambda_s)\left[-E\left(\frac{2\sqrt{\lambda_s}}{1+\lambda_s}\right)\right.\right. & \\ \qquad \left.\left. +2E\left(\frac{\pi-k_\lambda}{2}, \frac{2\sqrt{\lambda_s}}{1+\lambda_s}\right)\right]\right\}, & (\lambda, s) \in \mathcal{D} \end{cases} \tag{5.5}$$

where $\lambda_s = \lambda + is/2$, $E(x)$ and $E(\varphi, x)$[1] are complete and incomplete elliptic integrals of the second kind respectively, for a derivation of $\theta(s)$ see Appendix C.

[1]Formally the incomplete elliptic integral of the second kind is: $E(\varphi, k) = \int_0^\varphi \sqrt{1 - k^2\sin^2\alpha}\ d\alpha$. Taking the limit $\varphi \to \pi/2$ we obtain the complete elliptic integral of the second kind.

The region $\mathcal{D}$ is defined as the interior of a circle in the (λ, s) plane,

$$\lambda^2 + (s/2)^2 = 1. \tag{5.6}$$

Moreover it is worth noting we consider only $s > 0$ as $\theta(s) = \theta(-s)$, see Eq. (5.4). The long time properties of the MGF in the thermodynamic limit are encoded within this function $\theta(s)$ and through it the behaviour of the cumulants of the time-integrated transverse magnetization [56]. Although this function is not necessarily a LD function and therefore not necessarily convex, as described in Sec. 2.5.1, our approach is inspired by the thermodynamic formalism and so we examine the analytic properties of $\theta(s)$ to define the *full counting statistics (FCS) phases* of the system. To this end we define a dynamical order parameter $\kappa_s \equiv -\theta'(s)$ and a corresponding susceptibility $\chi_s \equiv \theta''(s)$ to identify and distinguish different FCS phases.

As previously mentioned the imaginary part of $\epsilon_k(s)$ changes sign at $k = k_\lambda$, this manifests itself as a transition line in the (λ, s) plane which separates the region $\mathcal{D}$ from the rest of the plane. Therefore for each $|\lambda| < 1$ there exists a wavevector k_λ and transition s value $s_c = 2 \sin k_\lambda$. Approaching the transition line from inside $\mathcal{D}$ the order parameter κ_s is continuous while the corresponding susceptibility diverges with a square-root singularity at s_c, $\chi_s \propto |s - s_c(\lambda)|^{-1/2}$. The only exception to this is at the endpoints of the FCS singularities, i. e. when we are at the static quantum critical points $(\lambda, s) = (\pm 1, 0)$, where the divergence is logarithmic in nature. The corresponding FCS phase diagram is shown in Fig. 5.1(a) along with slices of κ_s and χ_s in Fig. 5.1(b,c).

To gain further insight into the nature of these FCS phases we define the long time state $|s\rangle \equiv \lim_{t\to\infty} T_t(s)|i\rangle$, with an appropriate normalization. We refer to this class of states as the s-states and in this Chapter we consider the initial state $|i\rangle$ to be the ground state $|0\rangle$, however in the long time limit $|s\rangle$ is usually

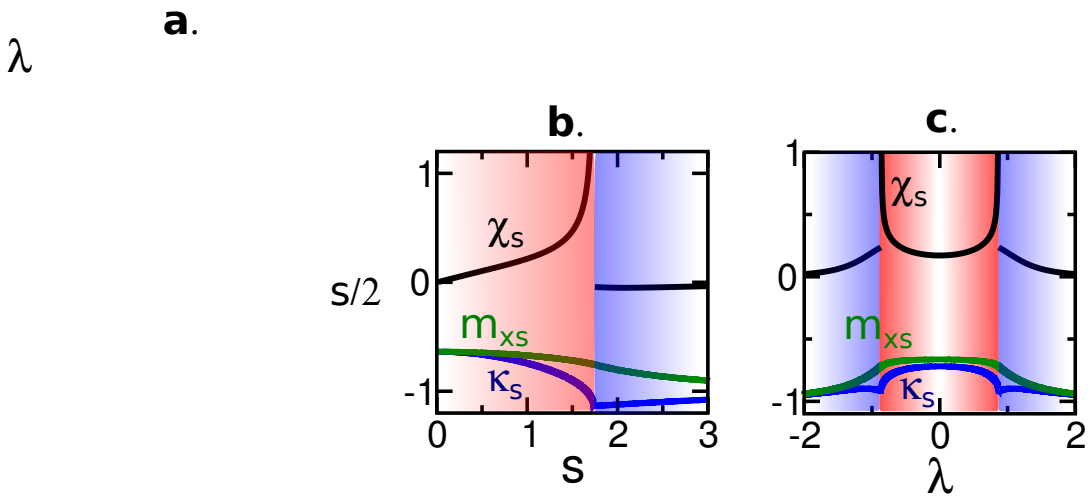

Figure 5.1: (a) FCS phase diagram of the TFIM with the time-integrated transverse magnetization as the observable of interest. A line of second order phase transitions in $\theta(s)$ separate the dynamically ordered and disordered phases. The black circles on the λ axis indicate the locations of the static quantum critical points while the regions I, II and III are defined by the structure of $|s\rangle$ (see main text). The yellow dashed lines indicate the cuts plotted in the subsequent panels. (b) The dependence on s for fixed λ of the order parameter κ_s (blue) and the corresponding susceptibility χ_s (black) which diverges at the FCS transition line when approached from inside $\mathcal{D}$. Also shown is the static magnetization m_{xs} as function of s, this is directly related to $\theta(s)$ (see main text). (c) The same as (b) but now with fixed s and varied λ.

independent of the initial state. The expectation value of an observable $\mathcal{O}$ in these states is then given by $\langle\mathcal{O}\rangle_s \equiv \lim_{t\to\infty} Z_t^{-1}(s)\langle 0|T_t^\dagger(s)\mathcal{O}T_t(s)|0\rangle$. Using the definitions of $\theta(s)$ and $|s\rangle$ it is very easy to show that for the operator of interest q, the s-biased expectation is related to the long time CGF via $\langle q\rangle_s = -\theta(s)/s$. It follows immediately from this that derivative of the *static* susceptibility in this s-state diverges at the transition line in the same manner as χ_s, therefore the 2nd order FCS transition corresponds to a 3rd order static phase transition in the $|s\rangle$ states [56, 64]. Using the BCS representation of the initial vacuum and then applying the operator $T_t(s)$ we find the state $|s\rangle$ in the long time limit, up to constants, is given by

$$|s\rangle = \bigotimes_{k>0} |s_k\rangle \tag{5.7}$$
$$\propto \begin{cases} \bigotimes_{k>0} |1_k, 1_{-k}\rangle_s & \lambda > 1, \\ \bigotimes_{k<k_\lambda} |0_k, 0_{-k}\rangle_s \bigotimes_{k>k_\lambda} |1_k, 1_{-k}\rangle_s & -1 < \lambda < 1, \\ \bigotimes_{k>0} |0_k, 0_{-k}\rangle_s & \lambda < -1. \end{cases}$$

In our case q is the total transverse magnetization $m_{xs} = N^{-1}\sum_i \langle\sigma_i^x\rangle_s$ which combined with the $|s\rangle$ state form in Eq. 5.7 we find

$$\begin{aligned} m_{xs} &= \frac{1}{N}\sum_{\mathrm{Im}(\epsilon_k^s)<0}\left(1 - \frac{2\left|\sin\left(\frac{\phi_k^s}{2}\right)\right|^2}{\cosh[2\mathrm{Im}(\alpha_k^s)]}\right) \\ &+ \frac{1}{N}\sum_{\mathrm{Im}(\epsilon_k^s)>0}\left(1 - \frac{2\left|\cos\left(\frac{\phi_k^s}{2}\right)\right|^2}{\cosh[2\mathrm{Im}(\alpha_k^s)]}\right), \end{aligned} \tag{5.8}$$

this quantity is shown in Fig. 5.1(b,c). For all values of (λ, s) we may define such a $|s\rangle$ state, the states inside and outside the region $\mathcal{D}$ are smoothly connected

but these states change in a singular fashion on crossing the FCS phase boundary. We denote these two regions *dynamically ordered* and *dynamically disordered* respectively, as the spectrum of H_s is smoothly connected to that of the original TFIM which define the static ordered and disordered phases, this is shown in Fig. 5.1(a). Furthermore standard complex analysis results, i. e. Darboux's theorem [111, 112], imply that the cumulants of the time-integrated magnetization Q_t are affected by the analytic properties of the CGF as a function of s. Formally we may appeal to the Hadamard factorization theorem to express the MGF in terms of its zeros in the complex s plane. Thus to understand the impact of the FCS transition line on the cumulants at $s = 0$ it is necessary to determine the location of all the transition points in the *complex* s plane. To do this we apply simple shift of variable $s \to s + i\bar{s}$ and immediately uncover a new transition surface in the $(\lambda, s, \bar{s})$ volume defined by

$$(\lambda - \frac{\bar{s}}{2})^2 + (\frac{s}{2})^2 = 1. \tag{5.9}$$

From this we see there is always a singularity, which lies on the imaginary s axis, related to the static critical point $\lambda_c = \pm 1$ for *all values* of λ. To complete our discussion we examine the cumulants $\langle\langle Q_t^n \rangle\rangle$ in both the ordered and disordered regime to determine the impact of the FCS transition line on their behaviour. In Fig. 5.2 we show the FCS phase diagram and take the two $\lambda = 0.01$ and $\lambda = 1.99$. These are equidistant from the static critical point and so the closest $\bar{s}_c$ transition points are equidistant to the $s = 0$ axis. One might naively expect that the cumulants would behave in a similar fashion, however for $\lambda = 0.01$ their exists a second dominant FCS transition point at nonzero s_c. This singularity makes the corresponding cumulants[2] very different [53, 64, 100], as shown in Fig. 5.2(b,d)

[2]We note that the cumulants were calculated by taking the logarithm of Eq. (5.3) and Taylor expanding each term in the resulting sum in powers of s. Differentiating each term in the sum with respect to $-s$, and setting $s = 0$, we resum the results to obtain the desired cumulants.

where the cumulants are plotted for 200 spins with periodic boundary conditions. Moreover the ratio of the cumulants at long times should be influenced by these singular features for $|\lambda| < 1$.

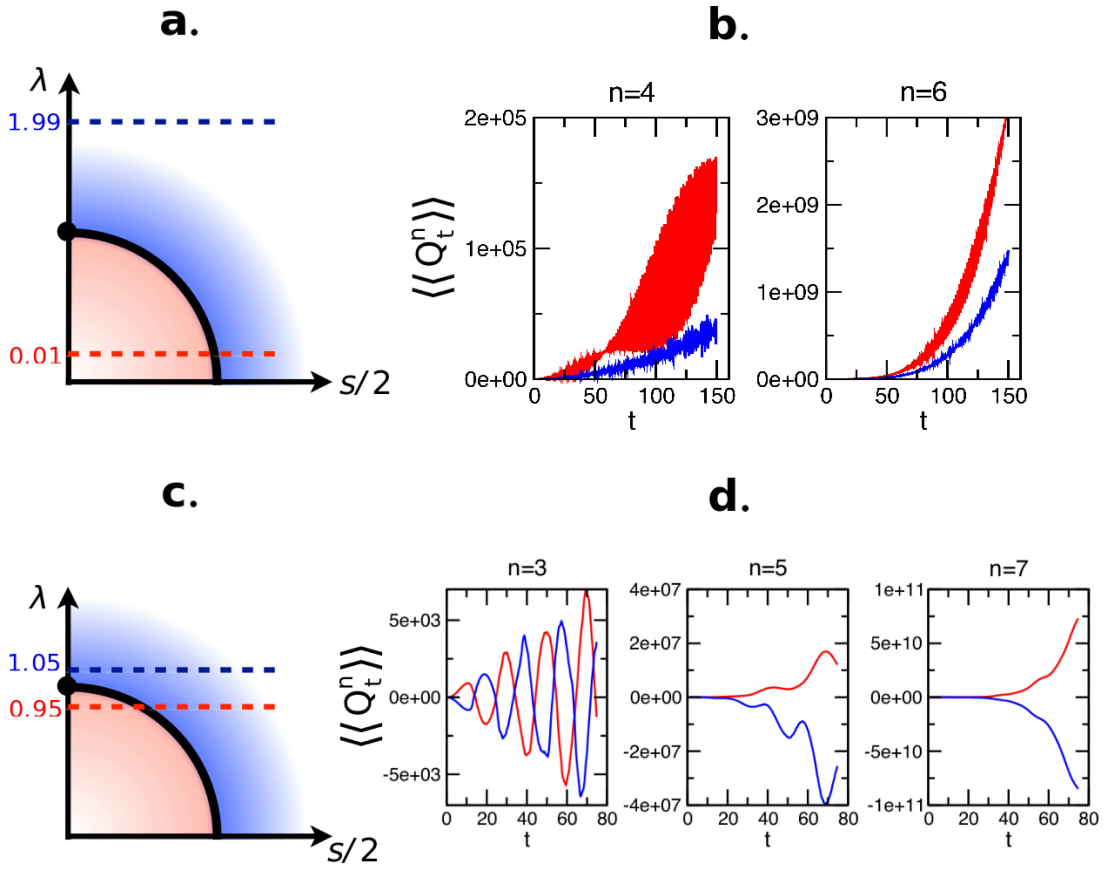

Figure 5.2: (a,b) The state points $\lambda = 0.01, 1.99$ are equidistant from the static singularity but the presence of an FCS singularity at $s_c \neq 0$ for $\lambda < 1$ implies their cumulants $\langle\langle Q_t^n \rangle\rangle$ are different. (c,d) The same as before but $\lambda = 0.95, 1.05$, the odd cumulants of Q_t for $\lambda < 1$ have opposite sign to the same cumulants at $\lambda > 1$ indicating that the fluctuation behaviour is very different.

Taking another two λ values close to static quantum critical point, $\lambda = 0.95$ and $\lambda = 1.05$. The correlation length of the ground state for both of these λ values is very similar, however in one instance the dominant $\bar{s}_c$ is positive and in the latter it is negative. This suggests that the cumulants at both these values are of

a similar magnitude but are out-of-phase with each other. Plotting the cumulants for $n = 3, 5, 7$ this is indeed the case, reflecting the *dynamically ordered/disordered* phase structure where for $|\lambda| < 1$ the fluctuations are of opposite sign to $|\lambda| > 1$. Due to the number of transition points it is difficult to resolve the exact effects of the FCS singularities on the cumulants in the ground state of the TFIM but we have shown at least qualitatively that some differences in behaviour may not be solely expected from knowledge of the statics of the system. Moreover using this non-Hermitian approach to FCS we will now show how one could potentially probe these singular features using a cold ion system.

5.2 Open Quantum Systems and Digital Simulation

The main barrier to experimentally probing or simulating the FCS singularities described in the previous Section stems from the non-Hermitian nature of the perturbation to the system of interest. In tackling this problem the key step is to consider the temporal evolution of the density matrix $\rho(t)$ generated by H_s, $\dot{\rho}(t) = -i[H, \rho(t)] - \frac{s}{2}\{q, \rho(t)\}$. As we now demonstrate, this evolution shows that one may obtain the MGF $Z(s, t)$ for the time-integrated observable Q_t from the waiting time distribution of an auxiliary open system and furthermore that any singular features of the FCS emerge as singularities in the waiting time distribution [39, 40]. Effectively this evolution equation is that of a full Lindblad Master equation, see Eq. (2.53), but without the recycling terms $\sum_i \gamma_i L_i \rho L_i^\dagger$. Given an observable of interest q we identify a set of jump operators L_i defined by $\sum_i L_i^\dagger L_i = q$ along with the decay rates $\gamma_i = s, \forall i$. The associated non-unitary evolution operator $T_t(s)$ is then the same operator which evolves the associated open system in between quantum jump events, thus $Z(s, t)$ equals the probability that no jumps have

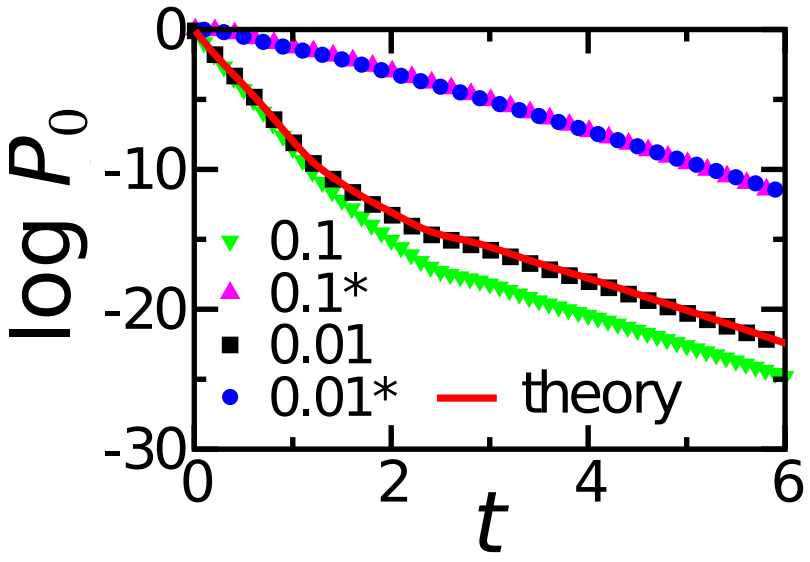

Figure 5.3: Comparison of numerical simulations of $P_0(t)$ with theory for a 6 spin Ising chain prepared in the ground state prepared at $\lambda = \cos(5\pi/6)$ for dimensionless time steps of length 0.1 and 0.01. The simulations marked with the label $*$ indicate equivalent simulations with the system initialized in $|-\rangle$.

occurred up to a time t in the auxiliary open system, $P_0(t)$.

In general this probability decays exponentially [125] in the long time limit supporting the scaling used in Eq. (2.70) for the closed problem. Therefore the MGF, and hence the FCS singularities, may be probed by preparing the system in an initial state and coupling the system to an appropriate Markovian environment. For the case of the TFIM and the time-integrated transverse magnetization to identify the appropriate environment we make a trivial shift in the observable of interest, $q = \sum_i(\sigma_i^x + 1)$. We then identify a set of quantum jump operators $L_i = \sqrt{2}|-\rangle_i\,{}_i\langle +|$ where $\sigma_i^x|\pm\rangle = \pm|\pm\rangle$, and i runs over the lattice. This auxiliary open system may be experimentally probed using the digital simulation techniques developed in cold ion systems [123, 124]. To simulate this open system we use an ancillary ion and Trotter decompose the time evolution of the system plus ancilla state, $|\psi\rangle_s \otimes |A\rangle_a$, into a series of unitary transformations each with a time step

δt. Each time step in this simulation is given by

$$\prod_{l=1}^{n_\diamond} G_l \prod_{k=1}^{N} e^{-i\sigma_k^z \sigma_{k+1}^z \delta t} \prod_{j=1}^{N} e^{-i\lambda\sigma_j^x \delta t} |\psi\rangle_s \otimes |0\rangle_a, \tag{5.10}$$

where the two most right operator terms evolve the system according to the two-body and single body operations of the TFIM's H and only act on the system subspace. In contrast the gate operations G_j act on the Hilbert space spanned by the system spin j and the ancilla. Preparing the two level ancilla initially in the state $|0\rangle_a$ these gate operations are defined as

$$\begin{aligned} G_j|+\rangle_j \otimes |0\rangle_a &= \cos\phi|+\rangle_j \otimes |0\rangle_a - i\sin\phi|-\rangle_j \otimes |1\rangle_a, \\ G_j|-\rangle_j \otimes |0\rangle_a &= |-\rangle_j \otimes |0\rangle_a, \end{aligned}$$

where the angle $\phi = \sqrt{2s\delta t}$. For $\phi \ll 1$, and small δt, the exponentials in Eq. (5.10) may be expanded and upon tracing out the ancilla ion it is easy to see that the evolution described by these unitary transformations is the desired Lindblad equation [126], at least to first order in δt. After each application of a gate G_j one measures the ancilla state in the $\{|0\rangle_a, |1\rangle_a\}$ basis; if the ancilla is in the $|1\rangle_a$ state a quantum jump has occurred and the system is reset and the experiment repeated. The upper limit on the final product of Eq. (5.10) is $n_\diamond = N$ for all the steps prior to a jump and for the final step it is $\leq N$, as the ancilla was measured in the state $|1\rangle_a$ after one of the gate operations. Repeating this experiment many times $P_0(t)$ can be estimated and hence the $Z(s,t)$ may be extracted at various s by tuning the decay rates for the dissipative dynamics [56].

Using this Trotter decomposition the $P_0(t)$ extracted from the digital simulations are shown in Fig. 5.3, and match the theoretical values indicating the survival probability can be found accurately at finite t. To study the longer time behaviour of $P_0(t)$ it is necessary to initialize the spins in the $|-\rangle$ state in place of the ground state $|0\rangle$. This state is annihilated by the jump operators and so $P_0(t)$ decays at a slower rate with increasing t, thus each experiment can run for longer with a

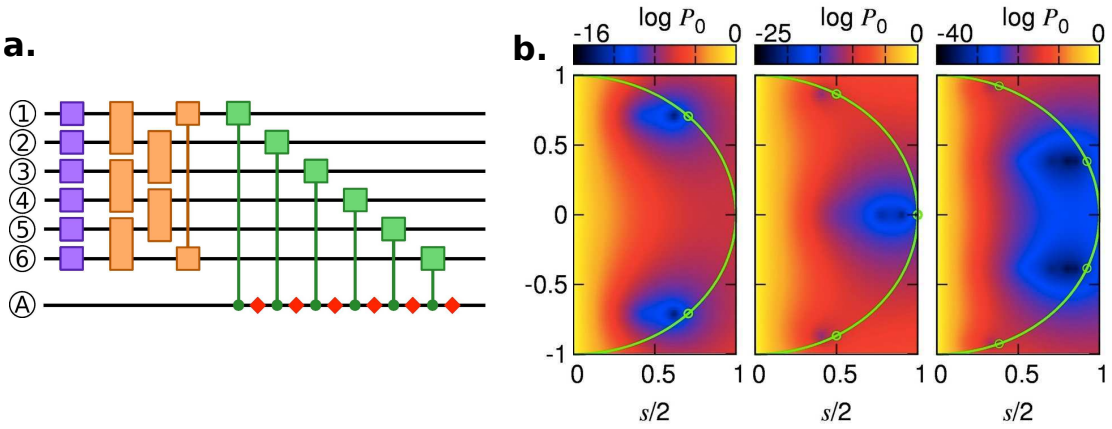

Figure 5.4: (a) These are the world lines of seven ions used to simulate an open 6 spin Ising ring for a single time step. The single spin operations (blue squares) capture the effects of the transverse field while the exchange interaction is simulated using two-ion gate operations (orange squares), together these simulate the coherent evolution. The dissipative dynamics require a two-ion gate which acts on the ancilla ion (green squares), where measurement on the ancilla (red diamonds) determine whether or not a quantum jump has occurred. (b) Simulations of the survival probability ($P_0(t)$) as a function of λ and $s/2$ for $4, 6$, and 8 ion Ising chains at $t = 5, 5$ and 8 respectively, with the system initialized in $|-\rangle$. The unit circle is marked with green overlays and circles at $(\lambda, s) = (\cos k, 2 \sin k)$ mark where features of the FCS transitions would be expected to be seen.

smaller chance of being terminated by the first quantum jump. Figure 5.4 shows the results of these simulations for small system sizes, $N = 4, 6, 8$, and times. Even within this small system size short time regime signatures of the singular features are observed, these lie close to the unit circle at positions $(\lambda, s) = (\cos k, 2 \sin k)$ where k are the wavevectors used to diagonalize the TFIM for finite N.

5.3 $\mathcal{PT}$-symmetry breaking

5.3.1 Theoretical Background

Standard formulations of quantum mechanics state that all observables, in particular the Hamiltonian, are Hermitian i. e. $H^\dagger = H$. This ensures that the outcomes of measurements are *real* (i. e. the operator spectra are real) and naturally this has implications on the dynamics, which are generated by H. However the requirement of a real spectrum implies there could in principle be systems which are described by *non-Hermitian* Hamiltonians. In the last decade, since the seminal work of Bender et al. [65], much interest has arisen in such Hamiltonians and their symmetry properties [66–71]. In this Section we focus on a particular class of non-Hermitian Hamiltonians which have real spectra and are symmetric under a particular space-time reflection. These Hamiltonians are symmetric under the application of a time-reversal operator $\mathcal{T}$ followed by a parity operation $\mathcal{P}$ and so are dubbed $\mathcal{PT}$-symmetric, this symmetry is more precisely defined as

$$[\mathcal{PT}, H] = 0. \tag{5.11}$$

For a given system there exist many $\mathcal{PT}$ operators all of which satisfy the properties that $\mathcal{T}$ is anti-linear [127] and $(\mathcal{PT})^2 = 1$. Together with Eq. (5.11) these conditions allow one to reformulate quantum mechanics using this new class of non-Hermitian operators without violating any of the original axioms of the theory. It is worth noting that originally the $\mathcal{PT}$ operator was taken to be a spatial reflection ($\boldsymbol{x} \to -\boldsymbol{x}$) combined with a time-reversal (i. e. complex conjugation). Now although $\mathcal{PT}$ commutes with the non-Hermitian operator its *eigenvectors* may be different to those of H. To see this we consider an eigenstate $|\phi\rangle$ of $\mathcal{PT}$

with a corresponding eigenvalue λ_0. From the properties of $\mathcal{PT}$ and $\mathcal{T}$ it follows directly that

$$\begin{aligned} |\phi\rangle &= (\mathcal{PT})\lambda_0|\phi\rangle \\ &= \lambda_0^*\lambda_0|\phi\rangle. \end{aligned} \tag{5.12}$$

This implies that $|\lambda_0|^2 = 1$ and thus the eigenvalue is simply a phase $\lambda_0 = e^{i\alpha}, \alpha \in \mathbb{R}$. We now consider $|\phi\rangle$ to also be an eigenstate of the non-Hermitian H with corresponding energy E, once again it is straightforward to show

$$E\lambda_0|\phi\rangle = E^*\lambda_0|\phi\rangle. \tag{5.13}$$

As λ_0 is a nonvanishing phase factor this implies that the energy E is real. If however $|\phi\rangle$ is not a simultaneous eigenstate of $\mathcal{PT}$ and H this conclusion breaks down and the energy E is in general *complex* with eigenvalues appearing in complex conjugate pairs. We refer to this case as the $\mathcal{PT}$-symmetry *broken* regime of H, conversely when the spectrum of H is real we describe the symmetry as being *unbroken*. It is important to highlight that the exact form of the $\mathcal{PT}$ operator is not specific, it is only required to obey the properties of anti-linearity and $(\mathcal{PT})^2 = 1$. Therefore when examining the spectral properties of a non-Hermitian Hamiltonian it is necessary to examine all potential $\mathcal{PT}$-symmetries and check if they are broken or unbroken to determine if the spectrum is real or complex. The connection to our work should be apparent, as the MGF $Z(s,t)$ is determined by the non-Hermitian H_s the spectral characteristics of H_s will naturally have a large impact on the cumulants of our time-integrated observables. We will demonstrate this explicitly throughout the remainder of this Section, beginning with warm-up example of single spin before studying the many-body TFIM.

5.3.2 Simple Example: Single Spin

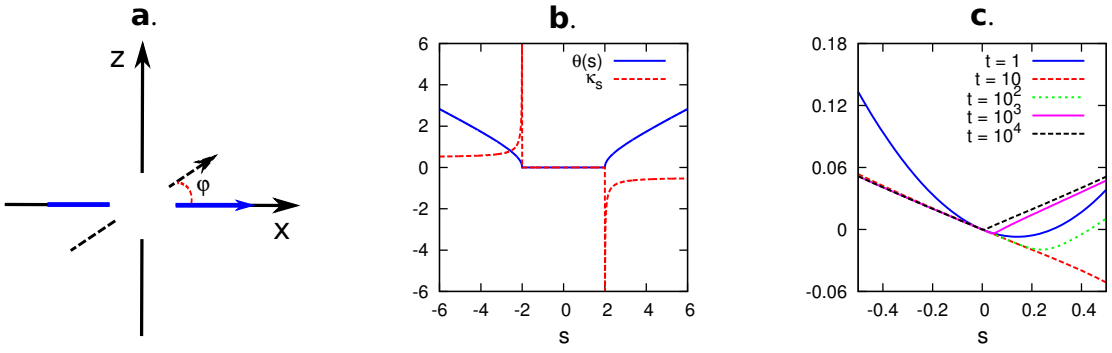

Figure 5.5: (a) Schematic diagram of a single spin which precesses about the x-direction, the time-integrated magnetization of interest is at angle φ with respect to the x-direction. (b) Time-integrated transverse magnetization (lies along z-direction, $\varphi = \pi/2$) for $\epsilon = 1$, the CGF $\theta(s)$ is zero for $|s| \leq 2$ and nonzero everywhere else. The breaking of the $\mathcal{PT}$-symmetry of H_s manifests as singularities in the CGF at $s = \pm 2$ and discontinuities in κ_s. Note we've assumed the initial state has non-zero overlap with the eigenstates of H_s, i. e. $c_\pm(s)$ in Eq. (5.17), are non-zero. (c) In the regime where H_s does not possess a $\mathcal{PT}$-symmetry ($\varphi \neq \pi/2$, here we take $\varphi = 0.1$) a singularity emerges at $s = 0$ in the scaled CGF in the long time limit. In this parameter regime the emergence of such a singularity is generally independent of the initial state (in this plot the system was initialized in $\frac{4}{5}|\uparrow\rangle + \frac{3}{5}|\downarrow\rangle$).

We apply the theoretical background discussed in the previous Subsection to a toy example of a single spin described by the Hamiltonian

$$H = \epsilon \sigma^x. \tag{5.14}$$

Following the prescription of Section 2.5.1 we examine the time-integrated magnetization in the $x - z$ plane, i. e. $q = \sigma^x \cos\varphi + \sigma^z \sin\varphi$, by perturbing H to

obtain

$$H_s = \epsilon\sigma^x - \frac{is}{2}(\sigma^x \ \cos\varphi + \sigma^z \ \sin\varphi). \tag{5.15}$$

This non-Hermitian Hamiltonian was originally discussed in a different context [68] but here we discuss the impact its spectrum has on the time-integrated magnetization of the original model defined by H. This operator is easily diagonalized and has eigenvalues $E_\pm = \pm\frac{1}{2}\sqrt{4\epsilon^2 - s^2 - 4is\epsilon\cos\varphi}$. Furthermore one can readily identify a $\mathcal{PT}$-symmetry, where the $\mathcal{PT}$ operator is composed of a parity operator $\mathcal{P} = \sigma^x$ and $\mathcal{T}$ is simply complex conjugation. We begin by examining the time-integrated transverse magnetization ($\varphi = \pi/2$), in this case the eigenvalues simplify to

$$E_\pm = \pm\frac{1}{2}\sqrt{4\epsilon^2 - s^2}. \tag{5.16}$$

From this we see that provided $4\epsilon^2 \geq s^2$ the eigenvalues of H_s are real and we are in the $\mathcal{PT}$ *unbroken* regime. Using this property of the spectrum it is easy to formally write down the MGF $Z(s,t)$, see Eq. 2.68, and to show that the cumulants of the time-integrated magnetization in the z-direction oscillate in time. This implies the temporal scaling of these cumulants is sublinear at long times and thus the scaled CGF is $\theta(s) = 0$. The picture changes dramatically when $4\epsilon^2 < s^2$ and we are in the $\mathcal{PT}$-symmetry *broken* regime, in this case the eigenvalues form complex conjugate pairs, and the MGF is

$$Z_t(s) = c_+(s)e^{2\mathrm{Im}(E_+)t} + c_-(s)e^{2\mathrm{Im}(E_-)t}. \tag{5.17}$$

The terms $c_\pm(s)$ are given by the overlaps of the initial state with the left and right eigenstates of H_s. Depending on the *sign* of s the MGF in the long time is dominated either by the imaginary part of E_+ or E_-. From Eq. (5.17) it is clear

that for finite s the MGF will grow exponentially with t in the long time limit and $\theta(s)$ will be finite.

Applying the thermodynamic approach we examine $\theta(s)$ along with the dynamical magnetization $\kappa_s = -\theta'(s)$ as a function of s. Within the *unbroken* regime, $\varphi = \pi/2$, both the dynamical free energy and dynamical magnetization are zero. Tuning s we may break the $\mathcal{PT}$-symmetry of H_s, leading to a square-root singularity in $\theta(s)$ at $s = \pm 2\epsilon$ and a corresponding diverging κ_s, this is shown in Fig. 5.5(b). Considering the time-integrated magnetization along a direction other than the z-axis, the energy eigenvalues $E_\pm$ always appear in complex conjugate pairs and the $\mathcal{PT}$-symmetry is broken $\forall s$. Examining the scaled CGF $\Theta(s,t)/t$ as a function of time we find a singularity emerges at $s = 0$ in the long time limit, see Fig. 5.5(c).

This singularity is due to the sign of s determining which eigenvalue dominates $Z(s,t)$ in the long time limit. This singularity implies that the cumulants grow faster than t in the long time limit. Furthermore due to the relationship to the survival probability in an associated open quantum system, see Sec. 5.2, we know the scaling in Eq. (2.70) is correct for $s \neq 0$, however the limits $t \to \infty$ and $s \to 0$ do not necessarily commute which manifests as this singularity.

Thus with this toy example we have demonstrated that using the counting field s one may break the $\mathcal{PT}$-symmetry of a problem and this can manifest itself in the dynamical order parameter κ_s. In this case κ_s diverges upon breaking the symmetry but as the problem is single-body in nature this cannot be attributed to any type of FCS phase transition. We also note that the breaking of the $\mathcal{PT}$-symmetry may impact the temporal scaling of cumulants at $s = 0$, and due to the many $\mathcal{PT}$ operators and time-integrated observables (Q_t) we can "count" in a given system, we expect these results to have a broad range of applicability. In the next Section we return to the many-body problem previously considered,

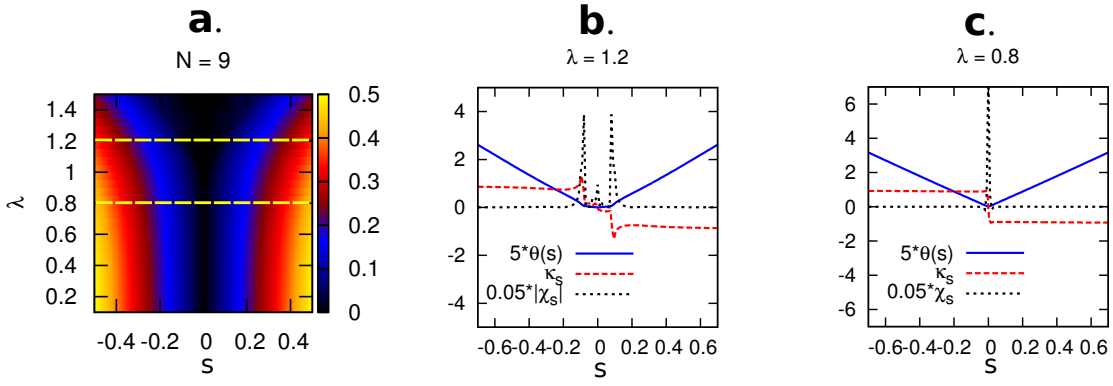

Figure 5.6: (a) Color density plot of the scaled CGF $\theta(s)$ in the (λ, s) plane for $N = 9$ spins. In the disordered regime $\lambda > 1$, there is a large region where $\theta(s) \approx 0$. (b,c) Plots of the scaled CGF along with dynamical order parameter and susceptibility as a function of s for $\lambda = 0.8$ and 1.2 for a system of 11 spins. In the ferromagnetic (ordered) regime there is a large peak in the susceptibility at $s = 0$, indicative of the cumulants scaling faster than t. In the paramagnetic regime the CGF is ~ 0 at $s = 0$, but tuning s the $\mathcal{PT}$-symmetry can be broken and the CGF will acquire a finite value, this is marked by peaks in χ_s.

the TFIM, but now focus on the properties of the time-integrated longitudinal magnetization and the connection to $\mathcal{PT}$-symmetry breaking.

5.4 Time-Integrated Longitudinal Magnetization

In this Section we return to the TFIM, and for simplicity rewrite its Hamiltonian in the form

$$H = -\sum_i \sigma_i^x \sigma_{i+1}^x - \lambda \sum_i \sigma_i^z, \tag{5.18}$$

the only difference between this and Eq. (5.1) is a rotation in the $x-z$ plane which maps $(\sigma_i^z, \sigma_i^x) \to (-\sigma_i^x, \sigma_i^z)$. Rather than consider the cumulants of the time-

integrated transverse magnetization as in Sec. 5.1 we instead focus on the time-integrated longitudinal magnetization $q_t = M_t^x \equiv \int_0^t \sum_i \sigma_i^x(t')dt'$, whose MGF is related to the appropriate non-Hermitian Hamiltonian

$$H_s = -\sum_i \sigma_i^x \sigma_{i+1}^x - \lambda \sum_i \sigma_i^z - \frac{is}{2} \sum_i \sigma_i^x. \tag{5.19}$$

This Hamiltonian is a discretized form of the massive Yang-Lee model [51, 52, 128, 129] of the TFIM and accordingly its critical properties have been studied in detail in Ref. [130], importantly a critical line in the (λ, s) plane was found which intersects the $s = 0$ axis at the static quantum critical points $\lambda = \pm 1$. Moreover this curve separates two regions in the (λ, s) plane where H_s has a real spectrum in one region and a complex spectrum in the other. This singular change in the spectral properties of H_s is associated with the breaking of an associated $\mathcal{PT}$-symmetry, which following Ref. [71] we will now describe.

Firstly to check that a $\mathcal{PT}$-symmetry may exist for our H_s we perform a similarity transformation by rotating the spins an angle $\pi/2$ about the z-axis

$$\begin{aligned} \mathcal{R} &= e^{\frac{i\pi}{4}\sum_i \sigma_i^z} = \prod_i \frac{1}{\sqrt{2}}(\mathbb{I}_i + i\sigma_i^z), \\ \tilde{H}_s &= \mathcal{R} H_s \mathcal{R}^{-1}. \end{aligned} \tag{5.20}$$

In the above Equation $\mathbb{I}_i$ denotes identity operator for site i, this similarity transformation preserves the spectral properties of H_s and maps the Pauli spin operators onto one another in the following way

$$\begin{aligned} &(\sigma_i^x, \sigma_i^y, \sigma_i^z) \to (-\sigma_i^y, \sigma_i^x, \sigma_i^z), \\ &\tilde{H}_s = -\sum_i \sigma_i^y \sigma_{i+1}^y - \lambda \sum_i \sigma_i^z + \frac{is}{2} \sum_i \sigma_i^y. \end{aligned} \tag{5.21}$$

From this expression we see that $\tilde{H}_s$ is a non-symmetric matrix with real entries, therefore implying that the spectrum is either *real* or consists of *complex conjugate pairs*[3]. Taking the anti-linear operator $\mathcal{T}$ to simply be complex conjugation, its effect on H_s is to map the spin operators onto one another via $\mathcal{T} : (\sigma_i^x, \sigma_i^y, \sigma_i^z) \to (\sigma_i^x, -\sigma_i^y, \sigma_i^z)$. If after this one applies a parity operator

$$\mathcal{P} = \prod_i \sigma_i^z, \tag{5.22}$$

whose effect is to map $(\sigma_i^x, \sigma_i^y, \sigma_i^z) \to (-\sigma_i^x, -\sigma_i^y, \sigma_i^z)$, it is straightforward to check that $[\mathcal{PT}, H_s] = 0$ and therefore constitutes a $\mathcal{PT}$-symmetry of the problem. One can therefore diagonalize both $\mathcal{PT}$ and H_s simultaneously and distinguish a region where they possess the same eigenvectors (the $\mathcal{PT}$-symmetry is *unbroken*) from one where they are different (the $\mathcal{PT}$-symmetry is *broken*).

Having identified the relevant $\mathcal{PT}$-symmetry of H_s, we examine its impact on the cumulants of time-integrated longitudinal magnetization in the ground state $|0\rangle$ of the TFIM. If H_s is fully diagonizable we can express the identity operator in terms of its left and right eigenvectors and the MGF will read

$$Z_t(s) = \sum_{a,b} e^{-i(E_a - E_b^*)t} \langle 0|L_a\rangle\langle R_a|R_b\rangle\langle L_b|0\rangle, \tag{5.23}$$

where E_a are eigenvalues of H_s and $|R_a\rangle$ ($|L_a\rangle$) is the associated right (left) eigenvector. Due to the non-Hermiticity of H_s these eigenvalues E_a may be complex and the associated left and right eigenstates are not related by Hermitian conjugation, $|R_a\rangle^\dagger \neq |L_a\rangle$. These eigenvectors form a biorthonormal vector space,

[3]One can quite readily see that in appropriate limits of parameter space that $\tilde{H}_s$ clearly has real spectrum (i. e. $s = 0$) or a complex spectrum ($\lambda = 0, |s| \gg 1$). Although there exist other classes of non-Hermitian Hamiltonian which can possess a real spectra, the property $\theta(s) = \theta(-s)$ is suggestive that an anti-linear operator $\mathcal{T}$ H_s is a symmetry of H_s and hence $\mathcal{PT}$ is the natural symmetry to consider.

$\langle L_a|R_b\rangle = \delta_{a,b}$, where the identity operator is given by $\mathbb{I} = \sum_a |L_a\rangle\langle R_a|$. It is worth noting that although the left and right eigenvectors are orthonormal with respect to each other, the eigenvectors $|R_a\rangle$ ($|L_a\rangle$) and $|R_b\rangle$ ($|L_b\rangle$) are in general not mutually orthogonal.

From this expression the long time MGF is dominated by the term (a, b) for which the imaginary component of $E_a - E_b^*$ is largest (provided the relevant vector overlaps in Eq. (5.23) are nonzero, i. e. $\langle R_a|R_b\rangle \neq 0$). In this case we know that H_s possesses a $\mathcal{PT}$-symmetry, hence the spectrum is either real (*unbroken* regime) or the eigenvalues form complex conjugate pairs (*broken* regime) and thus the long time the scaled CGF will be

$$\theta(s) = \begin{cases} 0 & \mathcal{PT}\text{-unbroken} \\ \max_a 2\,\mathrm{Im}(\varepsilon_a) & \mathcal{PT}\text{-broken} \end{cases}, \tag{5.24}$$

here ϵ_a is the complex eigenenergy per spin E_a/N. From the form of the scaled CGF it is clear that the $\mathcal{PT}$-symmetry will impact on the behaviour of the cumulants, in particular when the $\mathcal{PT}$-symmetry remains unbroken the cumulants of the longitudinal magnetization $\langle\langle Q_t^n \rangle\rangle$ will oscillate in time.

To confirm this we numerically extract $\theta(s)$ from Eq. (5.23) using exact diagonalization for small rings of size $N = 9, 11$. The scaled CGF is plotted in the (λ, s) plane in Fig. 5.6(a), even for these relatively small system sizes there is a clear change of behaviour in the CGF upon tuning λ. When the groundstate is ferromagnetically ordered, that is $\lambda < 1$, the CGF is non-zero for all $s \neq 0$. Upon tuning the transverse field such that the groundstate is paramagnetic, $\lambda > 1$, there exists a finite range of values for which $\theta(s) = 0$. Taking two fixed λ slices, one in each static phase (see Fig. 5.6(b,c)), we see that for $\lambda > 1$ the change in $\theta(s)$ from being 0 to $\neq 0$ is marked by a first order transition in κ_s and a corresponding peak in the susceptibility χ_s. Contrastingly the behaviour of the scaled CGF for $\lambda < 1$ is similar to that of the single spin in the regime where no $\mathcal{PT}$-symmetry exists,

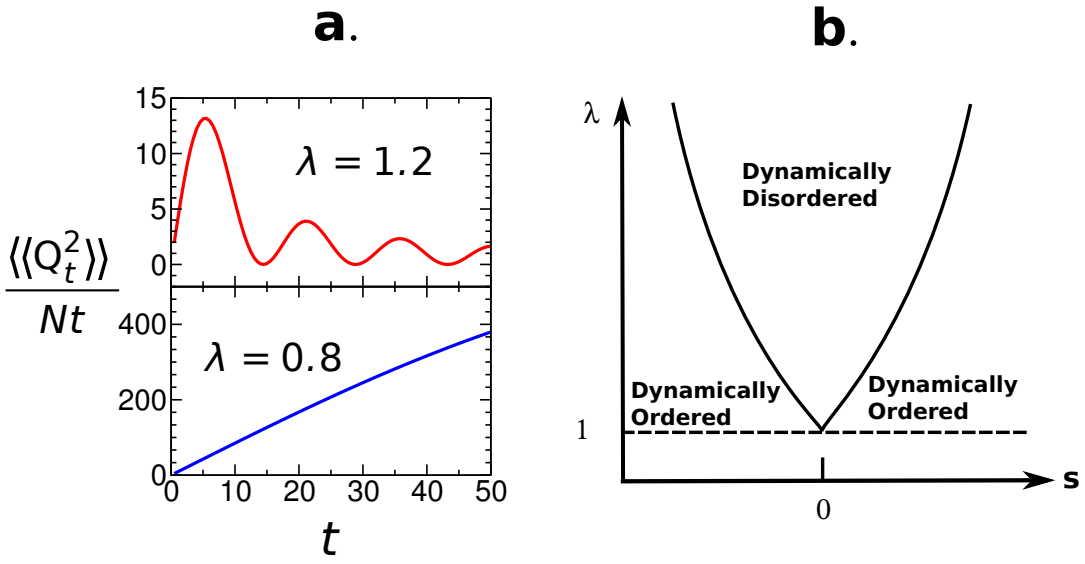

Figure 5.7: (a) Behaviour of the scaled second cumulant of the time-integrated longitudinal magnetization in both the ordered ferromagnetic state and disordered paramagnetic regime. (b) FCS phase diagram of the TFIM, with the time-integrated longitudinal magnetization as our observable of interest. There are two dynamical phases: a "dynamically ordered" phase where the $\mathcal{PT}$-symmetry of H_s is broken and the cumulants scale either linearly or super-linearly with t depending on s. The second phase is the "dynamically disordered" phase where the $\mathcal{PT}$-symmetry is unbroken and the cumulants oscillate in time. These two phases are separated by a 1st order FCS phase transition line.

see Fig. 5.5(c). This change of behaviour in $\theta(s)$ upon crossing the static quantum critical point also manifests itself in the temporal scaling of the cumulants of the longitudinal magnetization. Examining the scaled second cumulant, $\langle\langle Q_t^2 \rangle\rangle/(Nt)$, in both regimes we find for $\lambda > 1$ it oscillates and vanishes in the long time limit. In contrast for $\lambda < 1$ this scaled cumulant grows super-linearly in time and so diverges in the long time limit[4], see Fig. 5.7(a). This behaviour extends to higher order cumulants of the time-integrated longitudinal magnetization in the ground state. We note that this behaviour is very different from that of the 2nd cumulant of the time-integrated transverse magnetization discussed in Sec. 5.1. The cumulants either side of the critical point of the time-integrated magnetization have a very similar magnitude. A possible physical picture for this dramatic scaling change of the time-integrated longitudinal magnetization can be constructed by considering the form of the ground state in the limits of $\lambda = 0$ and $\lambda \to \infty$. In the first instance the ground state is described by all of the spins pointing up. Intuitively the time local correlators would be time-independent and the 2nd cumulant would evolve super-linearly in time. In the second limit the ground state is completely aligned with transverse field. The projection of the spins onto the longitudinal axis would oscillate in time thus leading to the oscillatory behaviour of $\langle\langle Q_t^2 \rangle\rangle$ observed in Fig. 5.7(a). Although this is a nice physical picture, we note it is hard to easily extend this argument to a general initial state but if one focusses on the $\mathcal{PT}$-symmetry properties of H_s it is clear that the role of the initial state is not so important.

Now in the thermodynamic limit, $N \to \infty$, the $\mathcal{PT}$-symmetry breaking at $\lambda = 1$

[4]For these small system sizes finite size effects are quite large, in particular the transition point would be expected to be at $\lambda \sim 0.7$. However, the change in the behaviour of the cumulants is a symmetry breaking process throughout the entire spectrum. Therefore in such small systems this does not need to occur exactly at the transition point, this is only the case in the thermodynamic limit.

becomes sharp and forms a curve of FCS phase transitions in the (λ, s) plane. The FCS phase diagram is shown in Fig. 5.7(b), and coincides with that previously found in Ref. [130]. This curve was previously identified as being critical, i. e. a 2nd order static critical line, but here marks a series of 1st order FCS transitions in the scaled CGF $\theta(s)$. Thus this transition line, where the $\mathcal{PT}$-symmetry breaks, is marked by discontinuous jumps in the order parameter κ_s. Interestingly these sharp changes in the time-integrated observables are not directly predictable from the static properties of the system. Imagine preparing the system at two values of λ, one in each static phase, equidistant but close enough to the quantum critical point such that universality comes into play. These two states will have the same correlation length, as close to the critical point it is determined solely by the distance to the quantum critical point $|\lambda - 1|^{-1}$, but the cumulants of M_t^x will be very different.

5.5 Dynamical Phase Transitions and FCS Phases

In this Section we study the analytic properties of the $|s\rangle$ state associated with the time-integrated transverse magnetization, as defined in Eq. (5.7). Specifically we consider the following quench protocol [76–78, 131]: firstly we connect the Ising chain to appropriate Markovian environments [56] and allow the system to evolve to the $|s\rangle$ state. We then remove the environments and perform a "quench" in the s-parameter whereby the $|s\rangle$ state evolves, in a non-trivial manner, under the original TFIM Hamiltonian, H:

$$|s_t\rangle = e^{-iHt}|s\rangle = \bigotimes_{k>0} e^{-iHt}|s_k\rangle = \bigotimes_{k>0} |s_{k,t}\rangle. \tag{5.25}$$

Using this protocol, which we refer to as the "s quench", we will examine the LD function associated with the return probability [73], see Eq. (2.80), and the

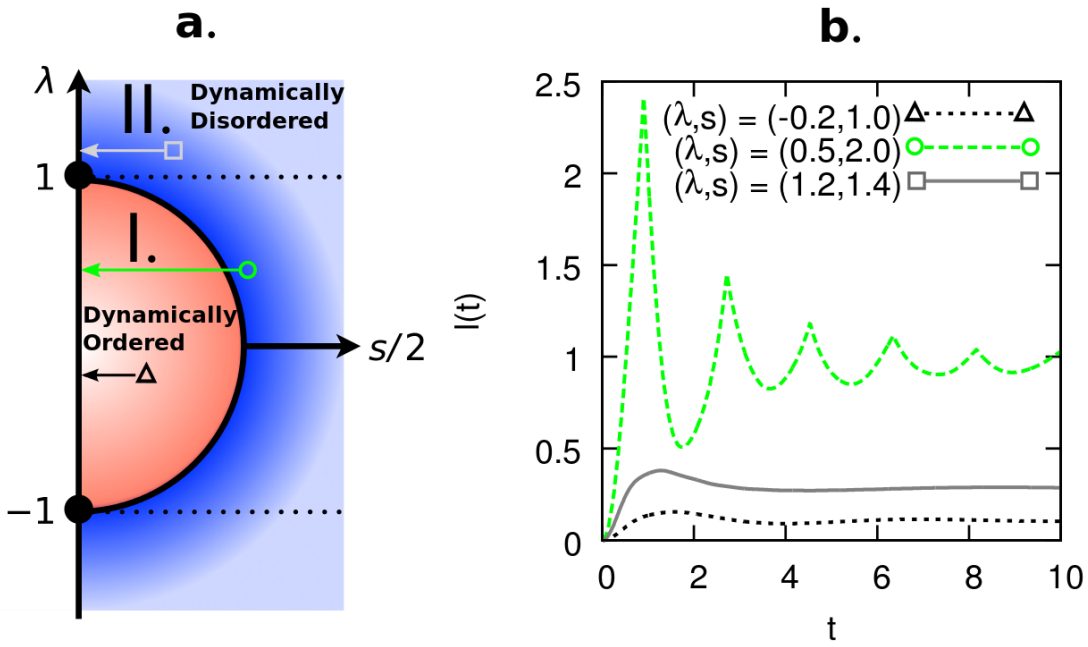

Figure 5.8: (a) FCS phase diagram of the TFIM, where the time-integrated transverse magnetization is the observable of interest. Regions I and II are the dynamically ordered and disordered regimes respectively. (b) Considering "quenches" from $(\lambda, s) \to (\lambda, 0)$ the LD function associated with the return probability of this protocol shows nonanalyticities when the "quench" crosses the FCS transition line. This is analogous to the effects seen upon quenching across a static quantum critical point.

possible connection between the FCS transition line uncovered in Sec. 5.1 and DPTs. Furthermore in the subsequent Section we will characterize the geometric properties of the states $|s\rangle(|s_t\rangle)$, expressed in terms of the free fermions which diagonalize H, using the Berry phase [57, 58, 132] and Chern number [60, 133].

Having introduced our nonequilibrium protocol and the necessary background to DPTs [79–81, 134], see Sec. 2.5.2, we now examine the evolution of $|s\rangle$ under H. Combining Eqs. (2.80) and (5.7) we find the LD function associated with the return probability is highly dependent on the critical wavevector $k_\lambda = \cos^{-1}\lambda$ and takes the form

$$l(t) = 2\mathrm{Re}\Big(\int_0^{k_\lambda} \log\Big[\frac{|\cos\alpha_k^s|^2 + |\sin\alpha_k^s|^2 e^{-2i\epsilon_k t}}{\cosh 2\mathrm{Im}(\alpha_k^s)}\Big]dk + \int_{k_\lambda}^{\pi} \log\Big[\frac{|\sin\alpha_k^s|^2 + |\cos\alpha_k^s|^2 e^{-2i\epsilon_k t}}{\cosh 2\mathrm{Im}(\alpha_k^s)}\Big]dk\Big). \tag{5.26}$$

Considering finite system sizes N and allowing the parameter t to be complex, this LD function will possess two sets of zeros at times:

$$\begin{aligned} t_j^{(1)} &= \frac{i}{\epsilon_k}(\log|\tan\alpha_k^s|^2 + i(2j+1)\pi)\,, \\ t_j^{(2)} &= \frac{i}{2\epsilon_k}(\log|\tan\alpha_k^s|^2 + i(2j+1)\pi)\,, \end{aligned} \tag{5.27}$$

where $j \in \mathbb{Z}$ and $\epsilon_k = \epsilon_k(s=0) = 2\sqrt{(\lambda-\cos k)^2 + \sin^2 k}$. The first set of zeros emerge when the integrand in Eq. (5.26) vanishes and the other set is attributed to when the integrands take the same value and the emergent nonanalytic behaviour at the k_λ limits of each integral. Whenever the complex angles α_k^s, which are directly related to the difference in Bogoliubov angles used to diagonalize H and H_s (see Sec. 5.1), are such that $|\cos\alpha_k^s| = |\sin\alpha_k^s|$ these zeros will lie on the real time axis. This condition is only ever satisfied when the $|s\rangle$ state lies in the dynamically disordered regime and $|\lambda| < 1$, see Fig. 5.8, here k_λ is well defined and the "s quench" crosses the FCS transition line. In the thermodynamic limit

crossing the FCS transition line leads to emergence of nonanalyticities in $l(t)$ at times

$$t_j^* = \frac{(2j+1)\pi}{2\epsilon_{k_\lambda}}, \frac{(2j+1)\pi}{\epsilon_{k_\lambda}}\,. \tag{5.28}$$

However when we "quench" from a state $|s\rangle$ such that no FCS transition points are "crossed", such as within the dynamically ordered regime or $|\lambda| > 1$, no DPTs emerge in the return probability rate function. The energy scale k_λ is the mode at which the free fermions of the original H are half occupied, $n_{s=0}(k_\lambda) = 1/2$ and so can be considered to be an infinite temperature critical mode [79]. This mode marks the onset of half-occupancy, where for modes $k < k_\lambda$ the occupancy is $< 1/2$ and for modes with $k > k_\lambda$ the occupancy is greater than a half. The emergence of these DPTs is similar to previous results where quenching across a static quantum critical point leads to the emergence of DPTs [79–81]. Here we see DPTs emerge even far from the static quantum critical points of the TFIM and although the FCS transition line can be postulated to be a quantum phase transition line in these extended $|s\rangle$ states it is not clear how it relates to the original model. To test this postulate we will examine the geometric properties of these $|s\rangle$ states in the final Section of this Chapter. Summarizing we have found evidence that static quantum criticality and DPTs are not necessarily intrinsically linked. Other studies have also shown that a quench across a quantum critical point is not necessary for DPTs to emerge [134, 135] and that FCS singular features do not necessarily emerge as DPTs under a "s quench".

5.6 Geometric Approach - Berry Phase and Chern Number

5.6.1 Geometric phase and Berry curvature

The role of geometry in theoretical physics cannot be understated, it underpins general relativity and emerges in amazing quantum phenomena such as the Aharonov-Bohm effect [132] and the quantum Hall effect. The integer quantum Hall effect may emerge in the presence of a magnetic field, and its associated Landau levels, and is characterized by a conductance plateaus

$$G = n\frac{e^2}{h}. \tag{5.29}$$

Here e is the fundamental charge and n is the filling factor which takes integer values ($n = 1, 2, 3, \ldots$). This filling factor is a topological invariant known as the *Chern number*, defined as the surface integral over parameter space of the associated *Berry curvature*. These numbers are topologically protected. It has emerged as the key quantity in classifying new topological phases of matter, such as topological insulators, and together with the Berry curvature provides a new geometric approach to quantum phase transitions. A final prominent geometric measure is the *Berry phase*, this physically manifests in the adiabatic transport of a quantum state around a closed parameter manifold [57]. Within this geometric approach quantum phase transitions manifest as extrema in the Berry curvature, and the associated geometric quantities [61, 136, 137], of the ground state manifold. Using this approach we will examine the geometric properties of the FCS transition line and "s quenched" states along with their relationship to DPTs. Prior to this we will describe these quantities in detail and exemplify their use with an application to the ground state manifold of the TFIM.

Consider now a parameter manifold, $\mathcal{M}$, where for each point in the manifold there is an associated set of parameters $\vec{\lambda}$ and a Hamiltonian. Thus every point on the manifold possesses an associated Hamiltonian and ground state $|0(\vec{\lambda})\rangle$ and a natural metric to describe $\mathcal{M}$ is the distance between these ground states [60, 138]. This distance is determined by tuning the parameter vector $\vec{\lambda}$ by an infinitesimal amount and evaluating the overlap of the new ground state and the old one,

$$1 - |\langle 0(\vec{\lambda})|0(\vec{\lambda} + d\vec{\lambda})\rangle|^2 = \sum_{\mu,\nu} g_{\mu\nu} d\lambda^\mu d\lambda^\nu, \tag{5.30}$$

where the metric $g_{\mu\nu}$ is the geometric tensor

$$g_{\mu\nu} = \langle 0(\vec{\lambda})|\overleftarrow{\partial_\mu}\partial_\nu|0(\vec{\lambda})\rangle - \langle 0(\vec{\lambda})|\overleftarrow{\partial_\mu}|0(\vec{\lambda})\rangle\langle 0(\vec{\lambda})|\partial_\nu|0(\vec{\lambda})\rangle. \tag{5.31}$$

The partial derivatives are with respect to an element of the parameter vector, $\partial_\mu = \partial/\partial\lambda^\mu$, and the diacritic arrow $\leftarrow$ indicates the partial derivative acts to the left. The associated Berry curvature, $F_{\mu\nu}$, is related to the imaginary part of this $g_{\mu\nu}$ via

$$F_{\mu\nu} = -2\mathrm{Im}[g_{\mu\nu}] = \partial_\mu A_\nu - \partial_\nu A_\mu, \tag{5.32}$$

where the quantity $A_\mu = i\langle 0(\vec{\lambda})|\partial_\mu|0(\vec{\lambda})\rangle$ is known as the Berry connection, due to its natural link to the Berry phase and curvature. These quantities are not gauge invariant (c. f. the magnetic vector potential) however the curl of the Berry connections (c. f. the magnetic field density), which defines $F_{\mu\nu}$, is gauge invariant. The Berry phase (B) is simply the line integral of the Berry connection, or via Stoke's theorem it is simply the surface integral of the $F_{\mu\nu}$. Furthermore if one considers $\mathcal{M}$ to be a two-dimensional parameter manifold, as we do here on out, then one may also define the Chern number (C):

$$\begin{aligned} B &\equiv \int_{\partial S} \vec{A}.d\vec{\lambda}, \\ C &\equiv \frac{1}{2\pi}\int_{\mathcal{M}} F_{\mu\nu} dS_{\mu\nu}. \end{aligned} \tag{5.33}$$

The Chern number is a topological invariant and takes integer value when the manifold is closed in a topological sense [60, 133, 139]. From a purely geometric stand point it is used to classify complex vector bundles, which are essentially complex vector spaces associated with each point in the manifold. In the context of classifying the ground state manifold and this vector space is one-dimensional and consists simply of $|0(\vec{\lambda})\rangle$.

To exemplify how to apply these concepts we take the example of the TFIM under a nonequilibrium quench protocol in the transverse field $\lambda_i \to \lambda_f$ and consider the geometry of the time-evolved groundstate $|u_t\rangle = e^{-iHt}|0(\lambda_i)\rangle$. This example was originally discussed in Ref. [140] and is the first model shown to possess DPTs. We will now relate these geometric quantities to the emergence of these DPTs in the TFIM. The quenched ground state $|u_t\rangle$ breaks up into contributions from each fermionic momentum sector

$$|u_{k,t}\rangle = [\cos\alpha_k^{\lambda_f} - i\sin\alpha_k^{\lambda_f} e^{-2i\epsilon_k(\lambda_f)t} c_k^\dagger c_{-k}^\dagger]|0_k, 0_{-k}\rangle. \tag{5.34}$$

Once again the fermionic operators $c_k(c_k^\dagger)$ diagonalize the TFIM Hamiltonian, see Appendix B, and the difference between Bogoliubov angles [55] involved in diagonalizing $H(\lambda_i)$ and $H(\lambda_f)$ are captured by $\alpha_k^{\lambda_f}$. Similarly the fermionic vacuum for each $|k|$ wavevector is written as $|0_k, 0_{-k}\rangle$ and is annihilated by $c_{\pm k}$. Furthermore the TFIM Hamiltonian, described in Eq. (3.17), is invariant under $U(1)$ global rotations in this fermion space

$$c_k \to c_k e^{-i\varphi}, \tag{5.35}$$

however the quenched states $|u_{k,t}\rangle$ *do not* obey this symmetry which is attributed to the spontaneous creation of excitations upon quenching and leads to a nontrivial geometry. Considering the rotated time-evolved states $|u_{k,t}(\varphi)\rangle$ a suitable two-dimensional manifold associated with these states M^2 is that spanned by

both the wavevectors k and the global phase φ. The Cooper pair-like nature of the excitations appearing in $|u_{k,t}(\varphi)\rangle$ means the phase factor φ has a factor of 2 preceding it and these states are only uniquely defined in the interval $\varphi \in [0, \pi]$. Moreover these states are uniquely defined for all $k \in [0, \pi]$ leading to a manifold $M^2 = [0, \pi] \times [0, \pi]$ where for each point in this manifold we associate the state $|u_{k,t}(\varphi)\rangle$.

It is important to note when computing the Berry curvature and geometric properties of M^2 that as k and φ are t independent so will the geometric properties of the manifold. This may initially seem surprising as states used in our computation are explicitly time-dependent. To determine the Berry curvature we need to evaluate the derivatives of $|u_{k,t}(\varphi)\rangle$ with respect to φ and k. Although the former is simple to evaluate, the derivative with respect to k is not immediately apparent as the fermionic states are also k dependent making it is necessary to employ perturbation theory [62] and expand $|0_k, 0_{-k}\rangle$ as

$$|0_{k+\delta k}, 0_{-(k+\delta k)}\rangle = |0_k, 0_{-k}\rangle + \frac{d}{dk}|0_k, 0_{-k}\rangle \delta k + \mathcal{O}(\delta k^2). \tag{5.36}$$

This perturbative expansion has an implicit gauge choice built in known as the parallel transport gauge, which is discussed in Appendix D. This gauge choice in conjunction with the orthogonality of excitations to the ground state means that

$$\frac{d}{dk}|0_k, 0_{-k}\rangle = \frac{d}{dk} c_k^\dagger |0_k, 0_{-k}\rangle = 0. \tag{5.37}$$

Using this result the calculation of the Berry curvature and Chern number is straightforward. Before proceeding to calculate the Chern number it is desirable to examine the form of the manifold M^2. Firstly in the limit $k = \pi$ the states are independent of the phase φ regardless of the quench protocol,

$$\sin \alpha_{k=\pi}^{\lambda_f} = 0,$$
$$|u_{\pi,t}(\varphi)\rangle = |u_\pi\rangle = \cos \alpha_{k=\pi}^{\lambda_f} |0_\pi, 0_{-\pi}\rangle. \tag{5.38}$$

However the infrared ($k \to 0$) behaviour of these states is more complex and depends on the quench protocol. Quenching within the same phase the $k = 0$ modes are φ independent as $\sin \alpha_{k\to 0}^{\lambda_f} = 0$, so the manifold M^2 is topologically equivalent to a 2-sphere, see Fig. 5.9. Quenching across the static quantum critical point at $\lambda = 1$ leads to the $k = 0$ states depending on a global phase set by φ

$$\sin \alpha_{k\to 0}^{\lambda_f} = 1,$$
$$|u_{0,t}(\varphi)\rangle = -ie^{2i\varphi} e^{-2i\epsilon_k(\lambda_f)t} |1_{k=0}, 1_{k=0}\rangle. \tag{5.39}$$

This global phase can be removed with an appropriate gauge transformation, specifically a global $U(1)$ rotation in the fermion space, which leads us to again conclude M^2 is topologically equivalent to a 2-sphere. From this we find the Berry curvature is simply $F_{k,\varphi} = -\partial_k \sin^2 \alpha_k^{\lambda_f}$, leading to a simple functional form of the Chern number $C = \sin^2 \alpha_0^{\lambda_f}$.

For quenches within the same phase, where *no DPTs* emerge [79], this takes the value $C = 0$ as no gauge fixing was required [140]. However on quenching across the quantum critical point this takes a value $C = 1$. Furthermore the occupation of this mode $n_{k=0}$ is equal to the Chern number. In thermal equilibrium at $T = 0K$ the $k = 0$ occupation should be zero due to the presence of a gap but due to the quench protocol this gap may close leading to population inversion. This inversion, and the subsequent emergence of DPTs, is captured by the non-trivial $C = 1$. In this manner we see that one may link the emergence of DPTs with a non-trivial Chern number. In the Section that follows we apply these ideas to the "s quenched" states $|s_{k,t}\rangle$, defined in Eq. (5.25), and study the geometric

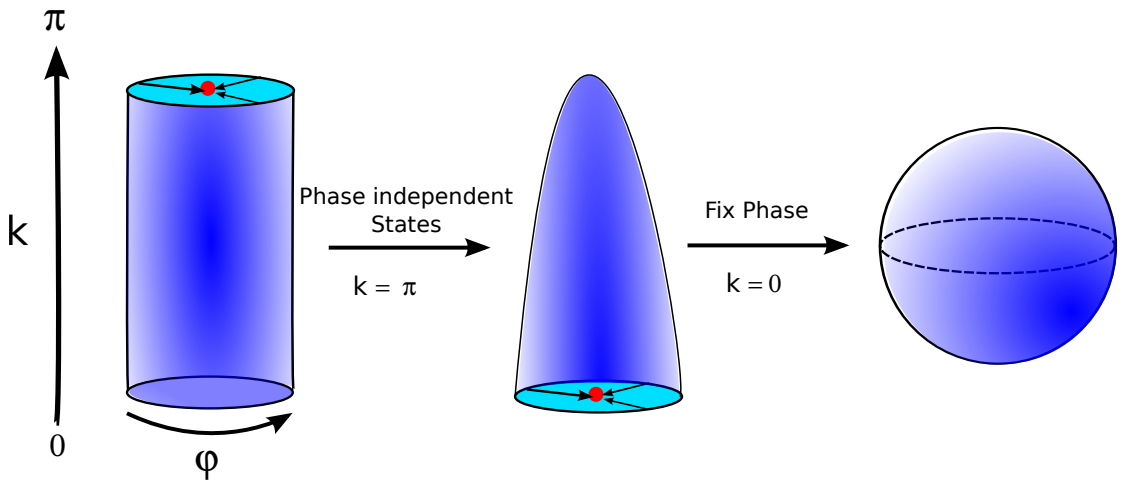

Figure 5.9: The parameter manifold M^2 is φ independent at $k = \pi$ and only depends on φ up to a gauge transformation in the infrared ($k \to 0$) limit, thus it is topologically equivalent to a S^2-sphere.

properties of the static $|s\rangle$ states to extend the links between geometry, static quantum criticality and DPTs to the FCS phases of the TFIM.

5.6.2 Geometry of $|s\rangle$ states

In this Section we characterize the geometry of $|s\rangle$ (5.7) and $|s_t\rangle$ (5.25), beginning with a more precise discussion of the mathematical form of the states $|s\rangle$ prior to performing the analysis. From Eq. (5.7) (and Eq. (5.25)) it is clear that the states $|s\rangle$ ($|s_t\rangle$) can be split up into contributions from each wavevector $|s_k\rangle(|s_{k,t}\rangle)$. These $|s\rangle$ states are the right eigenvectors of H_s, previous work has shown how the geometry of the manifold of a system's ground states may possess signatures of quantum criticality [60, 63, 136]. In analogous fashion we expect the geometric properties of $|s\rangle$ to show signatures of the FCS transition line (5.6). However as this is an atypical transition line it is unclear exactly what effect its presence would have on their geometry, more specifically on the Berry phase and Chern number.

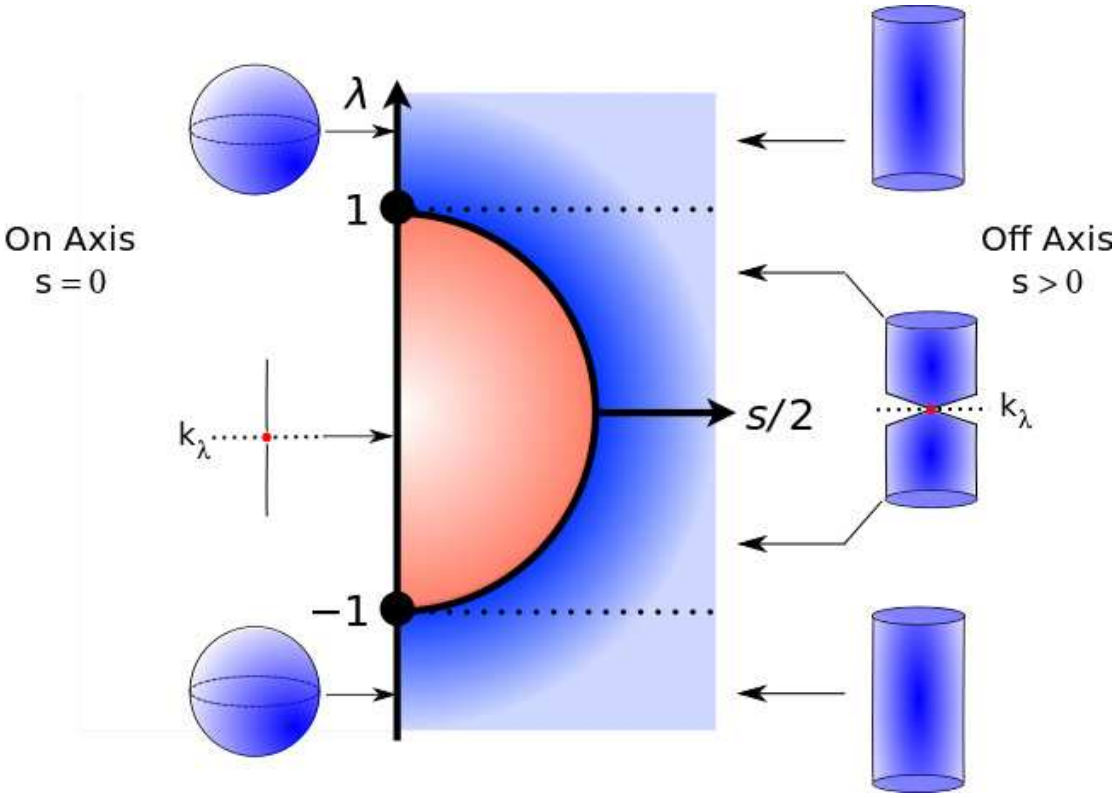

Figure 5.10: The manifold of s states at each point in the FCS phase diagram is independent of φ at the wavevector k_λ. For $|\lambda| < 1$ the states are completely φ independent in the limit $s \to 0$. In contrast when $|\lambda| > 1$ the manifold is topologically equivalent to a S^2-sphere at $s = 0$.

To examine the geometric properties of these states it is necessary to first express $|s\rangle$ (and $|s_t\rangle$) in terms of the free fermions of the *original* TFIM.

This is done by inverting the BCS relationship of Eq. (5.2) and fixing the normalization of each fermionic occupation state $|n_k, n_{-k}\rangle_s$ to be 1, from this we

immediately find

$$|0_k, 0_{-k}\rangle_s = \frac{1}{\sqrt{\cosh 2\mathrm{Im}(\alpha_k^s)}}\Big(\cos\alpha_k^s|0_k, 0_{-k}\rangle - i\sin\alpha_k^s|1_k, 1_{-k}\rangle\Big),$$
$$|1_k, 1_{-k}\rangle_s = \frac{1}{\sqrt{\cosh 2\mathrm{Im}(\alpha_k^s)}}\Big(\cos\alpha_k^s|1_k, 1_{-k}\rangle - i\sin\alpha_k^s|0_k, 0_{-k}\rangle\Big). \tag{5.40}$$

We then perform a global rotation on the free fermion operators ($c_k \to c_k e^{-i\varphi}$) of H to introduce a global phase shift φ (5.35). Combining this phase shift with Eqs. (5.7) and (5.40) we readily obtain the phase dependent state $|s(\varphi)\rangle$. Once again the parameter manifold M^2 consists of the wavevectors k and φ, with each point defining a state $|s_k(\varphi)\rangle$, see Fig. 5.10. We find from Eq. (5.33) the Berry phase associated with this adiabatic evolution (defined by the global phase shifts) is

$$B = \int_0^\pi \langle s(\varphi)|i\partial_\varphi|s(\varphi)\rangle d\varphi. \tag{5.41}$$

To examine the FCS transition line it is necessary to work in the limit of large system size $N \to \infty$ where the wavevectors k become dense on the interval $[0, \pi]$. In this limit we introduce an appropriately scaled geometric density defined as $\tilde{\beta} \equiv \lim_{N\to\infty} B/N$, we now insert the states $|s(\varphi)\rangle$ and after performing the integral over φ we obtain

$$\tilde{\beta} = -\int_{k_\lambda}^{\pi} \frac{|\cos\alpha_k^s|^2}{\cosh 2\mathrm{Im}(\alpha_k^s)} dk - \int_0^{k_\lambda} \frac{|\sin\alpha_k^s|^2}{\cosh 2\mathrm{Im}(\alpha_k^s)} dk. \tag{5.42}$$

We numerically integrate the RHS of the above Equation for various representative slices through the (λ, s) plane and plot the resulting $\tilde{\beta}$ in Fig. 5.11(a). There is no clear analytic difference in this density between the dynamically ordered

and disordered regimes in the FCS phase diagram. However if one examines the derivative of this density, $d\tilde{\beta}/ds$, the FCS transition line is marked by local maxima in the derivative of the geometric phase density , see Fig. 5.11. The presence of extrema in the derivative of the geometric phase density has previously been used as a signature of quantum criticality in the ground state manifold of a family Hamiltonians [61, 63, 136, 137]. Here we find similar features but in the manifold of extended $|s\rangle$ states which mark FCS singularities defined by the spectral properties of H_s. Thus we have shown one may use the Berry phase to identify FCS singular points, this is attributed to the Berry phase probing the energy level structure (as marked by k_λ appearing in Eq. (5.42)) of H_s.

To connect this observation with the emergence of DPTs on "s quenching" across the FCS singular point we perform an analysis on the Chern number C associated with the manifold of quenched states. Firstly the quenched states $|s_t\rangle$ may be split up into separate momenta contributions:

$$\begin{aligned}|s_{k,t}\rangle &= \tau(k_\lambda - k)\frac{1}{\mathcal{N}}(\cos\alpha_k^s - i\sin\alpha_k^s e^{-2i\epsilon_k t}c_k^\dagger c_{-k}^\dagger)|0_k, 0_{-k}\rangle \\ &+ \tau(k - k_\lambda)\frac{1}{\mathcal{N}}(-i\sin\alpha_k^s + \cos\alpha_k^s e^{-2i\epsilon_k t}c_k^\dagger c_{-k}^\dagger)|0_k, 0_{-k}\rangle \\ &+ \delta_{k,k_\lambda}[\cos\phi_{k_\lambda} - i\sin\phi_{k_\lambda}e^{-2i\epsilon_{k_\lambda}t}c_{k_\lambda}^\dagger c_{-k_\lambda}^\dagger]|0_{k_\lambda}, 0_{-k_\lambda}\rangle, \end{aligned} \tag{5.43}$$

here $\tau(x)$ is simply the Heaviside step function and δ_{k,k_λ} is the Kronecker delta function. We work in the thermodynamic limit and perform the global phase shift on the $s = 0$ free fermions and consider the states $|s_{k,t}(\varphi)\rangle$. To calculate the Chern number associated with these states it is necessary to evaluate the Berry curvature $F_{k,\varphi}$ and combine it with Eq. (5.33). Working in the thermodynamic limit we make use of the identity $\delta_{k,k'} = \tau(k-k') + \tau(k'-k) - 1$ and the parallel transport

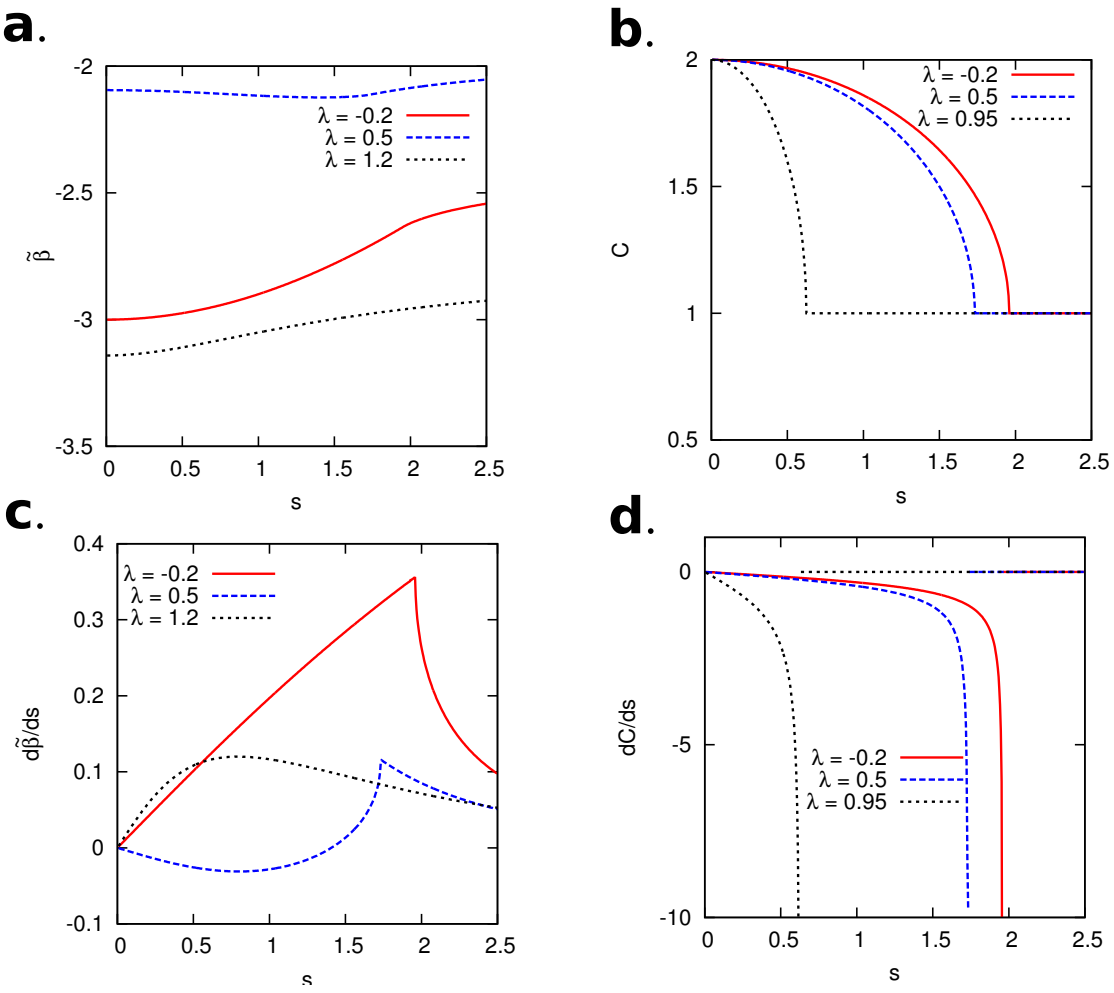

Figure 5.11: (a,c) No singular features are readily apparent in the Berry phase density at the FCS transition line. However the derivative of the Berry phase density, $d\tilde{\beta}/ds$, has extremum which are located at the FCS transition line. For $|\lambda| > 1$ no such extremum are present due to the lack of FCS transition points in this parameter regime. (b,d) The Chern number C associated with the manifold of $|s_{k,t}\rangle$ states has a "kink" at the FCS transition line, this leads to a divergence of the derivative dC/ds. These features are normally observed at static quantum criticality but now mark the FCS transition line.

gauge [62] to find the non-trivial functional form of the Chern number [64]

$$
\begin{aligned}
C = & \frac{2(|\cos\alpha^s_{k_\lambda}|^2 - |\sin\alpha^s_{k_\lambda}|^2)}{\cosh 2\mathrm{Im}(\alpha^s_{k_\lambda})} \\
& + \mathrm{Im}\Big(\int_0^{k_\lambda} \frac{2i(\sin\alpha^s_k)^*\cos\alpha^s_k\partial_k\alpha^s_k}{\cosh 2\mathrm{Im}(\alpha^s_k)}dk\Big) \\
& - \mathrm{Im}\Big(\int_{k_\lambda}^{\pi} \frac{2i(\cos\alpha^s_k)^*\sin\alpha^s_k\partial_k\alpha^s_k}{\cosh 2\mathrm{Im}(\alpha^s_k)}dk\Big) \\
& - \mathrm{Im}\Big(\int_{k_\lambda}^{\pi} \frac{2i|\cos\alpha^s_k|^2(\cos\alpha^s_k(\sin\alpha^s_k)^* - \mathrm{h.c.})\partial_k\alpha^s_k}{\cosh^2 2\mathrm{Im}(\alpha^s_{k_\lambda})}dk\Big) \\
& - \mathrm{Im}\Big(\int_0^{k_\lambda} \frac{2i|\sin\alpha^s_k|^2(\cos\alpha^s_k(\sin\alpha^s_k)^* - \mathrm{h.c.})\partial_k\alpha^s_k}{\cosh^2 2\mathrm{Im}(\alpha^s_{k_\lambda})}dk\Big). \qquad (5.44)
\end{aligned}
$$

Here the superscript $*$ denotes standard complex conjugation and h. c. denotes Hermitian conjugation of the term appearing previous. Recalling that the emergence of DPTs may be attributed to a non-trivial change in the form of C [140] we plot C as a function of s for various slices in the FCS phase diagram. The states $|s_{k,t}(\varphi)\rangle$ spanning the manifold M^2 are different in nature to $|u_{k,t}(\varphi)\rangle$ discussed in the previous Section, in particular they have a non-trivial dependence on $\varphi\ \forall(k \neq k_\lambda)$. This leads to M^2 having a cylindrical form away from $s = 0$, with a "pinch" at the wavevector $k = k_\lambda$. In the limit $s \to 0$ the manifold returns to a closed form, either a 2-sphere for $|\lambda| > 1$ or for $|\lambda| < 1$ a "line" where φ only plays the role of a global phase $\forall k$, this manifests itself as an integer Chern number, see Fig. 5.11(b). The emergence of DPTs on "quenching" across the FCS transition line is marked by an "kink" in C (see Fig. 5.11(b,d)), similar in form to that seen in the dynamical order parameter $-\theta'(s)$ discussed in Sec. 5.1. This "kink" leads to a divergence in the derivative dC/ds at the FCS transition line, this divergence is very similar to that of the dynamical susceptibility χ_s at the FCS transition line [56, 64].

One may ask the question as to why only extrema emerge in these geometric quantities and not divergences? To answer this we note that the FCS transition line is associated with the closing of a gap in the complex spectrum of H_s occurs

at a incommensurate wavevector, or *excited-state* of H_s. The lack of divergences is then attributed to our choice of initial state; the closing of this gap is single particle in nature while our states $|s\rangle(|s_t\rangle)$ are multi-particle in nature. In the thermodynamic limit the multi-particle nature of these states suppresses the single particle divergences and leads to extrema emerging in the associated Berry phase derivative and Chern number [63]. These features indicate that the FCS transition line has the geometric hallmarks of a regular quantum critical point, and one could think of it as the static quantum critical point of some other Hermitian Hamiltonian. However it is difficult to construct such a Hamiltonian as it must also be related to the original TFIM H and so will be subject of future work. This is in contrast to the non-Hermitian H_s we have studied throughout this Chapter.

6. Conclusions

This thesis examined the generating functions of dynamical observables from a thermodynamic perspective in a number of classical and quantum systems (both open and closed). The trajectory phase transitions associated with the time-integrated energy in the 1d Glauber-Ising chain were found to be single points on a whole transition curve which existed in the complex s plane. Applying the dynamical equivalent of Lee-Yang theory, we extracted the positions of these singular points using the high order cumulants of the mode-resolved time-integrated energy at $s = 0$ at short times. If one could not resolve the contributions from each mode to the cumulants and instead used the full cumulants the results became highly dependent on the inverse temperature β. At high temperatures there existed a few dominant singular points which could be identified using this approach, however at low temperatures all the singular points become important and this Lee-Yang approach fails to converge to any transition point. Future work will focus on extending the time interval over which the approximation in this approach is valid by extracting higher-order Lee-Yang zeros.

The thermodynamics of trajectories approach to open quantum systems was extended to quadrature trajectories focussing on simple optical systems, such as the dissipative 3-level and two coupled 2-level systems, along with the micromaser which possessed a very rich dynamical phase diagram. We found a new dynamical

order parameter, the quadrature "activity", which could serve as an alternative order parameter to the jump activity in both the 3-level system and micromaser. In the former case the correlation of the order parameters was studied in detail by examining the typical quadrature "activity" in biased ensembles of jump trajectories and vice-versa. It was demonstrated that when the system was more jump active the Y quadrature "activity" was increasingly negative. Conversely a positive quadrature "activity" corresponded to the system emitting few quanta and appearing jump inactive. Moreover in the 3-level system and micromaser both the quadrature and jump activities displayed a crossover in dynamical behaviour, at $s = 0$, upon tuning the conjugate "counting" field s. These crossovers became sharp in the appropriate limits and reflect the bistability in the corresponding probability distributions. Such bistabilities emerge in "phase space" portraits of the associated marginal distributions of the quadratures. We also studied two coupled 2-level systems where the individual 2-level subsystems were driven by lasers of different polarization. Unlike the other examples this difference in driving was not reflected in the jump activity but was indeed captured by the quadrature "activity" upon applying the corresponding s bias. Future work will extend the dynamical Lee-Yang zero approach of classical stochastic systems to other trajectory ensembles and will tackle the problem of how to resolve rich phase diagrams, such as that of the micromaser, where many trajectory transition points may exist close to $s = 0$.

After this a study of the generating functions of time-integrated observables in closed quantum systems, using the transverse field Ising model as our primary example, was presented. To extend our previous thermodynamics of trajectories to such systems we treated the generating functions of these observables as dynamical partition sums and "free energies", even though in general no large deviation principle exists. These generating functions may be calculated using a variation on full counting statistics methods where we deform the system of interest's Hamil-

tonian to form a non-Hermitian operator. Using the TFIM as an example, both the time-integrated transverse and longitudinal magnetization in the ground state were examined. In both cases a new FCS transition line emerged on tuning the counting field s, of which the static critical points were the end points. These new FCS phase transition lines influenced the behaviour of the cumulants and in the case of the longitudinal magnetization their impact was dramatic due to the breaking of an associated $\mathcal{PT}$-symmetry. These symmetries of the deformed non-Hermitian operator impact their spectral properties and hence the long time temporal scaling of the associated cumulants. Such symmetries may spontaneously break and their impact can not be predicted solely from the correlation length of the groundstate of the system. With our variation on FCS we showed that one can map the MGF to the survival probability of an associated open quantum system to probe such FCS singularities. It was shown that small cold-ion systems in conjunction with digital simulation techniques could be used to experimentally probe the FCS singularities of the transverse magnetization in the TFIM.

To capture these new FCS singularities, a new class of state ($|s\rangle$) was introduced and studied for the case of the transverse magnetization. Evolving these states under the $s = 0$ system Hamiltonian results in the emergence of DPTs in the return provided, provided the evolution "crosses" the FCS transition line. Furthermore the geometry of these states exhibits singular features, as captured by the Berry phase and Chern number, at the FCS transition line similar to that of a systems ground state at a quantum critical point. Although one could argue that the FCS transition line and the $|s\rangle$ states are directly related to the ground state and quantum critical point of some other Hermitian Hamiltonian, how to find such a Hamiltonian is highly non-trivial. Of the many directions future studies could pursue, establishing a method, similar to the Lee-Yang approach discussed previously, to extract these singular features using measurements of **static** observables is of particular interest. This would provide a greater understanding

of the connection between the time-integrated observables, static observables and the Lee-Yang theory of phase transitions. Further work will also include a study of the entanglement properties of states $|s\rangle$ close to FCS transitions and will extend this approach to other systems such as the XXZ-model.

Before finishing we now make some more general comments about the research presented in this thesis and the connections between the areas presented. By considering the generating function, as opposed to the characteristic function, one is able to consider the statistics of dynamical observables within a thermodynamic framework. This allows one to use the tools of equilibrium statistical physics to understand these dynamical observables. From a theoretical point of view this is a nice result as one can use "old" ideas to understand new physics. A good example of this is the development of a dynamical Lee-Yang theory in Chapter 3 to determine trajectory phase transition locations at long times from short time cumulants. This in turn gives at least some qualitative information about the long time distribution of the dynamical observable. The results of Chapters 3-5 further demonstrate that theoretically this approach is a useful tool to have at one's disposal. However as with most things the usefulness of this approach is dependent on the type of problem and the questions one wishes to ask. A particular issue, especially from an experimental point of view, is the physical accessibility of the counting field s. Although one can circumnavigate this problem using a Lee-Yang approach or an ancilla system or even mapping to an open system, it would be interesting to find a system where s is a natural physical parameter. Finally throughout this thesis we have seen that the singularities associated with time-integrated observables are related to equilibrium phase transitions and DPTs. Below is a table highlighting the connections; from this table it is apparent that the open quantum system trajectory phase transitions are not simply related to the other types of system discussed here.

Definitions	
$z = \tau + it$	$\tilde{s} = s + i\bar{s}/2$
$\mathbb{I} = \sum_n \|n\rangle\langle n\|$	$H_{\tilde{s}} = H - (s + i\bar{s}/2)q$
General: $\langle n\|e^{-zH_{\bar{s}}}\|0\rangle$	LD function: $\Theta^{(n)}(\tilde{s}, z)$
Dynamical and Related Equilibrium Quantities	
Classical:$Z(s,t) = \langle -\|e^{\tau \mathbb{W}_s}\|eq.\rangle$ LD:$-\Theta^{(0)}(s,\tau)$	Eq: Boundary Part. Funct. (BPF) $\langle 0\|e^{-\tau(-H_s)}\|0\rangle$ (Lee-Yang zeros)
Closed:$Z(s,t) = \langle 0\|T_t^\dagger(\bar{s})T_t(\bar{s})\|0\rangle$ $= \sum_n \|\langle n\|e^{-itH_{\bar{s}}}\|0\rangle\|^2$ LD:$\max_n 2\mathrm{Re}[\Theta^{(n)}(\bar{s}, it)]$	Eq: BPF imaginary length Open: Survival Probability
DPTs:$L(s,t) = \|\langle 0\|e^{-itH_s}\|0\rangle\|^2$ LD: $2\mathrm{Re}[\Theta^{(0)}(s,it)]$	Eq: BPF imaginary length $\langle 0\|e^{-itH_s}\|0\rangle$(Fisher zeros)
Open: $Z(s,t) = \mathrm{Tr}(e^{t\mathbb{W}_s}\rho)$ LD: $\theta(s)$	Eq: System+Spin Chain (Jumps only) LD not related to $\Theta^{(n)}(\tilde{s}, z)$

A. Time-reversal invariance and symmetrizing the classical deformed Master operator

A classical unbiased stochastic Master operator is time-reversal invariant if its associated energy operator and transition rates obey detailed balance : $W(\mathcal{C}'|\mathcal{C})e^{-\beta E(\mathcal{C})} = W(\mathcal{C}|\mathcal{C}')e^{-\beta E(\mathcal{C}')}$, here $E(\mathcal{C})$ is the energy of the configuration $\mathcal{C}$. Provided the biased ensembles of trajectories are also time-reversal invariant, this may be deduced from the form of the associated $\mathbb{W}_s$, the deformed Master operator may be symmetrized using a similarity transformation

$$\mathbb{H}_s = e^{\frac{\beta\hat{E}}{2}}\mathbb{W}_s e^{-\frac{\beta\hat{E}}{2}}, \tag{A.1}$$

where $\hat{E}$ is the energy operator. This operator is Hermitian and can be considered a "quantum Hamiltonian" but to see exactly how the s-ensemble maps to a closed quantum system we must examine the full MGF. The steady state equilibrium of the unbiased Master operator is simply the Boltzmann distribution $|eq.\rangle = \frac{1}{Z}\sum_{\mathcal{C}} e^{-\beta E(\mathcal{C})}|\mathcal{C}\rangle$, where Z is the equilibrium partition function. From this it is trivial to see that the flat state ($\langle -| = \sum_{\mathcal{C}}\langle\mathcal{C}|$) is related to the equilibrium distribution via the energy operator: $\frac{1}{Z}\langle -|e^{-\beta\hat{E}} = \langle eq.|$.

Focussing on the biased ensemble of trajectories in the equilibrium distribution

we insert identities into the definition of the MGF to find

$$\begin{aligned} Z(s,t) &= \langle -|e^{\mathbb{W}_s t}|eq.\rangle \\ &= \langle 0|e^{\mathbb{H}_s t}|0\rangle, \end{aligned} \tag{A.2}$$

where $|0\rangle = \frac{1}{\sqrt{Z}} e^{\beta \hat{E}/2}|eq.\rangle$ is the state associated with the largest eigenvalue of $\mathbb{H}_{s=0}$. The MGF in Eq. A.2 is thus expressed as a quantum expectation value, where $|0\rangle$ is the groundstate of $-\mathbb{H}_{s=0}$.

B. Diagonalizing the TFIM and H_S

The dynamics of the time-integrated energy of the 1d Glauber-Ising chain are governed by the Hamiltonian $\mathbb{H}_s$ described in Eq. (3.16). This spin Hamiltonian may be diagonalized by first mapping the spins to Jordan-Wigner fermions and then performing a Bogoliubov rotation. The first step, the Jordan-Wigner transformation, expresses the spin operators σ_i^x, σ_i^+ and σ_i^- to fermionic creation and annihilation operators, $b_i^\dagger$ and b_i, via

$$\begin{aligned}\sigma_i^x &= 1 - 2b_i^\dagger b_i, \\ \sigma_i^+ &= \prod_{j<i}(1 - 2b_j^\dagger b_j)b_i, \\ \sigma_i^- &= \prod_{j<i}(1 - 2b_j^\dagger b_j)b_i^\dagger.\end{aligned} \tag{B.1}$$

Furthermore $\mathbb{H}_s$ is translationally invariant and so is block diagonal in momentum space, we thus switch to the Fourier representation of these Fermionic operators

$$b_i = \frac{1}{\sqrt{N}} \sum_k e^{-ikr_i} b_k. \tag{B.2}$$

In this representation the Hamiltonian is given by

$$\begin{aligned}\mathbb{H}_s =&\frac{1}{2}\sum_k (2[s+\lambda-1+\cos k]b_k^\dagger b_k \\ &- i\sqrt{\gamma\lambda}[b_{-k}b_k + b_{-k}^\dagger b_k^\dagger - (s+2-\lambda)]).\end{aligned} \tag{B.3}$$

Restricting ourselves to the even N spin sector, with periodic boundary conditions, the wavevector k takes values $k = \pi n/N$ where $n = -N+1, -N+3, \ldots, N-1$. To eliminate the terms which do not preserve the total fermion number $(b_{-k}b_k, b_{-k}^\dagger b_k^\dagger)$ we perform a Bogoliubov rotation

$$\begin{aligned} b_k &= \cos\frac{\phi_k^s}{2}c_k + i\sin\frac{\phi_k^s}{2}c_{-k}^\dagger, \\ b^\dagger &= \cos\frac{\phi_k^s}{2}c_k^\dagger - i\sin\frac{\phi_k^s}{2}c_{-k}. \end{aligned} \tag{B.4}$$

This transformation preserves the canonical commutation relations, $\{c_k, c_{k'}^\dagger\} = \delta_{k,k'}$, the Bogoliubov angles ϕ_k^s satisfy $\phi_{-k}^s = -\phi_k^s$ and are fixed such that only fermion number conserving terms appear in the Hamiltonian. This condition forces the angles to satisfy

$$\tan\phi_k^s = -\frac{\sqrt{\gamma\lambda}\sin k}{s+1-\cos k}, \tag{B.5}$$

with these transformations we arrive at Eq. (3.17). Next to calculate the MGF $Z(s,t)$ we express the vacuum $|0\rangle_{s=0}$ of $\mathbb{H}_{s=0}$ as a BCS state of the $s \neq 0$ Hamiltonian $\mathbb{H}_s$,

$$\begin{aligned}|0\rangle_{s=0} &= \frac{1}{\mathcal{N}}\exp\Big(\sum_k c_{-k}^\dagger c_k^\dagger\Big)|0\rangle_s \\ &= \bigotimes_{k>0}[\cos\alpha_k^s|0_k, 0_{-k}\rangle_s - i\sin\alpha_k^s|1_k, 1_{-k}\rangle_s],\end{aligned} \tag{B.6}$$

where the second line follows from expanding the exponential and using the Bogoliubov rotation in Eq. (B.4). In the first line $\mathcal{N}$ denotes the normalization factor, $\bigotimes$ denotes the direct product, the states $|n_k, n_{-k}\rangle$ indicate the occupation of fermionic modes with wavevector $\pm k$ which diagonalize $\mathbb{H}_s$ and the angles α_k^s are equal to half the difference of ϕ_k^s and $\phi_k^{s=0}$.

In Chapter 5 we consider a non-Hermitian operator H_s related to the TFIM. This can be diagonalized again using a Jordan-Wigner transformation followed by a Bogoliubov rotation, where in Eq. (B.4) we make the replacement $c_k \to A_k$ and $c_k^\dagger \to \bar{A}_k$. Although the excitations are still fermionic, $\{A_k, \bar{A}_{k'}\} = \delta_{k,k'}$, due to the non-Hermitian nature of our perturbed Hamiltonian these creation and annihilation operators are not Hermitian conjugate to each other i. e. $A_k^\dagger \neq \bar{A}_k$. Working through an identical calculation one find the Bogoliubov angles are now subject to the constraint

$$\tan \phi_k^s = \frac{\sin k}{is/2 + \lambda - \cos k}, \tag{B.7}$$

where λ is the transverse field strength.

C. CGF of Time-Integrated Transverse Magnetization in TFIM

Recalling the complex spectrum $\epsilon_k(s) = 2\sqrt{(\lambda + \frac{is}{2} - \cos k)^2 + \sin^2 k}$ and Eq. (5.4), in the continuum limit the scaled CGF is given by

$$\theta(s) = \frac{2}{\pi}|\mathrm{Im}\int_0^\pi \sqrt{(\lambda + \frac{is}{2} - \cos k)^2 + \sin^2 k}\; dk|. \tag{C.1}$$

Focussing on $s > 0$, in the dynamically disordered phase the imaginary component of $\epsilon_k(s)$ is always $> 0\ \forall k$. Furthermore setting $k \to \pi - k$ one can readily see that $\int_0^\pi \sqrt{(\lambda + \frac{is}{2} - \cos k)^2 + \sin^2 k}\; dk = \int_0^\pi \sqrt{(\lambda + \frac{is}{2} + \cos k)^2 + \sin^2 k}\; dk$. With these observations in hand, and denoting $\lambda_s = \lambda + is/2$, we find

$$\begin{aligned}
\theta(s) &= \frac{2}{\pi}\mathrm{Im}\Big[\int_0^\pi \sqrt{1 + \lambda_s^2 + 2\lambda_s \cos k}\; dk\Big] \\
&= \frac{2}{\pi}\mathrm{Im}\Big[(1+\lambda_s)\int_0^\pi \sqrt{1 + \frac{2\lambda_s}{(1+\lambda_s)^2}(1 - \cos k)}\; dk\Big] \\
&= \frac{2}{\pi}\mathrm{Im}\Big[(1+\lambda_s)\int_0^\pi \sqrt{1 - \frac{4\lambda_s}{(1+\lambda_s)^2}\sin^2\frac{k}{2}}\; dk\Big] \\
&= \frac{4}{\pi}\mathrm{Im}\Big[(1+\lambda_s)\int_0^{\frac{\pi}{2}} \sqrt{1 - \frac{4\lambda_s}{(1+\lambda_s)^2}\sin^2 k}\; dk\Big].
\end{aligned} \tag{C.2}$$

The integral appearing in the last line of Eq. (C.2) is a complete elliptical integral of the second kind. A similar expression may be found in the dynamically ordered regime by noting that for $k < k_\lambda$ the imaginary part of $\epsilon_k(s)$ is < 0 and > 0 when $k > k_\lambda$. Dividing the integral over k up into the ranges $[0, k_\lambda]$ and $[k_\lambda, \pi]$ and performing similar manipulations one readily arrives at the functional form of Eq. (5.5).

D. Parallel Transport Gauge

Consider the ground state $|0(\boldsymbol{\xi})\rangle$ of a Hamiltonian $H(\boldsymbol{\xi})$ both of which depend on the parameters $\boldsymbol{\xi}$. When adiabatically transporting this wavefunction around a closed loop in parameter space we can choose a gauge where the phase of the state remains constant under infinitesimal changes in the parameters $\boldsymbol{\xi}$, this is the parallel transport gauge. This gauge is implicitly built into most expressions in standard perturbation theory and results in a vanishing Berry phase. To see this we first recall the Berry connection

$$A(\boldsymbol{\xi}) = i\langle 0(\boldsymbol{\xi})|\nabla_{\boldsymbol{\xi}}|0(\boldsymbol{\xi})\rangle. \tag{D.1}$$

To calculate this quantity it is necessary to use perturbation theory

$$|0(\boldsymbol{\xi}+\Delta\boldsymbol{\xi})\rangle \simeq |0(\boldsymbol{\xi})\rangle + \sum_{n\neq 0}|n(\boldsymbol{\xi})\rangle \frac{\langle n(\boldsymbol{\xi})|H(\boldsymbol{\xi}+\Delta\boldsymbol{\xi}) - H(\boldsymbol{\xi})|0(\boldsymbol{\xi})\rangle}{E_0(\boldsymbol{\xi}) - E_n(\boldsymbol{\xi})}, \tag{D.2}$$

where $|n(\boldsymbol{\xi})\rangle$ are the excited states of the unperturbed system. Due to the orthogonality of the excited states to the ground state we find the Berry connection should be 0. Crucially this arises from the choice in gauge, the parallel transport gauge, which ensures that an infinitesimal change in $|0(\boldsymbol{\xi})\rangle$ is orthogonal to $|0(\boldsymbol{\xi})\rangle$. As written in Eq. D.2 this choice of gauge is incompatible with state vectors which are globally single valued upon adiabatic transport around a closed loop in parameter space, however this incompatibility may be rectified by the inclusion of a

phase factor

$$|0(\boldsymbol{\xi}+\Delta\boldsymbol{\xi})\rangle \simeq e^{-i\Delta\phi}\Big[|0(\boldsymbol{\xi})\rangle + \sum_{n\neq 0}|n(\boldsymbol{\xi})\rangle \frac{\langle n(\boldsymbol{\xi})|H(\boldsymbol{\xi}+\Delta\boldsymbol{\xi})-H(\boldsymbol{\xi})|0(\boldsymbol{\xi})\rangle}{E_0(\boldsymbol{\xi})-E_n(\boldsymbol{\xi})}\Big]. \quad \text{(D.3)}$$

Here $\Delta\phi$ plays the role of an arbitrary gauge phase, and in the limit $\Delta\boldsymbol{\xi}\to 0$ this should vanish. In this limit one can Taylor expand the phase factor $e^{-i\Delta\phi}$ to 1st order in $\Delta\phi$. This leads to a nonvanishing Berry connection

$$A(\boldsymbol{\xi}) = i\langle 0(\boldsymbol{\xi})|\nabla_{\boldsymbol{\xi}}|0(\boldsymbol{\xi})\rangle = i(1-\Delta\phi), \quad \text{(D.4)}$$

and thus with a suitable choice of this gauge phase the single valuedness of the state vector can be restored.

Bibliography

[1] L. Peliti. *Statistical mechanics in a nutshell*. Princeton University Press, 2011.

[2] D. Chandler. *Introduction to Modern Statistical Mechanics*. Oxford University Press, Oxford, 1987.

[3] J. C. Maxwell. On the dynamical evidence of the molecular constitution of bodies. *Nature*, 11:357–359, 1875.

[4] D. Ruelle. *Thermodynamic formalism*. Cambridge University Press, 2004.

[5] M. Merolle, J. P. Garrahan, and D. Chandler. Space-time thermodynamics of the glass transition. *Proceedings of the National Academy of Sciences USA*, 102(31):10837, 2005.

[6] V. Lecomte, C. Appert-Rolland, and F. van Wijland. Thermodynamic formalism for systems with markov dynamics. *Journal of Statistical Physics*, 127(1):51, April 2007.

[7] J. P. Garrahan, R. L. Jack, V. Lecomte, E. Pitard, K. van Duijvendijk, and F. van Wijland. Dynamical first-order phase transition in kinetically constrained models of glasses. *Physical Reviews Letters*, 98:195702, May 2007.

[8] J. P. Garrahan, R. L Jack, V. Lecomte, E. Pitard, K. van Duijvendijk, and F. van Wijland. First-order dynamical phase transition in models of glasses: an approach based on ensembles of histories. *Journal of Physics A: Mathematical and Theoretical*, 42(7):075007, 2009.

[9] L. O. Hedges, R. L. Jack, J. P. Garrahan, and D. Chandler. Dynamic order-disorder in atomistic models of structural glass formers. *Science*, 323(5919):1309, 2009.

[10] E. Pitard, V. Lecomte, and F. van Wijland. Dynamic transition in an atomic glass former: A molecular-dynamics evidence. *Europhysics Letters*, 96(5):56002, 2011.

[11] C. Giardina, J. Kurchan, V. Lecomte, and J. Tailleur. Simulating rare events in dynamical processes. *Journal of Statistical Physics*, 145(4):787–811, 2011.

[12] M. Gorissen, J. Hooyberghs, and C. Vanderzande. Density-matrix renormalization-group study of current and activity fluctuations near nonequilibrium phase transitions. *Physical Review E*, 79:020101, February 2009.

[13] R. L. Jack and P. Sollich. Large deviations and ensembles of trajectories in stochastic models. *Progress of Theoretical Physics Supplement*, 184:304–317, 2010.

[14] Y. S. Elmatad, R. L. Jack, D. Chandler, and J. P. Garrahan. Finite-temperature critical point of a glass transition. *Proceedings of the National Academy of Sciences USA*, 107(29):12793, 2010.

[15] G. Biroli and J. P. Garrahan. Perspective: The glass transition. *The Journal of Chemical Physics*, 138(12), 2013.

[16] C. A. Angell. Formation of glasses from liquids and biopolymers. *Science*, 267(5206):1924–1935, 1995.

[17] M. D. Ediger, C. A. Angell, and Sidney R. Nagel. Supercooled liquids and glasses. *The Journal of Physical Chemistry*, 100(31):13200–13212, 1996.

[18] C. A. Angell, K. L. Ngai, G. B. McKenna, P. F. McMillan, and S. W. Martin. Relaxation in glassforming liquids and amorphous solids. *Journal of Applied Physics*, 88(6):3113–3157, 2000.

[19] P. G. Debenedetti and F. H. Stillinger. Supercooled liquids and the glass transition. *Nature (London)*, 410:259–267, 2001.

[20] V. Lubchenko and P. G. Wolynes. Theory of structural glasses and supercooled liquids. *Annual Review of Physical Chemistry*, 58(1):235–266, 2007.

[21] A. Heuer. Exploring the potential energy landscape of glass-forming systems: from inherent structures via metabasins to macroscopic transport. *Journal of Physics: Condensed Matter*, 20(37):373101, 2008.

[22] A. Cavagna. Supercooled liquids for pedestrians. *Physics Reports*, 476(46):51 – 124, 2009.

[23] D. Chandler and J. P. Garrahan. Dynamics on the way to forming glass: Bubbles in space-time. *Annual Review of Physical Chemistry*, 61(1):191–217, 2010.

[24] L. Berthier and G. Biroli. Theoretical perspective on the glass transition and amorphous materials. *Reviews of Modern Physics*, 83:587–645, June 2011.

[25] F. Ritort and P. Sollich. Glassy dynamics of kinetically constrained models. *Advances in Physics*, 52(4):219–342, 2003.

[26] J. P. Garrahan, P. Sollich, and C. Toninelli. *Kinetically constrained models, in Dynamical Heterogeneities in Glasses, Colloids and Granular Materials, edited by L. Berthier, G. Biroli, J.-P. Bouchaud, L. Cipelletti, and W. van Saarloos*, 2011.

[27] J. Jäckle and S. Eisinger. A hierarchically constrained kinetic ising model. *Zeitschrift fr Physik B Condensed Matter*, 84(1):115–124, 1991.

[28] J. P. Garrahan and D. Chandler. Geometrical explanation and scaling of dynamical heterogeneities in glass forming systems. *Physical Review Letters*, 89:035704, July 2002.

[29] J. P. Garrahan and I. Lesanovsky. Thermodynamics of quantum jump trajectories. *Physical Review Letters*, 104(16):160601, April 2010.

[30] J. P. Garrahan, A. D. Armour, and I. Lesanovsky. Quantum trajectory phase transitions in the micromaser. *Physical Review E*, 84(2):021115, August 2011.

[31] A. Budini. Large deviations of ergodic counting processes: A statistical mechanics approach. *Physical Review E*, 84(1):011141, July 2011.

[32] C. Ates, B. Olmos, J. P. Garrahan, and I. Lesanovsky. Dynamical phases and intermittency of the dissipative quantum ising model. *Physical Review A*, 85:043620, April 2012.

[33] T. Karzig and F. von Oppen. Signatures of critical full counting statistics in a quantum-dot chain. *Physical Review B*, 81:045317, January 2010.

[34] D. A. Ivanov and A. G. Abanov. Phase transitions in full counting statistics for periodic pumping. *Europhysics Letters*, 92(3):37008, November 2010.

[35] D. A. Ivanov and A. G. Abanov. Characterizing correlations with full counting statistics: Classical ising and quantum xy spin chains. *Physical Review E*, 87:022114, February 2013.

[36] G. A. Álvarez, E. P. Danieli, P. R. Levstein, and H. M. Pastawski. Decoherence as attenuation of mesoscopic echoes in a spin-chain channel. *Physical Review A*, 82:012310, July 2010.

[37] J. Li, Y. Liu, J. Ping, S.-S. Li, X.-Q. Li, and Y. Yan. Large-deviation analysis for counting statistics in mesoscopic transport. *Physical Review B*, 84(11):115319, September 2011.

[38] C. W. Gardiner. *Handbook of stochastic methods*. Springer, 1986.

[39] M. B. Plenio and P. L. Knight. The quantum-jump approach to dissipative dynamics in quantum optics. *Reviews of Modern Physics*, 70:101–144, January 1998.

[40] C. W. Gardiner and P. Zoller. *Quantum Noise*. Springer, 2004.

[41] Y. V Nazarov, editor. *Quantum Noise in Mesoscopic Physics*. Kluwer Academic Publishers, 2003.

[42] M. Esposito, U. Harbola, and S. Mukamel. Nonequilibrium fluctuations, fluctuation theorems, and counting statistics in quantum systems. *Reviews of Modern Physics*, 81:1665–1702, December 2009.

[43] N. G. Van Kampen. *Stochastic Processes in Physics and Chemistry*. North-Holland Personal Library, 2007.

[44] J. P. Eckmann and D. Ruelle. Ergodic theory of chaos and strange attractors. *Reviews of Modern Physics*, 57:617–656, July 1985.

[45] P. Gaspard. *Chaos, Scattering and Statistical Mechanics*. Cambridge University Press, 2005.

[46] H. Touchette. The large deviation approach to statistical mechanics. *Physics Reports*, 478(1-3):1, July 2009.

[47] G. Greiner, O. Mandel, T. Esslinger, T. Hänsch, and I. Bloch. Collapse and revival of the matter wave field of a boseeinstein condensate. *Nature*, 419:51–54, 2002.

[48] T. Kinoshita, T. Wenger, and D. Weiss. A quantum newton's cradle. *Nature*, 440:900–903, 2006.

[49] M. Cheneau, P. Barmettler, D. Poletti, M. Endres, P. Schauß, T. Fukuhara, C. Gross, I. Bloch, C. Kollath, and S. Kuhr. Light-cone-like spreading of correlations in a quantum many-body system. *Nature*, 481:484 –487, 2012.

[50] M. Gring, M. Kuhnert, T. Langen, T. Kitagawa, B. Rauer, M. Schreitl, I. Mazets, D. Adu Smith, E. Demler, and J. Schmiedmayer. Relaxation and prethermalization in an isolated quantum system. *Science*, 337(6100):1318–1322, 2012.

[51] T. D. Lee and C. N. Yang. Statistical theory of qquations of state and phase transitions. ii. lattice gas and ising model. *Physical Review*, 87:410, August 1952.

[52] C. N. Yang and T. D. Lee. Statistical theory of equations of state and phase transitions. i. theory of condensation. *Physical Review*, 87:404, August 1952.

[53] C. Flindt and J. P. Garrahan. Trajectory phase transitions, lee-yang zeros, and high-order cumulants in full counting statistics. *Physical Review Letters*, 110:050601, January 2013.

[54] J. M. Hickey, S. Genway, I. Lesanovsky, and J. P. Garrahan. Thermodynamics of quadrature trajectories in open quantum systems. *Physical Review A*, 86:063824, December 2012.

[55] S. Sachdev. *Quantum Phase Transitions*. Cambridge University Press, 2011.

[56] J. M. Hickey, S. Genway, I. Lesanovsky, and J. P. Garrahan. Time-integrated observables as order parameters for full counting statistics transitions in closed quantum systems. *Physical Review B*, 87:184303, May 2013.

[57] M. V. Berry. Quantal phase factors accompanying adiabatic changes. *Proceedings of the Royal Society of London. A. Mathematical and Physical Sciences*, 392(1802):45–57, 1984.

[58] B. Simon. Holonomy, the quantum adiabatic theorem, and berry's phase. *Physical Review Letters*, 51:2167–2170, December 1983.

[59] J. Samuel and R. Bhandari. General setting for berry's phase. *Physical Review Letters*, 60:2339–2342, June 1988.

[60] M. Kolodrubetz, V. Gritsev, and A. Polkovnikov. Classifying and measuring geometry of a quantum ground state manifold. *Physical Review B*, 88:064304, August 2013.

[61] A. Hamma. Berry phases and quantum phase transitions. *arXiv:quant-ph/0602091*, 2006.

[62] R. Resta. Manifestations of berry's phase in molecules and condensed matter. *Journal of Physics: Condensed Matter*, 12(9):R107, 2000.

[63] Y.-Q. Ma and S. Chen. Geometric phase and quantum phase transition in an inhomogeneous periodic xy spin-$\frac{1}{2}$ model. *Physical Review A*, 79:022116, February 2009.

[64] J. M. Hickey, S. Genway, and J. P. Garrahan. Dynamical phase transitions, time-integrated observables, and geometry of states. *Physical Review B*, 89:054301, February 2014.

[65] C. M. Bender and S. Boettcher. Real spectra in non-hermitian hamiltonians having $\mathcal{PT}$ symmetry. *Physical Review Letters*, 80:5243–5246, June 1998.

[66] C. M. Bender, D. C. Brody, and H. F. Jones. Complex extension of quantum mechanics. *Physical Review Letters*, 89:270401, December 2002.

[67] C. M. Bender, D. C. Brody, and H. F. Jones. Extension of $\mathcal{PT}$-symmetric quantum mechanics to quantum field theory with cubic interaction. *Physical Review D*, 70:025001, July 2004.

[68] C. M. Bender. Making sense of non-hermitian hamiltonians. *Reports on Progress in Physics*, 70(6):947, 2007.

[69] A. Mostafazadeh. Pseudo-hermitian representation of quantum mechanics. *International Journal of Geometric Methods in Modern Physics*, 07(07):1191–1306, 2010.

[70] S. Weigert. $\mathcal{PT}$-symmetry and its spontaneous breakdown explained by antilinearity. *Journal of Optics B: Quantum and Semiclassical Optics*, 5(3):S416, 2003.

[71] O. A. Castro-Alvaredo and A. Fring. A spin chain model with non-hermitian interaction: the ising quantum spin chain in an imaginary field. *Journal of Physics A: Mathematical and Theoretical*, 42(46):465211, 2009.

[72] James M. Hickey, Emanuele Levi, and Juan P. Garrahan. Cumulants of time-integrated observables of closed quantum systems and $\mathcal{PT}$ symmetry with an application to the quantum ising chain. *Physical Review B*, 90:094301, September 2014.

[73] A. Silva. Statistics of the work done on a quantum critical system by quenching a control parameter. *Physical Review Letters*, 101:120603, September 2008.

[74] A. Polkovnikov, K. Sengupta, A. Silva, and M. Vengalattore. *Colloquium* : Nonequilibrium dynamics of closed interacting quantum systems. *Reviews of Modern Physics*, 83:863–883, August 2011.

[75] A. Gambassi and A. Silva. Large deviations and universality in quantum quenches. *Physical Review Letters*, 109:250602, December 2012.

[76] D. Schuricht and F. H. L. Essler. Dynamics in the ising field theory after a quantum quench. *Journal of Statistical Mechanics: Theory and Experiment*, 2012(04):P04017, 2012.

[77] P. Calabrese, F. H. L. Essler, and M. Fagotti. Quantum quench in the transverse field ising chain: I. time evolution of order parameter correlators. *Journal of Statistical Mechanics: Theory and Experiment*, 2012(07):P07016, 2012.

[78] P. Calabrese, F. H. L. Essler, and M. Fagotti. Quantum quenches in the transverse field ising chain: Ii. stationary state properties. *Journal of Statistical Mechanics: Theory and Experiment*, 2012(07):P07022, 2012.

[79] M. Heyl, A. Polkovnikov, and S. Kehrein. Dynamical quantum phase transitions in the transverse-field ising model. *Physical Review Letters*, 110:135704, March 2013.

[80] F. Pollmann, S. Mukerjee, A. G. Green, and J. E. Moore. Dynamics after a sweep through a quantum critical point. *Physical Review E*, 81:020101, February 2010.

[81] C. Karrasch and D. Schuricht. Dynamical phase transitions after quenches in nonintegrable models. *Physical Review B*, 87:195104, May 2013.

[82] J. Bricmont. Science of chaos or chaos in science? *Annals of the New York Academy of Sciences*, 775(1):131–175, 1995.

[83] J. M. Hickey, C. Flindt, and J. P. Garrahan. Trajectory phase transitions and dynamical lee-yang zeros of the glauber-ising chain. *Physical Review E*, 88:012119, July 2013.

[84] S. Genway, J. P. Garrahan, I. Lesanovsky, and A. D. Armour. Phase transitions in trajectories of a superconducting single-electron transistor coupled to a resonator. *Physical Review E.*, 85:051122, May 2012.

[85] V. Gorini and A. Kossakowski. Nlevel system in contact with a singular reservoir. *Journal of Mathematical Physics*, 17(7):1298–1305, 1976.

[86] G. Lindblad. On the generators of quantum dynamical semigroups. *Communications in Mathematical Physics*, 48(2):119–130, 1976.

[87] H.P. Breuer and F. Petruccione. *The Theory of Open Quantum Systems*. Oxford University Press Oxford, 2007.

[88] M.O. Scully and S. Zubairy. *Quantum Optics*. Cambridge University Press, 1997.

[89] I. Affleck, T. Kennedy, E. H. Lieb, and H. Tasaki. Rigorous results on valence-bond ground states in antiferromagnets. *Physical Review Letters*, 59:799–802, August 1987.

[90] M. Fannes, B. Nachtergaele, and R.F. Werner. Finitely correlated states on quantum spin chains. *Communications in Mathematical Physics*, 144(3):443–490, 1992.

[91] C. Schön, E. Solano, F. Verstraete, J. I. Cirac, and M. M. Wolf. Sequential generation of entangled multiqubit states. *Physical Review Letters*, 95:110503, September 2005.

[92] F. Verstraete and J. I. Cirac. Continuous matrix product states for quantum fields. *Physical Review Letters*, 104:190405, May 2010.

[93] T. J. Osborne, J. Eisert, and F. Verstraete. Holographic quantum states. *Physical Review Letters*, 105:260401, December 2010.

[94] I. Lesanovsky, M. van Horssen, M. Guta, and J. P. Garrahan. Characterization of dynamical phase transitions in quantum jump trajectories beyond the properties of the stationary state. *Physical Review Letters*, 110:150401, April 2013.

[95] L. S. Levitov and G. B. Lesovik. Charge distribution in quantum shot noise,. *JETP Letters*, 58:230, 1993.

[96] L. S. Levitov, H. Lee, and G. B. Lesovik. Electron counting statistics and coherent states of electric current. *Journal of Mathematical Physics*, 37(10):4845, October 1996.

[97] Y. V. Nazarov and M. Kindermann. Full counting statistics of a general quantum mechanical variable. *European Physics Journal B*, 35:413, 2003.

[98] S. Pilgram, A. N. Jordan, E. V. Sukhorukov, and M. Büttiker. Stochastic path integral formulation of full counting statistics. *Physical Review Letters*, 90:206801, May 2003.

[99] C. Flindt, T. Novotný, A. Braggio, M. Sassetti, and A.-P. Jauho. Counting statistics of non-markovian quantum stochastic processes. *Physical Review Letters*, 100:150601, April 2008.

[100] C. Flindt, C. Fricke, F. Hohls, T. Novotný, K. Netocny, T. Brandes, and R. J. Haug. Universal oscillations in counting statistics. *Proceedings of the National Academy of Sciences USA*, 106(25):10116, June 2009.

[101] M. E. Fisher in. *Boulder Lectures in Theoretical Physics*, volume 7. University of Colorado, Boulder, 1965.

[102] I. P. Levkivskyi and E. V. Sukhorukov. Noise-induced phase transition in the electronic mach-zehnder interferometer. *Physical Review Letters*, 103:036801, July 2009.

[103] Y. Utsumi, O. Entin-Wohlman, A. Ueda, and A. Aharony. Full-counting statistics for molecular junctions: Fluctuation theorem and singularities. *Physical Review B*, 87:115407, March 2013.

[104] R. A. Blythe and M. R. Evans. Lee-yang zeros and phase transitions in nonequilibrium steady states. *Physical Review Letters*, 89:080601, August 2002.

[105] I. Bena, M. Droz, and A. Lipowski. Statistical mechanics of equlibrium and nonequilibrium phase transitions: The yang–lee formalism. *International Journal of Modern Physics B*, 19(29):4269, 2005.

[106] B.-B Wei and R.-B. Liu. Lee-yang zeros and critical times in decoherence of a probe spin coupled to a bath. *Phys. Rev. Lett.*, 109:185701, October 2012.

[107] G. H. Fredrickson and H. C. Andersen. Kinetic ising model of the glass transition. *Physical Review Letters*, 53:1244–1247, September 1984.

[108] C. Flindt, T. Novotný, A. Braggio, and A.-P. Jauho. Counting statistics of transport through coulomb blockade nanostructures: High-order cumulants and non-markovian effects. *Physical Review B*, 82:155407, October 2010.

[109] D. Kambly, C. Flindt, and M. Büttiker. Factorial cumulants reveal interactions in counting statistics. *Physical Review B*, 83:075432, February 2011.

[110] R. J. Glauber. Time-dependent statistics of the ising model. *Journal of Mathematical Physics*, 4:294, 1963.

[111] R. B. Dingle. *Asymptotic Expansions: Their Derivation and Interpretation*. Academic Press, London, 1973.

[112] M. V. Berry. Universal oscillations of high derivatives. *Proceedings of the Royal Society A*, 461(2058):1735, 2005.

[113] R. S. Bhalerao, N. Borghini, and J. Y. Ollitrault. Analysis of anisotropic flow with lee–yang zeroes. *Nuclear Physics A*, 727(3):373, 2003.

[114] C. Fricke, F. Hohls, N. Sethubalasubramanian, L. Fricke, and R. J. Haug. High-order cumulants in the counting statistics of asymmetric quantum dots. *Applied Physics Letters*, 96(20), 2010.

[115] C. Fricke, F. Hohls, C. Flindt, and R. J. Haug. High cumulants in the counting statistics measured for a quantum dot. *Physica E*, 42:848, 2010.

[116] J. Zamastil and F. Vinette. Determination of singularities of a function from its perturbation expansion. *Journal of Physics A: Mathematical and General*, 38:4009, 2005.

[117] E. D. Siggia. Pseudospin formulation of kinetic ising models. *Physical Review B*, 16:2319–2320, September 1977.

[118] H. Walther, B. T. H. Varcoe, B.-G. Englert, and T. Becker. Cavity quantum electrodynamics. *Reports on Progress in Physics*, 69(5):1325, 2006.

[119] P. Filipowicz, J. Javanainen, and P. Meystre. Theory of a microscopic maser. *Physical Review A*, 34:3077–3087, October 1986.

[120] E. Barkai, Y. Jung, and R. Silbey. Theory of single-molecule spectroscopy: Beyond the ensemble average. *Annual Review of Physical Chemistry*, 55(1):457–507, 2004.

[121] R. B. Lehoucq, D. C. Sorensen, and C. Yang. Arpack user's guide: Solution of large-scale eigenvalue problems with implicitly restorted arnoldi methods (software, environments, tools). 1998.

[122] HSL. A collection of fortran codes for large scale scientific computation. 2011.

[123] J. T. Barreiro, M. Müller, P. Schindler, D. Nigg, T. Monz, M. Chwalla, M. Hennrich, C. F. Roos, P. Zoller, and R. Blatt. An open-system quantum simulator with trapped ions. *Nature(London)*, 470:486–491, 2011.

[124] R. Blatt and C. F Roos. Quantum simulations with trapped ions. *Nature Physics*, 13(8):277, 2012.

[125] M. Horssen van and M. Guta. Large deviations, central limit and dynamical phase transitions in the atom maser. *arXiv:1206.4956v2 [quant-ph]*, 2013.

[126] M. Müller, K. Hammerer, Y. L. Zhou, C. F. Roos, and P. Zoller. Simulating open quantum systems: from many-body interactions to stabilizer pumping. *New Journal of Physics*, 13(8):085007, 2011.

[127] E. P. Wigner. Normal form of antiunitary operators. *Journal of Mathematical Physics*, 1(5):409–413, 1960.

[128] J. L. Cardy. Conformal invariance and the yang-lee edge singularity in two dimensions. *Physical Review Letters*, 54:1354–1356, Apr 1985.

[129] A.A. Belavin, A.M. Polyakov, and A.B. Zamolodchikov. Infinite conformal symmetry in two-dimensional quantum field theory. *Nuclear Physics B*, 241(2):333 – 380, 1984.

[130] G. Von Gehlen. Critical and off-critical conformal analysis of the ising quantum chain in an imaginary field. *Journal of Physics A: Mathematical and General*, 24(22):5371, 1991.

[131] P. Calabrese, F. H. L. Essler, and M. Fagotti. Quantum quench in the transverse-field ising chain. *Physical Review Letters*, 106:227203, June 2011.

[132] Y. Aharonov and J. Anandan. Phase change during a cyclic quantum evolution. *Physical Review Letters*, 58:1593–1596, April 1987.

[133] T. Frankel. *The Geometry of Physics: An Introduction*. Cambridge University Press, 2004.

[134] M. Fagotti. Dynamical phase transitions as properties of the stationary state: Analytic results after quantum quenches in the spin-1/2 xxz chain. *arXiv:1308.0277 [cond-mat.stat-mech]*, 2013.

[135] V. Szabolcs and D. Balázs. Disentangling dynamical phase transitions from equilibrium phase transitions. *arXiv:1401.2865 [cond-mat.str-el]*, 2013.

[136] A. C. M. Carollo and J. K. Pachos. Geometric phases and criticality in spin-chain systems. *Physical Review Letters*, 95:157203, October 2005.

[137] S.-L. Zhu. Scaling of geometric phases close to the quantum phase transition in the *xy* spin chain. *Physical Review Letters*, 96:077206, February 2006.

[138] J.P. Provost and G. Vallee. Riemannian structure on manifolds of quantum states. *Communications in Mathematical Physics*, 76(3):289–301, 1980.

[139] D. J. Thouless. Topological interpretations of quantum hall conductance. *Journal of Mathematical Physics*, 35(10):5362–5372, 1994.

[140] M. P. L. Heyl. *Nonequilibrium phenomena in many-body quantum systems*. Ludwig-Maximilians-Universität München, July 2012.